IS-T--1451

DE91 000664

Electrocatalysis of Anodic Oxygen-transfer Reactions at Modifie Lead Dioxide Electrodes

by

Hsiao, Yun-Lin

PHD Thesis submitted to Iowa State University

Ames Laboratory, U.S. DOE

Iowa State University

Ames, Iowa 50011

Date Transmitted: September 21, 1990

PREPARED FOR THE U.S. DEPARTMENT OF ENERGY

UNDER CONTRACT NO. W-7405-Eng-82.

Electrocatalysis of anodic oxygen-transfer reactions at modified lead dioxide electrodes

Yun-Lin Hsiao

Under the supervision of Professor Dennis C. Johnson
From the Department of Chemistry
Iowa State University

This dissertation describes results of the studies of anodic oxygen-transfer reactions at the electrochemically deposited lead dioxide electrodes modified by incorporation of spatially separated catalytic sites at the electrode surface. These active surface sites were created either by co-depositing the PbO_2 films with dopants (i.e., Bi^{3+}, As^{5+}, Cl^- and OAc^-) or by oxidative electrosorption of Bi^{3+} at the pre-deposited oxide films to produce the Bi^{5+}-adsorbed PbO_2. The incorporated cations and anions were speculated to substitute for the surface Pb^{4+} and O^{2-} ions, respectively.

Studies showed that the dopants influence (i) the deposition kinetics, (ii) the electrocatalytic properties, (iii) the surface morphologies, and (iv) the preferential orientations of the exposed crystallite planes of the doped oxides, as studied by cyclic voltammetry, scanning electron microscopy (SEM), and X-ray diffraction spectrometry (XRD). Results obtained from X-ray fluorescence spectrometry (XRF) revealed that the electrode activity was related to the densities of dopants in the modified electrodes, which

were controlled by the concentration ratio of [dopant]/[Pb^{2+}] in the deposition solutions.

The anion-doped PbO_2 electrodes exhibited significant catalytic activities for anodic O-transfer reactions for numerous compounds in 1 M H_2SO_4 when compared with that in 1 M $HClO_4$. The HSO_4^- ions were concluded to be adsorbed at the electrode surface by an ion-exchange mechanism with the exchangeable anions at the electrode surface (i.e., Cl^- for Cl-PbO_2 and OAc^- for OAc-PbO_2). Investigations of mass changes at electrode surface resulting from the anion exchange were performed using an Electrochemical Quartz Crystal Microbalance (EQCM).

Catalytic production of adsorbed hydroxyl radicals ($^{\cdot}OH_{ad}$) was concluded to be a prerequisite for an O-transfer reaction as well as the O_2 evolution process. Enhanced rates of O_2 evolution were observed at modified PbO_2 electrodes, which suggested a catalyzed mechanism for the anodic discharge of H_2O to form the adsorbed OH radicals. This reaction was concluded to be the rate-limiting step for both O-transfer and O_2-evolution processes.

DISCLAIMER

Electrocatalysis of anodic oxygen-transfer reactions at modified lead dioxide electrodes

by

Yun-Lin Hsiao

A Dissertation Submitted to the

Graduate Faculty in Partial Fulfillment of the

Requirements for the Degree of

DOCTOR OF PHILOSOPHY

Department: Chemistry
Major: Analytical Chemistry

Approved:

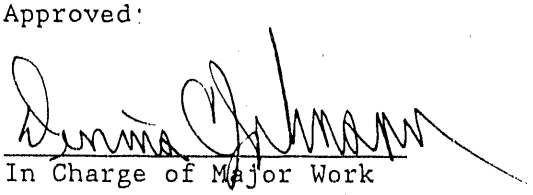

In Charge of Major Work

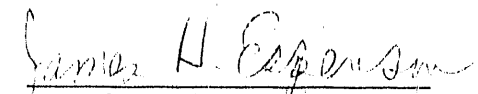

For the Major Department

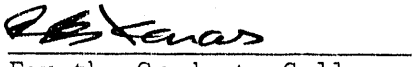

For the Graduate College

Iowa State University
Ames, Iowa

1990

TABLE OF CONTENTS

LIST OF SYMBOLS AND ABBREVIATIONS

A	- surface area of the rotated disc electrode (cm^2)
Ae	- electrochemically active surface area of EQCM
Au/QC	- gold-coated quartz crystal
Bi-PbO_2	- bismuth(V)-doped lead dioxide
Bi^{5+}/PbO_2	- bismuth(V)-adsorbed lead dioxide
C^b	- bulk concentration of analyte (mol L^{-1})
Cl-PbO_2	- chloride-doped lead dioxide
D	- diffusion coefficient (cm^2 s^{-1})
DMSO	- dimethyl sulfoxide
$DMSO_2$	- dimethyl sulfone
E	- applied electrode potential
E'	- standard reduction potential
$E_{1/2}$	- half-wave potential
E_d	- disc potential of a rotating ring-disc electrode
E_p	- peak potential
EQCM	- electrochemical quartz crystal microbalance
E_r	- ring potential of a rotating ring-disc electrode
F	- Faraday constant (96,487 coul eq^{-1})
df	- change of mechanical resonant frequency at EQCM (Hz)
I	- current (mA)
I_d	- disc current of a rotating ring-disc electrode (mA)
I_{O2}	- current produced for O_2 evolution (mA)
I_r	- ring current of a rotating ring-disc electrode (mA)

K	- proportionality constant of quartz crystal (cm^2 Hz mg^{-1})
k	- heterogeneous rate constant (cm s^{-1})
Δm	- mass change at the EQCM (ng)
n	- number of electron transferred (eq mol^{-1})
OAc-PbO_2	- acetate-doped lead dioxide
O-t	- oxygen-transfer
$^{\cdot}OH_{ad}$	- adsorbed hydroxyl radical
Δq	- net charge passed for electrode reaction at EQCM (coul)
r	- ionic radii (Å)
RDE	- rotating disc electrode
RRDE	- rotating ring-disc electrode
SCE	- saturated calomel electrode (0.243 V vs. NHE)
SEM	- scanning electron microscopy
t	- time (s)
XRD	- x-ray diffraction spectrometry
XRF	- x-ray fluorescence spectrometry
w	- rotation velocity of the disc electrode (rev min^{-1})
v	- kinematic viscosity (cm^2 s^{-1})
Θ	- X-ray diffraction angle

DEDICATION

To my parents

CHAPTER I.

GENERAL INTRODUCTION

Electrocatalysis

The electrochemical reaction of solution reactants requires inert electrodes. However, the electrode surfaces (which may differ widely from the bulk property) could react, at least temporarily, with the reactants (or intermediate product) of the overall electrode process. These interactions can occur by way of chemisorption, electrosorption or complexation with active centers of the electrode surface (1). Therefore, the rate of many electrochemical reactions can depend extensively on the nature of the electrode surface, and this is what electrocatalysis is about.

Some electrochemical reactions, although thermodynamically favorable, do not occur at a significant rate at commonly available electrodes. For such reactions to occur, it is necessary to find or modify a catalytic electrode, which will increase the rate of the reactions by several orders of magnitude. The advantages of electrocatalysis over homogeneous catalysis are twofold; first, separation of catalyst from reaction products is not necessary; second,

electrode potential can be controlled to enhance the reaction rate. This dissertation describes mainly the electrocatalysis of anodic O-transfer reactions at the modified lead dioxide films that have been electrochemically deposited on Au anodes in acidic solutions of Pb^{2+} salt.

What are Anodic Oxygen-transfer Ractions?

An anodic O-transfer reaction is defined as the oxidation reaction which involves the transfer of oxygen from water molecules to the electrochemical products. Some examples are shown below.

$$Mn^{2+} + 4H_2O \longrightarrow MnO_4^- + 8H^+ + 5e \quad [1]$$

$$Cr^{3+} + 7/2H_2O \longrightarrow 1/2Cr_2O_7^{2-} + 7H^+ + 3e \quad [2]$$

$$DMSO + H_2O \longrightarrow DMSO_2 + 2H^+ + 2e \quad [3]$$

$$C_6H_5\text{-}CH_3 \longrightarrow C_6H_5\text{-}CH_2OH \longrightarrow C_6H_5\text{-}CHO \longrightarrow C_6H_5\text{-}COOH \quad [4]$$

Most anodic O-transfer reactions are slow at conventional anodes, such as Pt, Au, glassy carbon (GC), and PbO_2. Therefore, there is great need in the electrochemical sciences for developing electrode materials that are electrochemically active for anodic O-transfer reactions.

Relation between O-transfer and O_2 Evolution

The prerequisite for successful O-transfer reaction is proposed to be the anodic discharge of H_2O to produce the adsorbed OH radicals (2).

This process has been determined to be the rate limiting step for both O_2 evolution and O-transfer reactions (3). In the absence of solution reactants, O_2 evolution from the electrode surface is the only reaction. The competition between the O-transfer and O_2 evolution for the adsorbed OH radicals can be described by the mechanism shown as follows.

$$\xrightarrow{S[OH]} \quad 2S[\ ] + O_2 + 2H^+ + 2e \qquad [5]$$

$$S[\ ] + H_2O \longrightarrow S[OH] + H^+ + e \qquad [6]$$

$$\xrightarrow[S[R]]{} \quad 2S[\ ] + RO + H^+ + e \qquad [7]$$

where S[ ] is the vacant surface site, and S[OH] and S[R] represent the adsorbed OH radical and reactant, respectively. The surface vacant sites, S[ ], can be repopulated via anodic discharge of H_2O. Since the process requires adsorption of both OH radicals and reactants, the electrode surface is believed to play an important role in catalyzing the oxidation of water. The goal pursued in this research for development of the catalytic anodes is the modification of PbO_2 electrodes to achieve the catalytic discharge of water, and to create active sites for reactant adsorption to promote the O-transfer reactions without severe concomitant evolution of O_2.

The understanding of the exact details of the O_2 evolution mechanism at electrode surfaces is still in a controversial stage. A brief review of the literature since the early 1960s work shows that the following three mechanisms have received strong support.

Mechanism I

This mechanism demands that two OH radicals are adsorbed on adjacent electrode sites (4). It is favorable that the two OH radicals can be adsorbed on the adjacent sites simultaneously. However, this requires proper spacing of the active sites to achieve concerted reaction steps.

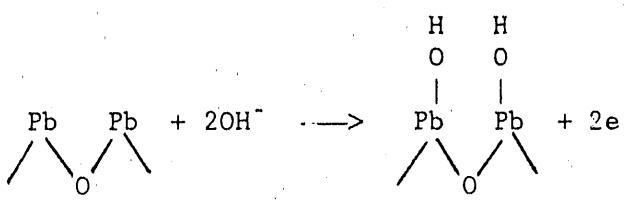

[8]

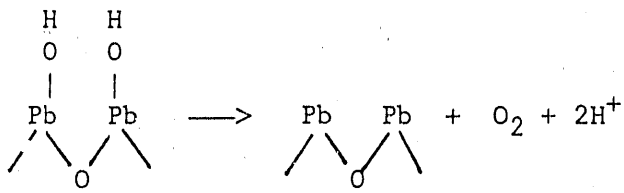

[9]

Mechanism II

This mechanism requires the adsorption of two OH radicals on one edge site (5). Edge-site Pb ions are in a low coordination state, so it is possible for two OH to adsorb. The mechanism for oxygen evolution on edge Pb is shown as followed.

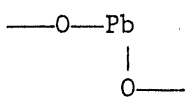

edge Pb(IV)

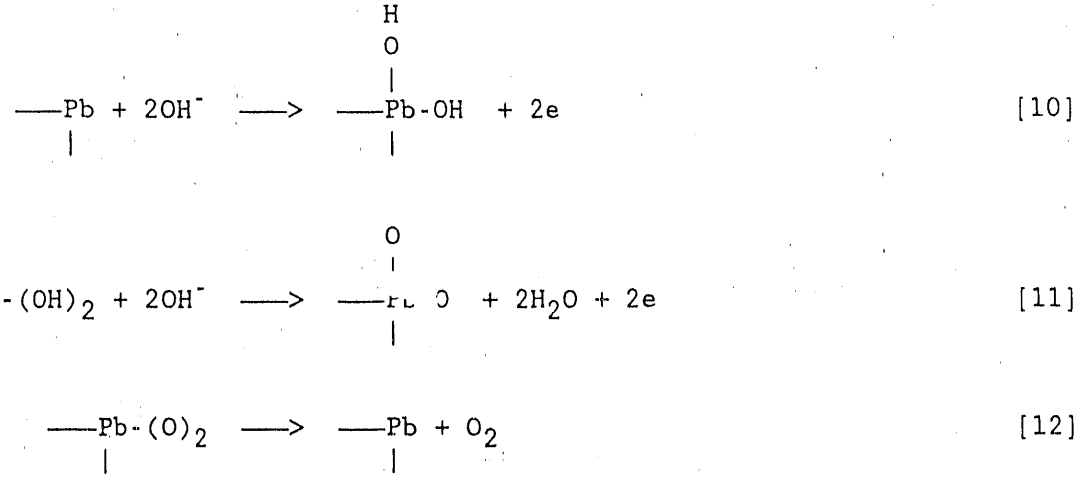

[10]

[11]

[12]

Mechanism III

This mechanism involves the adsorption of one OH radical onto a pre-adsorbed OH (6). Such type of reaction is more likely to occur on face rather than edge Pb, and the mechanism is illustrated in the following.

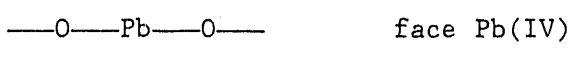

face Pb(IV)

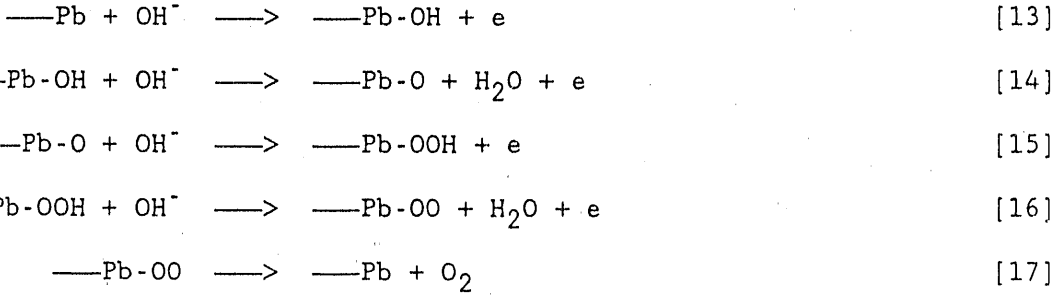

[13]

[14]

[15]

[16]

[17]

This mechanism requires the formation and breakage of the Pb-O bond for O_2 evolution to occur. If step [17] is rate limiting, then a weak bond strength of Pb-O is favorable to achieve a fast evolution of O_2 from the electrode surface. On the other hand, if reaction [13] is rate limiting, then it demands a stronger Pb-O bond for the formation of a high surface coverage by adsorbed OH radicals.

The following illustration shows the extent of overlapping of orbitals of two OH radicals adsorbed at (A) edge Pb, and (B) face Pb (5).

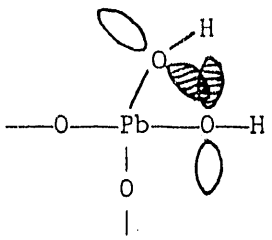

(A) edge Pb(IV)

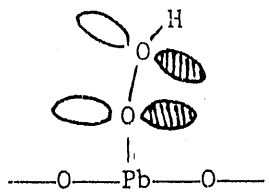

(B) face Pb(IV)

It has been reported that there is a greater charge donation to the electrode from the O-atoms adsorbed on the edges and corners than on the faces of a $SrFeO_3$ anode (5). Also reported was that the activation energy for two oxygen atoms to combine to give site-on bonded O_2 from an edge adsorbed O_2 is less than 0.8 eV on a $SrFeO_3$ anode (5), but no data were reported for that at face sites. Although it needs to break two Pb-O bonds to form one O_2 from the edge Pb rather than only one as from the face adsorbed O-O, edge cations are still concluded to catalyze O_2

evolution better than face cations (5).

How to Modify Lead Dioxide Electrodes?

It is of interest to use PbO_2 as a catalytic anode material because of its low cost, ease of preparation, existence of an oxygen-rich surface, inertness in most acidic and alkaline solutions, and a high O_2 evolution overpotential which allows for the application of large positive potential values without resulting in severe anodic discharge of water. The existing surface cation (Pb) and anion (O) sites make possible the modification of this oxide electrode by co-deposition with metallic (cationic) as well as nonmetallic (anionic) dopants. Modification of lead dioxide electrodes by anion-doping will be discussed in Chaps. II - V. Anions investigated included chloride (Cl^-), acetate (OAc^-), monohydrogen sulfate (HSO_4^-), and sulfate (SO_4^{2-}). Chapter VI will focus on the electrocatalytic properties of lead dioxide electrodes chemically modified by incorporation or adsorption of Bi^{5+}.

The anodic discharge of water to produce adsorbed OH radicals ($\cdot OH_{ad}$) has been determined to be the rate-limiting step for both O-transfer and O_2 evolution processes (3). Since the number of $\cdot OH_{ad}$ produced is constant at a fixed potential value, it seems possible to create a large number of active sites for reactant adsorption to enhance catalytic O-transfer reactions while simultaneously suppressing the process of O_2 evolution.

References

1. Beck, F.; Schulz, H. J. Electroanal. Chem. 1987, 229, 339.

2. Larew, L. A.; Gordon, J. S.; Hsiao, Y.-L.; Buttry, D. A.; Johnson, D. C. J. Electrochem. Soc. 1990, 137, 3071.

3. (a) Erdey-Gruz, T.; Shafarik, I. Proceedings of the 4th Conference on Electrochemistry Moscow; Academy of Science: Moscow, 1956; pp241-251. (b) Bockris, J. O'M. J. Chem. Phys. 1956, 24, 817. (c) Bockris, J. O'M. ed. Modern Aspects of Electrochemistry; Butterworth: London, 1954; pp 226-230.

4. (a) Epifanov, G. I. Solid State Physics; Mir Publishers: Moscow, 1977. (b) Damjanovic, A.; Dey, A.; Bockris, J. O'M. Electrochim. Acta, 1966, 11, 791. (c) Matsumoto, Y.; Kurimoto, J.; Sata, E. J. Electroanal. Chem. 1979, 102, 77. (d) Matsumoto, Y.; Sato, E. Electrochim. Acta, 1979, 24, 421. (e) Matsumoto, Y.; Sato, E. Electrochim. Acta, 1980, 25, 585. (f) Matsumoto, Y.; Kurimoto; Sato, E. Electrochim. Acta, 1980, 25, 539. (g) Mastumoto, Y.; Manabe, H.; Sato, E. J. Electrochem. Soc. 1980, 127, 811. (h) Mastumoto, Y.; Yamada, S.; Nishita, T.; Sato, E. J. Electrochem. Soc. 1980, 127, 2360.

5. Anderson, A. B. J. Electrochem. Soc. 1989, 136, 158.

6. (a) Rasiyah, P.; Tseung, C. C.; Hibbert, D. B. J. Electrochem. Soc. 1982, 129, 1724. (b) Kobussen, A. G. C.; Willems, H.; Broers,G. H. J. J. Electroanal. Chem. 1982, 142, 85. (c) Kobussen, A. G. C.; Broers, G. H. J. J. Electroanal. Chem. 1981, 126, 221.

CHAPTER II.

ELECTROCATALYSIS OF ANODIC OXYGEN-TRANSFER REACTIONS AT CHLORIDE-DOPED LEAD DIOXIDE ELECTRODES[1]

"Chemistry really means 'Chem is try'."

- unknown

Abstract

The electrocatalytic activities were compared for pure and chloride-doped beta-PbO_2 (Cl-PbO_2) films on gold and platinum substrates. Rate constants were increased significantly for oxidations of Mn^{2+}, toluene, benzyl alcohol, dimethylsulphoxide (DMSO) and benzaldehyde in acidic media by the incorporation of Cl^- into the oxide films. These reactions are concluded to occur by the electrocatalytic transfer of oxygen from H_2O to the reaction products. Results of X-ray diffraction studies indicate the Cl-PbO_2 film continues to have the slightly distorted rutile structure of pure beta-PbO_2. The observed electrocatalytic phenomena are concluded to be the beneficial

---

[1]Published in Hsiao, Y.-L.; Johnson, D. C. J. Electrochem. Soc. 1989, 136, 3704-3711.

consequence of surface defects generated when Cl^- serves for charge compensation within the surface matrix and, thereby, increases the number of surface sites capable of adsorbing hydroxyl radicals which are transferred in the electrocatalytic O-transfer reactions.

Introduction

Recently, much interest has been focused on the development of new anode materials (1). For oxidation reactions coupled to the transfer of oxygen from H_2O in aqueous solvents to the reaction products, metal oxides especially play an important role. Great interest in the electrocatalytic properties of PbO_2-film electrodes is a result of the successful application of this oxide in numerous anodic electrosynthetic reactions of commercial importance (2). The beta-form of PbO_2, having a slightly distorted rutile structure, is electrodeposited from perchloric acid solutions of Pb^{2+} (3, 4). However, it is noted that numerous oxidation reactions at pure beta-PbO_2 electrodes are under extreme kinetic control. Hence, a goal of this research continues to be the modification of PbO_2-film electrodes to increase their electrocatalytic properties for anodic O-transfer reactions.

Yeo and Johnson (5) reported that Bi(III) which had been incorporated into beta-PbO_2 films by co-electrodeposition had a significant electrocatalytic effect in the oxidation of several compounds in acidic media, including Mn(II) (rate increase of ca. 25X) and phenol (rate increased by > 100X). The electrocatalytic effects of

numerous other "doping" ions are now also under study. A general mechanism was proposed by Yeo et al. (6) for anodic O-transfer electrocatalysis at the "doped" oxide electrodes. According to this mechanism, labile surface-bound oxygen, probably existing as adsorbed hydroxyl radicals, are generated as intermediate products of the O_2-evolution reaction. These surface-bound oxygen species are transferred to products of the electrocatalyzed anodic reactions as illustrated by Equations 1-3 where M[ ] respresents the unpopulated surface site, M[OH] is the populated site, R is the reactant, and RO is the product of a one-oxygen transfer reaction.

$$M[\ ] + H_2O \longrightarrow M[OH] + H^+ + e \qquad [1]$$

$$M[OH] + R \longrightarrow M[\ ] + RO + H^+ + e \qquad [2]$$

$$\text{net:} \quad R + H_2O \longrightarrow RO + 2H^+ + 2e \qquad [3]$$

The concomitant evolution of oxygen, given by Equation 4, is not desired.

$$M[OH] + H_2O \longrightarrow O_2 + 3H^+ + 3e \qquad [4]$$

The chief goal of this research on doped PbO_2-film electrodes is the selective catalysis of O-transfer reactions (Equation 3) without similar increases in the rate of O_2 evolution (Equation 4).

Recent work in this laboratory (7) on co-deposition of various metal oxides with PbO_2 revealed an unexpected catalytic contribution

from Cl^- which was present as the counter ion of the doping metal cation. Reported here were the results of the effects of doping beta-PbO_2 with Cl^- for electrocatalysis of the oxidations of Mn(II), DMSO, toluene, benzyl alcohol, and benzaldehyde in 1.0 M H_2SO_4. Increases in rate constants by more than 80X are reported for DMSO and benzaldehyde.

Experimental

Apparatus

Exhaustive electrolysis data were obtained using a model 363 potentiostat (EG & G Princeton Applied Research) and a model SR-255 A/B strip chart recorder (Heath). Heterogeneous rate constants and current-potential curves were obtained by cyclic voltammetry at a Au rotated disk electrode (RDE, 0.164 cm^2) in a PIR rotator with a RDE3 potentiostat (Pine Instrument) and a model 2000 X-Y recorder (Houston Instrument). A three-compartment electrolysis cell was used with the Pt-wire counter electrode separated from the working solution by a fritted-glass junction. The saturated calomel electrode (SCE) reference contacted the working solution through a Harber-Luggin capillary.

Scanning Electron Micrographs (SEM) were obtained with a model JSM-840A microscope (Jeol). X-ray diffraction data were obtained with a model D500 diffractometer (Siemens).

Reagents

All chemicals were analytical reagent grade and solutions were prepared from water purified in a NANOpure-II deionization system

(SYBRON/Barnstead). The supporting electrolyte was 1.0 M $HClO_4$ for electrodeposition of oxide films and 1.0 M H_2SO_4 for kinetic testing and exhaustive electrolysis.

Procedure

Prior to electrodeposition, the Au RDE was polished with 0.5-um alumina powder (Buehler Ltd.) followed by rinsing with deionized water. Then, the electrode potential was cycled between the scan limits of 0.5 V and 1.8 V in 1.0 M $HClO_4$ until a reproducible cyclic voltammogram was obtained which represented the clean Au surface. Pure beta-PbO_2 films were electrolytically deposited on the Au RDE (900 rev min^{-1}) at 1.6 V in 1.0 M $HClO_4$ containing 1.4 mM $Pb(NO_3)_2$. A uniformly black oxide film was achieved during a 20-min deposition. The deposition conditions for Cl-PbO_2 were the same as those for pure PbO_2 except for addition of NaCl (0.14 - 1.4 mM) to the deposition solution, i.e., $[Cl^-]/[Pb^{2+}]$ = 0.1 - 1.0. The color of pure PbO_2 is black; however, the Cl-doped PbO_2 was reddish purple and the color did not vary noticeably as a function of the values of the ratio $[Cl^-]/[Pb^{2+}]$ tested.

For exhaustive electrolysis, the oxide films were deposited on large metal-screen electrodes (ca. 20 cm^2 for Au and ca. 30 cm^2 for Pt) for 20 min from 1.0 M $HClO_4$ containing 1.4 mM Pb^{2+} and 1.0 mM Cl^-, i.e., $[Cl^-]/[Pb^{2+}]$ = 0.7. The electrodes were rinsed with deionized water after preparation and used immediately, unless specified to the contrary. Concentration of analytes were 10 mM. Toluene, benzyl alcohol and benzaldehyde were oxidized at 1.7 V vs. SCE. Both Mn(II)

and DMSO were oxidized at 1.6 V vs. SCE. The total charge passed was calculated from the area under the current-time (i-t) curves with a planimeter (Keuffel & Esser Co.).

Reactions under mixed transport-kinetic control at the rotated electrodes were assumed to be consistent with the Koutecky-Levich equation below (8-11).

$$I = \frac{n_{eff}FADC^b}{d + D/k_{app}} \qquad [5]$$

In Equation 5, n_{eff} (eq mol^{-1}) is the effective number of electrons up to and including the rate determining step, k_{app} is the apparent heterogeneous rate constant (cm s^{-1}), C^b is the bulk concentration of reactant, d is the thickness of the diffusion layer, and F, A, and D have their usual electrochemical significance. For the RDE, the diffusion layer thickness is given by

$$d = 1.61D^{1/3}v^{1/6}w^{-1/2} \qquad [6]$$

where v is kinematic viscosity (cm^2 s^{-1}), and w is the angular velocity of electrode rotation (s^{-1}).

Values of n_{eff} and k_{app} were calculated from the slopes and intercepts, respectively, of plots of 1/I vs. $1/w^{1/2}$, as indicated by Equation 7.

$$\frac{1}{I} = \frac{1}{n_{eff}FAk_{app}C^b} + \frac{1}{0.62n_{eff}FAD^{2/3}\nu^{-1/6}C^b}\left(\frac{1}{w^{1/2}}\right) \quad [7]$$

All values of I were corrected for the background current measured in the absence of reactant.

Results and Discussion

Dimethyl sulfoxide (DMSO)

Figure 1 shows plots of $1/I$ vs. $1/w^{1/2}$ for the oxidation of DMSO at the pure PbO_2 and Cl-PbO_2 films on the Au RDE in 1.0 M H_2SO_4. Since k_{app} is inversely proportional to the intercept (Equation 7), the Cl-PbO_2 electrodes are readily concluded to exhibit greater electrocatalytic activity than pure PbO_2. Calculated values of n_{eff} and k_{app} are given in Table I, and the maximum increase in k_{app} as a result of Cl^- doping is ca. 80X. The average value of n_{eff} = ca. 2 eq mol^{-1} is consistent with the oxidation of DMSO to dimethyl sulphone ($DMSO_2$). The reactivity of the Cl-PbO_2 films was dramatically larger than that of the pure PbO_2, with the maximum value observed for $[Cl^-]/[Pb^{2+}]$ = 0.7.

Manganese(II)

Figure 2 shows the plots of $1/I$ vs. $1/w^{1/2}$ for the oxidation of Mn^{2+} at 1.6 V at the pure PbO_2 electrode (curve a) and Cl-PbO_2 electrode (curve b) in 1.0 M H_2SO_4. Curve b for Cl-PbO_2 is linear over the entire range of $1/w^{1/2}$ values, whereas Curve a for pure PbO_2 exhibits a distinct change in slope at intermediate values of $1/w^{1/2}$ to produce the

two linear segments $\underline{a}_1$ and $\underline{a}_2$. This is concluded to be a consequence of a change in n_{eff} with increasing w values for the poorly catalyzed reaction at the PbO_2 surface.

Consider the simple ee mechanism shown by Equation 8, where n_1 and n_2 represent the electrons transferred and k_1 and k_2 represent the heterogeneous rate constants of the respective steps in the overall reaction. The values of n_{eff} and k_{app} calculated from plots of 1/I vs. $1/w^{1/2}$ are expected to change as the rotational velocity (w) of the RDE is varied over a large range. For very small w, such that $d = D/k_2 >> D/k_1$, $n_{eff} = n_1 + n_2$ and $k_{app} = k_2$ in Equation 7. For large values of w, such that $D/k_2 >> d = D/k_1$, $n_{eff} = n_1$ and $k_{app} = k_1$. In the extreme case of very fast kinetics (i.e., $d >> D/k_1 + D/k_2$), the reaction is under purely mass-transport control with $n_{eff} = n_1 + n_2$ and the intercept of the $1/I$-$1/w^{1/2}$ plot is virtually zero.

$$A \xrightarrow{n_1,\ k_1} B \xrightarrow{n_2,\ k_2} C \qquad (k_2 > k_1) \qquad [8]$$

A brown residue was observed to form on the surface of the pure PbO_2-film electrode during operation at large w values corresponding to segment $\underline{a}_1$ (curve a) in Fig. 2. This residue is concluded to be $MnO_2(s)$, produced according to Equation 9. For a pure PbO_2-film electrode at small w values (segment a_2), the solution quickly became purple and the predominant product is concluded to be MnO_4^-, according to Equation 10. A purple product was clearly visible at the Cl-PbO_2 electrode for all w values tested (curve b), and no brown residue of

MnO_2 was observed to have accumulated even after prolonged operation at large w values. Because the slope of the $1/I\text{-}1/w^{1/2}$ plots is inversely related to n_{eff} (Equation 7), the ratio of slopes for the two linear segments in curve a (i.e., a_1/a_2) is predicted to be 2.5. The experimental value of 2.3 is considered to be in satisfactory agreement with the conclusion that segment a_1 corresponds to Equation 9, and segment a_2 and curve b correspond to Fquation 10.

$$Mn^{2+} + 2H_2O \longrightarrow MnO_2(s) + 4H^+ + 2e \quad [9]$$

$$Mn^{2+} + 4H_2O \longrightarrow MnO_4^- + 8H^+ + 5e \quad [10]$$

This conclusion is consistent with the expectation that the production of the Mn(VII), i.e., the product with the highest oxygen content, is facilitated by the electrode with the highest O-transfer activity, (i.e., the Cl-PbO_2 electrode).

Toluene, benzyl alcohol, and benzaldehyde

The observation described above for Mn(II) led to the consideration of the possible step-wise oxidation of toluene to benzoic acid, as suggested by Equation 11.

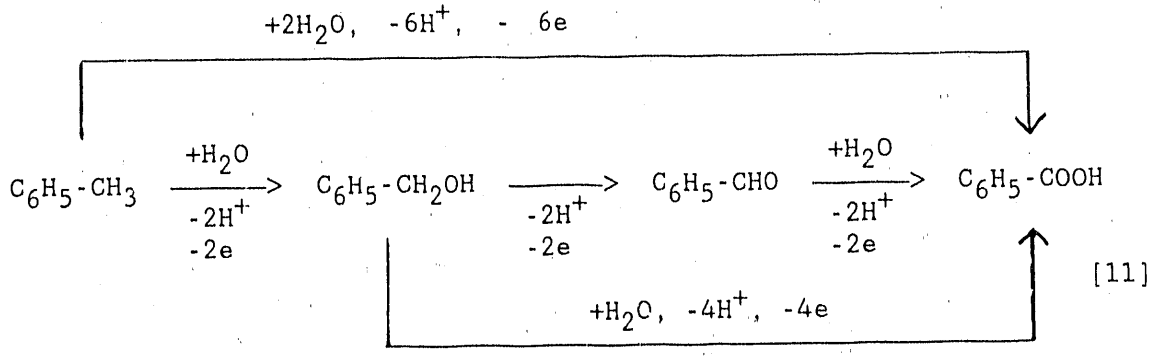

[11]

Other possible products of toluene oxidation can include benzoquinone and carbon dioxide (n = 12 eq mol^{-1}), as indicated by Equation 12, or, perhaps, complete oxidation to carbon dioxide (n = 36 eq mol^{-1}), as indicated by Equation 13.

$$C_6H_5CH_3 + 4H_2O \longrightarrow C_6H_4O_2 + CO_2 + 12H^+ + 12e \qquad [12]$$

$$C_6H_5CH_3 + 14H_2O \longrightarrow 7CO_2 + 36H^+ + 36e \qquad [13]$$

Plots of 1/I vs. $1/w^{1/2}$ are shown in Figs. 3A-C for the oxidations of toluene, benzyl alcohol and benzaldehyde, respectively, at the PbO_2 electrode (curve a) and Cl-PbO_2 electrode (curves b). Toluene (Fig. 3A) and benzyl alcohol (Fig. 3B) are moderately reactive at the pure PbO_2-film electrode at 1.7 V in 1 M H_2SO_4, whereas virtually no anodic activity was observed for benzaldehyde for the PbO_2 electrode. From a brief inspection of the intercepts of these plots, it is quite apparent that the relative values of k_{app} decrease in the order: toluene > benzyl alcohol >> benzaldehyde. For the Cl-PbO_2 film electrode, the

oxidation rates were increased for all compounds and anodic reactivity was observed for benzaldehyde. However, the order of reactivities remained the same as observed for the pure PbO_2 electrode. A summary of k_{app} values is given in Table II.

Based on examination of the slopes of linear portions of the $1/I$ *vs.* $1/w^{1/2}$ plots in Figs. 3A-C for low values of w, the values of n_{eff} for oxidation of toluene and benzyl alcohol were determined to have been increased by a factor of 2.3 and 2.7, respectively, by the Cl^- doping. A tentative conclusion is that the oxidations of toluene and benzyl alcohol at the rotated PbO_2-film electrode terminate with benzaldehyde as a primary product for the w values represented here. However, benzaldehyde is not the final product of oxidation at the Cl-PbO_2 electrode under the conditions of controlled-potential, exhaustive electrolysis as indicated by values n_{tot} equal to ca. 10 eq mol^{-1} for benzyl alcohol and ca. 20 eq mol^{-1} for benzaldehyde (see Table 2). Because n_{tot} was larger for benzaldehyde than for benzyl alcohol, it is concluded tentatively that a mixture of oxidation products was obtained, with the distribution depending on the starting material. It should be noted that there was no anodic activity observed for benzoic acid. More satisfactory explanation of these data must await the results of a complete study of the product distribution.

Data shown in Figs. 3A-C for high values of w (i.e., low $1/w^{1/2}$) deviate in a negative fashion from the linearized estimates shown. This is concluded, by analogy to the interpretation of data in Fig. 2, to be evidence for ee mechanisms in the various anodic reactions. Reliable

linear estimates of the data for high w could not be obtained and, as a result, no attempt was made to estimate values of n_{eff} in these regions of the plots.

Oxygen evolution overpotential and electrocatalysis

A working premise in this research is that anodic O-transfer catalysis is coupled to the mechanism for O_2 evolution, as described by Equations 1-4. Accordingly, the rates of the O-transfer and O_2-evolution reactions are both controlled by the surface coverage of adsorbed hydroxyl radicals (12). Hence, it is expected that any alteration to the oxide films which causes an increased activity for anodic O-transfer reactions will result in a decreased overpotential for the O_2-evolution reaction (η_{oer}). The challenge, then, is to optimize the desired O-transfer reactivity without undue increase to the simultaneous background signal for O_2 evolution.

Figure 4 shows so-called "Tafel plots" for the O_2-evolution process in 1.0 M $HClO_4$. The plots are interpreted on the basis of Equation 14, where η is the overpotential, k_2 is the Tafel slope, and k_1 is the value of log(I) at $\eta = 0$, for which I is the exchange current (I_o) (13).

$$\log(I) = k_1 + k_2 \cdot \eta \qquad [14]$$

Curve a (Fig. 4) corresponds to a pure PbO_2 film and Curve b to a Cl-PbO_2 film, both electrodeposited on the Au RDE. The data were taken from voltammetric curves recorded during the positive scan (10 mV s^{-1}) starting at 1.4 V and terminating at 1.8 V. The values obtained for the

Tafel slope (k_2) are 102 mV/decade for PbO_2 and 114 mV/decade for Cl-PbO_2. These are concluded to be in satisfactory agreement with the value of 120 mV/decade reported typically for O_2 evolution in acidic media. It is concluded that the mechanism of O_2 evolution is the same for the two electrodes (14). The values obtained for exchange current (I_o) were $10^{-6.17}$ for PbO_2 and $10^{-4.76}$ for Cl-PbO_2. The increase in I_o for O_2 evolution at the Cl-PbO_2 electrode, in comparison to PbO_2, is consistent with the observed increase in O-transfer catalysis on the basis of the mechanism in Equations 1-4.

Scanning electron microscopy

Attention must be given to the possibility that the observed increases in O_2 evolution and O-transfer reactivity were the result of an increase in the surface roughness as a result of Cl^- doping, i.e., an increase in the total surface area. This seems unlikely in this case because an increase in area of ca. 25 would be required to account for the increase in I_o for O_2 evolution. Further evidence was obtained by examination of the film electrodes with Scanning Electron Microscopy (SEM); the micrographs are shown in Fig. 5-a for PbO_2 and Fig. 5-b for Cl-PbO_2 on Au substrates. The surface morphology for doped and undoped PbO_2 films is quite different with the smallest grain size observed for the Cl-PbO_2. However, it appears from the micrographs that the surface roughness factor may be slightly greater for the PbO_2 film than for the Cl-PbO_2 film.

The rate of electrodeposition of the oxide films from Pb^{2+}

solutions was observed to be changed by the addition of Cl^-. This is clearly evident by a substantial difference in the peak current at 1.25 V for the cathodic stripping of the oxide deposited during consecutive potential cycles within the limits 0.5 V and 1.8 V. Values of peak current are shown as a function of scan number in Fig. 6 for a Au RDE in 1 M $HClO_4$ solutions of 0.7 mM Pb^{2+} with no Cl^- (Curve a) and 0.7 mM Pb^{2+} plus 28.5 uM Cl^- (Curve b). The peak shapes were virtually identical and, therefore, the peak height is reliable for an approximate comparison of the quantity of oxide stripped (and deposited) during each potential cycle. The increase with cycle number of the quantity of PbO_2 deposited at a Au RDE in 1.0 M $HClO_4$ has been discussed by Chang and Johnson (15). They determined that an ultra-thin film of lead oxide (PbO) remains following cathodic stripping of bulk PbO_2. This film serves for nucleation in the next cycle of deposition.

It is apparent in Fig. 6a that the quantity of PbO_2 stripped becomes constant after approximately the 10th cycle. Clearly from Fig. 6b, the presence of Cl^- is determined to inhibit the nucleation and growth of the oxide film and a constant quantity of deposited Cl-PbO_2 was not produced until approximately after the 20th cycle. We conclude tentatively that the alteration in the nucleation kinetics is a consequence of adsorption on the Au surface and is at least partially responsible for the observed differences in the surface morphology of the PbO_2 and Cl-PbO_2 surfaces (see Fig. 5). An additional factor may be that some of the Cl^- reaching the electrode is oxidized to Cl_2 or, perhaps, a higher oxidation state of chlorine, e.g., ClO_3^-.

Nevertheless, when a very thick deposit of Cl-PbO_2 was dissolved in 30% H_2O_2, the addition of $AgNO_3$ produced a positive test for Cl^-.

Values of k_{app} were determined not to vary significantly with changes in the thickness of the oxide films. However, k_{app} was found to be a function of the substrate material. Values of k_{app} for oxidation of DMSO are given in Table III for PbO_2 and Cl-PbO_2 on Au and Pt substrates. The largest k_{app} was obtained for Cl-PbO_2 on Au. It is considered probable that the lack of agreement between the k_{app} values is a consequence of differences in the true surface area which are a result of differences in nucleation and growth rates at the two metal substrates.

Stability of electrode activity

It is common to expect that electrocatalytic properties of altered surfaces will deteriorate in use because of degradation of the surface through fouling or dissolution of reactive surface species. However, surprisingly, the reactivity of Cl-PbO_2 films increased with time if stored in 1.0 M $HClO_4$. Exhaustive electrolysis of DMSO in 1.0 M H_2SO_4 was performed for a Cl-PbO_2 film on the Pt-screen electrode at 1.6 V. Reactivity was estimated on the basis of the slope of plots of $-\ln(I_t/I_o)$ vs. t, made according to Equation [15] where t is time, I_t is the time dependent current, and I_o is the initial current in the electrolysis (16).

$$-\ln(I_t/I_o) = \lambda t \qquad [15]$$

The larger the value of λ, the faster is the oxidation reaction.

Normalized values of the reactivity shown in Fig. 7 correspond to successive values of λ divided by the value determined for the first electrolysis in the series. The electrode was maintained under open-circuit conditions in 1.0 M $HClO_4$ between each electrolysis period. As shown in Fig. 7, the electrocatalytic activity increased over the first 90-hr period and then gradually decreased. However, it is noteworthy that even after 460 hrs, the activity continued to be greater than that for the freshly prepared electrode. It is speculated that the crystal structure of the Cl-PbO_2 film is slowly changed to a more active form during the first 90-hr period, and, thereafter, gradual dissolution of Cl^- occurs from the oxide surface.

X-ray powder diffraction

The X-ray diffraction powder pattern is shown in Fig. 8A for Cl-PbO_2 which was deposited on a Au wire electrode, removed, and ground with a mortar and pestle before obtaining the diffraction pattern. The diffraction pattern is consistent with the ß-form of pure PbO_2 which has a slightly distorted rutile structure (17) and the peak identification shown in Fig. 8A is based on that assignment. It was concluded above that Cl^- ions are incorporated within the PbO_2 matrix. It is expected that these Cl^- ions can provide partial charge compensation for Pb^{4+} cations with a resulting decrease in local lattice stability by disruption of bridging oxygen bonds (i.e., -Pb-O-Pb-).

The powder pattern diffractometer was applied to PbO_2 and Cl-PbO_2 films on Au substrates and the results are shown in Fig. 8B. The peaks

for Cl-PbO_2 are significantly broader than for PbO_2, which indicates a smaller crystallite size for the Cl-PbO_2. However, the initial visual comparison of the micrographs in Fig. 5 leads to the opposite conclusion, i.e., the particle size of Cl-PbO_2 appears to be larger than for PbO_2. These apparently contradictory conclusions are reconciled if the most readily seen particles (0.5-1 um dia.) in the Cl-PbO_2 micrograph are actually aggregates of smaller crystallites. Very close visual examination of the micrograph reveals the absence of smooth surfaces on these particles which would be expected if they were single crystals. There is a definite increase in intensities of the peaks corresponding to the (101) and (121) crystalline planes, relative to that of (020) planes, for the Cl-PbO_2 film in comparison to the PbO_2 film. This is evidence for a change in preferred orientation as a result of the presence of Cl^-.

The diffraction pattern of a Cl-PbO_2 film kept at open-circuit potential for 4 hrs in 1.0 M $HClO_4$ is shown in Fig. 8C. New peaks are seen for low diffraction angles and an enhancement in the intensity corresponding to (101) plane is apparent. Since the electrocatalytic reactivity of the Cl-PbO_2 films is increased by storage in 1.0 M $HClO_4$, it is concluded that the enhanced intensity for (101) plane, as compared to the (020) and (121) planes, is correlated with the improved catalytic properties. A comparison of relative diffraction peak intensities is summarizied in Table IV.

Conclusion

It is concluded that any chemical or physical process applied to the surface of PbO_2 electrodes which results in an increase in the density of surface defects will cause a decrease in the O_2-evolution overpotential and a corresponding increase in the rates of surface-catalyzed anodic O-transfer reactions. For the case of Cl-PbO_2, the Cl^- ions incorporated within the oxide are tentatively concluded to disrupt the lattice structure by providing partial charge compensation for Pb^{4+} cations. This incorporation of Cl^- results in disruption of the bonding order of Pb^{4+} and, probably, some decrease in oxygen content of the doped oxide. Hence, at the surface of Cl-PbO_2 electrodes, there is a corresponding increase in the density of partially filled orbitals from the Pb^{4+} centers which are available for adsorption of hydroxyl radicals and which has the effect of increasing the surface activity of M[OH] (see Equations 1-2).

References

1. Southampton Electrochemistry Group, "Instrumental Methods in Electrochemistry"; Southampton Electrochemistry Group; Ellis Horwood Limited: Chichester, England, 1985, p. 231.
2. Weinberg, N. L.; H. R. Weinberg, H. R. Chem. Rev. 1968, 68, 449.
3. "Encyclopedia of Electrochemistry of the Elements"; Bard, A. J.; vol. 1, Marcel Dekker Inc.: New York, 1973, chap. I-5.
4. Carr, J. P; N. A. Hampson, N.A. Chem. Rev. 1972, 72, 679.
5. Yeo, I-H; Johnson, D. C. J. Electrochem. Soc. 1987, 134, 1973.

6. Yeo, I-H; Kim, S.; Jacobson, R.; Johnson, D. C. J. Electrochem. Soc. in press.

7. Feng, J.; Johnson, D. C. unpublished results, Chemistry Dept., Iowa State University, Ames, Iowa, 1987.

8. Levich, V. G. "Physicochemical Hydrodynamics"; Prentice Hall: Englewood Cliffs, NJ, 1962, p. 75.

9. Koutecky, J; Levich, V. G. Zh. Fiz. Khim. 1956, 32, 1565.

10. Oyama, N.; Anson, F. C. Anal. Chem. 1980, 52, 1192.

11. Beck, F.; Schulz, H. J. Electroanal. Chem. 1987, 229, 339.

12. Yeo, I-H. Ph.D. Dissertation, Iowa State University, Ames, Iowa, 1987.

13. Tafel, J. Z. Phys. Chem. 1905, 50, 641.

14. "Kinetics of Electrochemical Metal Dissolution"; Kiss, L.; Elsevier Science Publishing Co., Inc.: New York, NY, 1988, p. 60.

15. Chang, H; Johnson, D. C. J. Electrochem. Soc. 1989, 136, 17.

16. Lingane, J. J. J. Amer. Chem. Soc. 1945, 67, 1916.

17. Harada, H. J. Appl. Crystallogr. 1981, 14, 141.

Table 1. Kinetic data for oxidation of DMSO as a function of $[Cl^-]/[Pb^{2+}]$ in the electrodeposition solution

$[Cl^-]/[Pb^{2+}]$	$10^2 \cdot k_{app}$ (cm s^{-1})[a]
0.0	0.05 ± 0.02
0.1	1.8 ± 0.3
0.2	2.5 ± 0.4
0.3	1.6 ± 0.3
0.5	2.8 ± 0.1
0.7	3.9 ± 0.2
0.9	1.5 ± 0.2

[a]Assumed: $n_{eff} = 2.0$ eq mol^{-1}.

Table II. Kinetic data for oxidation of Mn^{2+}, DMSO, toluene, benzyl alcohol and benzaldehyde in 1 M H_2SO_4

Reactant (5.0 mM)	$E_{applied}$ (V vs. SCE)	n_{tot}[a] (eq mol^{-1})	$10^2 n_{eff} \cdot k_{app}$ (eq mol^{-1} cm s^{-1})	
		@ Cl-PbO_2	@ PbO_2	@ Cl-PbO_2[b]
Mn^{2+}	1.60	5.08 ± 0.01	1.82 ± 0.06	50.0 ± 2.5
DMSO	1.60	2.07 ± 0.01	0.108 ± 0.08	7.79 ± 0.04
Toluene	1.70	3.10 ± 0.2	0.321 ± 0.022	5.05 ± 0.10
Benzyl alcohol	1.70	9.66 ± 0.28	0.136 ± 0.052	1.98 ± 0.03
Benzaldehyde	1.70	20.2	NR[c]	0.70 ± 0.02

[a]Values of n_{tot} were obtained by exhaustive electrolysis at a Cl-PbO_2 electrode.

[b]Deposition condition: $[Cl^-]/[Pb^{2+}] = 0.7$.

[c]No reaction.

Table III. Heterogeneous rate constants of oxidation of DMSO at various electrodes at 1.6 V in 1 M H_2SO_4

$$DMSO + H_2O \xrightarrow{k_{app}} DMSO_2 + 2H^+ + 2e$$

Film	Substrate	$10^3 \cdot k_{app}$[a] (cm s^{-1})
none	Au	0,02 ± 0,01
none	Pt	0,4 ± 0,01
PbO_2	Pt	0,1 ± 0,3
PbO_2	Au	0,5 ± 0,2
Cl-PbO_2	Pt	10 ± 1,6
Cl-PbO_2	Au	40 ± 3,4

[a]Assumed: n_{eff} = 2 eq mol^{-1}.

Table IV. Integrated intensity of X-ray diffraction peaks of designated crystal planes for the various oxide films

Film	I_{101}[a]	I_{121}	I_{020}
Pure PbO_2	432	946	1203
Cl-PbO_2[b]	2020	2211	339
Cl-PbO_2[c]	3918	2210	109

[a]Integrated peak intensity for specified orientation.

[b]Freshly prepared oxide film.

[c]Oxide film after storage for 4 hrs in 1 M $HClO_4$.

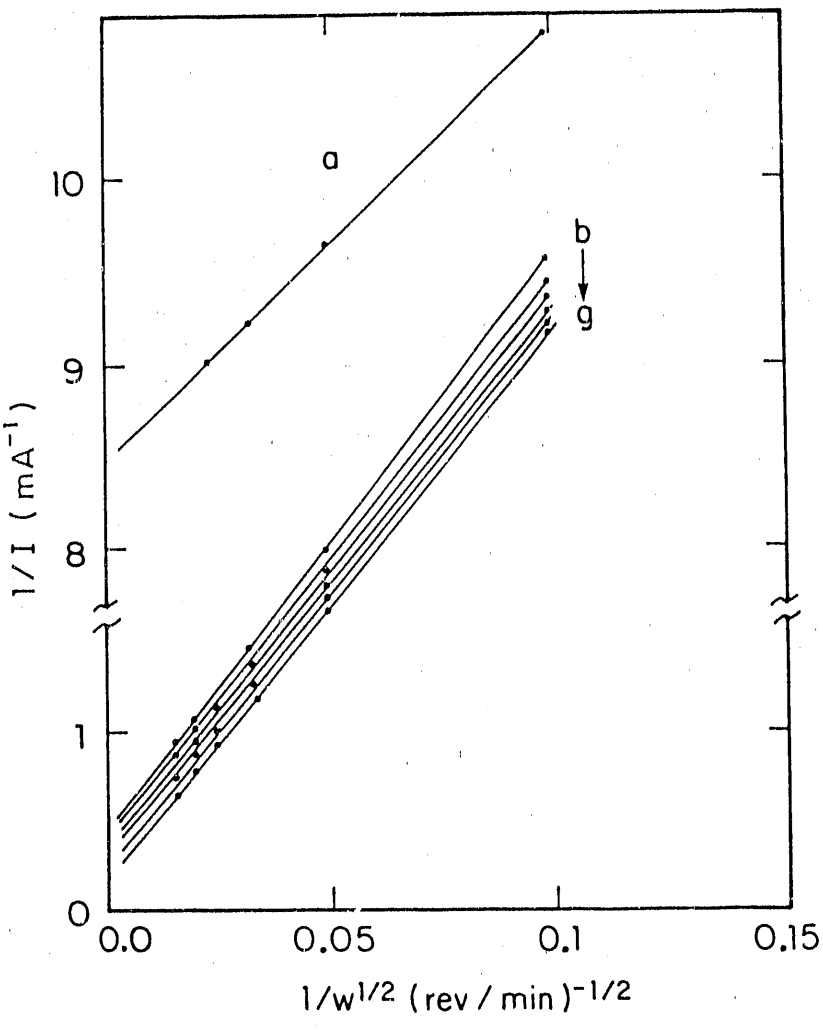

Figure 1. Plots of 1/I vs. $1/w^{1/2}$ for the oxidation of 5.0 mM DMSO at 1.6 V for a PbO_2 electrode (a) and Cl-PbO_2 electrodes (b-g) in 1.0 M H_2SO_4

$[Cl^-]/[Pb^{2+}]$: (a) 0.0, (b) 0.9, (c) 0.3, (d) 0.1, (e) 0.2, (f) 0.5, and (g) 0.7.

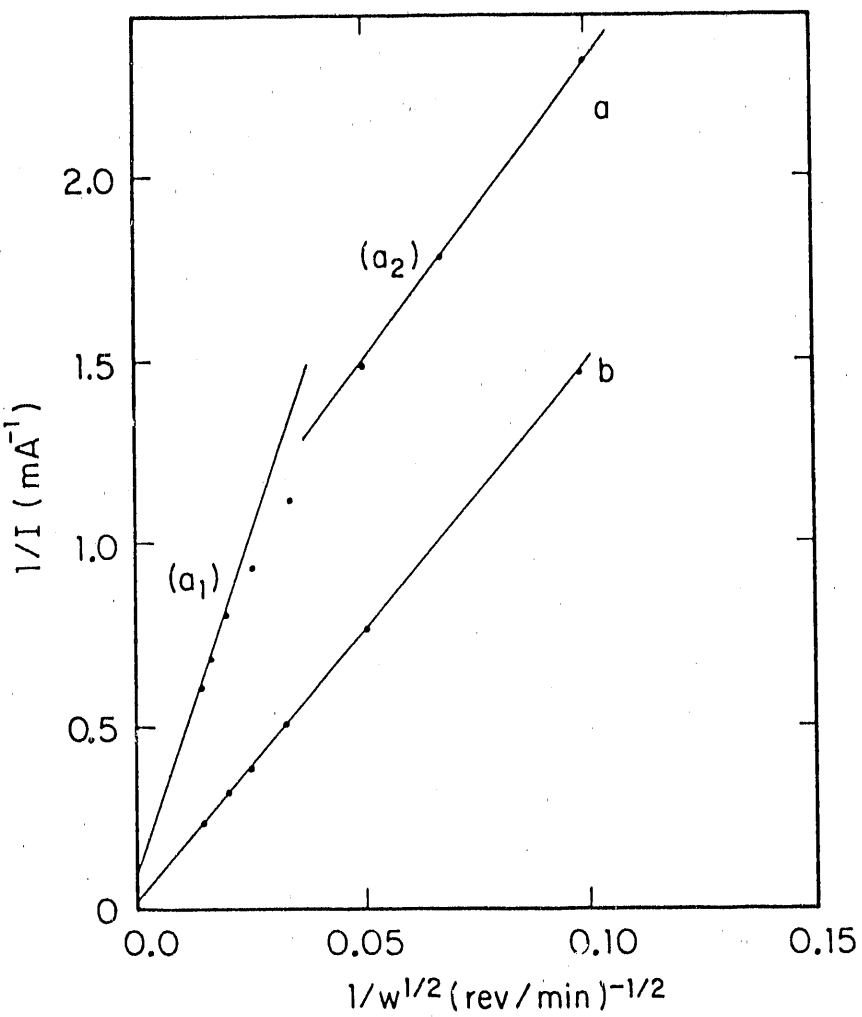

Figure 2. Plots of 1/I vs. $1/w^{1/2}$ for the oxidation of 5.0 mM Mn^{2+}

Conditions: E = 1.6 V, 1 M H_2SO_4

Electrodes: (a) pure PbO_2 film on Au,
(b) Cl-PbO_2 film on Au ($[Cl^-]/[Pb^{2+}]$ = 0.7)

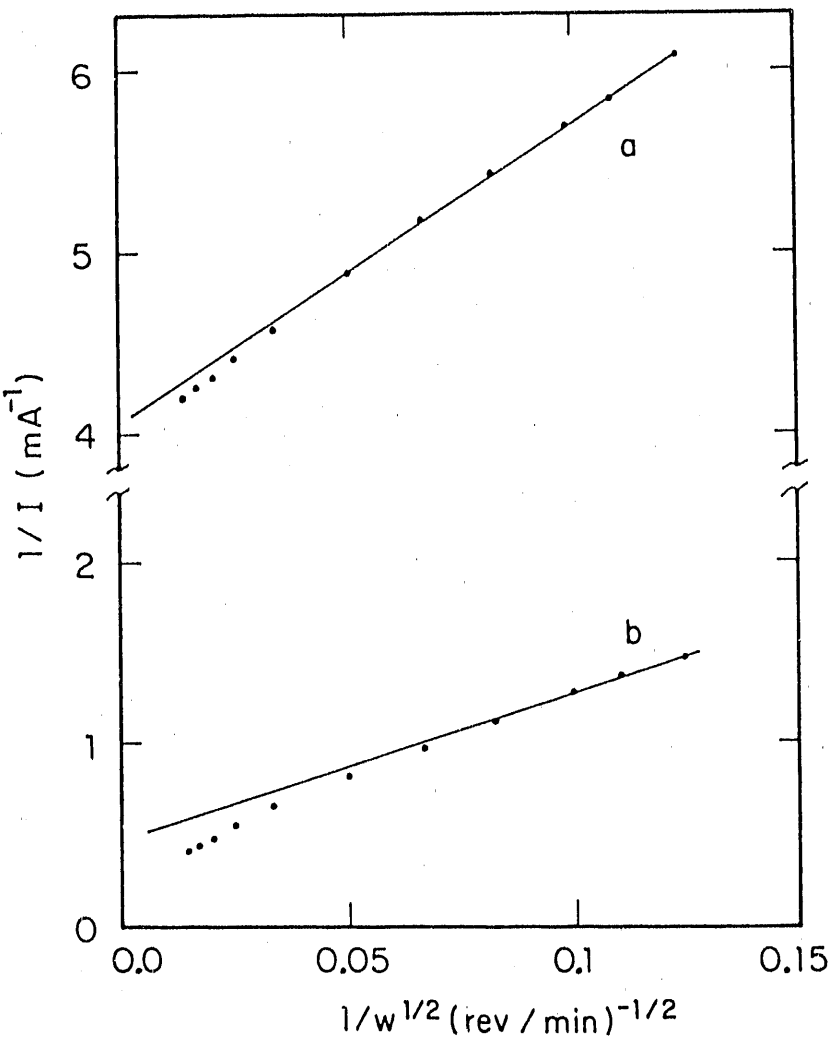

Figure 3A. Plot of 1/I vs. $1/w^{1/2}$ for the oxidation of 5.0 mM toluene

Conditions: E = 1.7 V, 1 M H_2SO_4

Electrodes: (a) pure PbO_2 film on Au
(b) Cl-PbO_2 film on Au ($[Cl^-]/[Pb^{2+}]$ = 0.7)

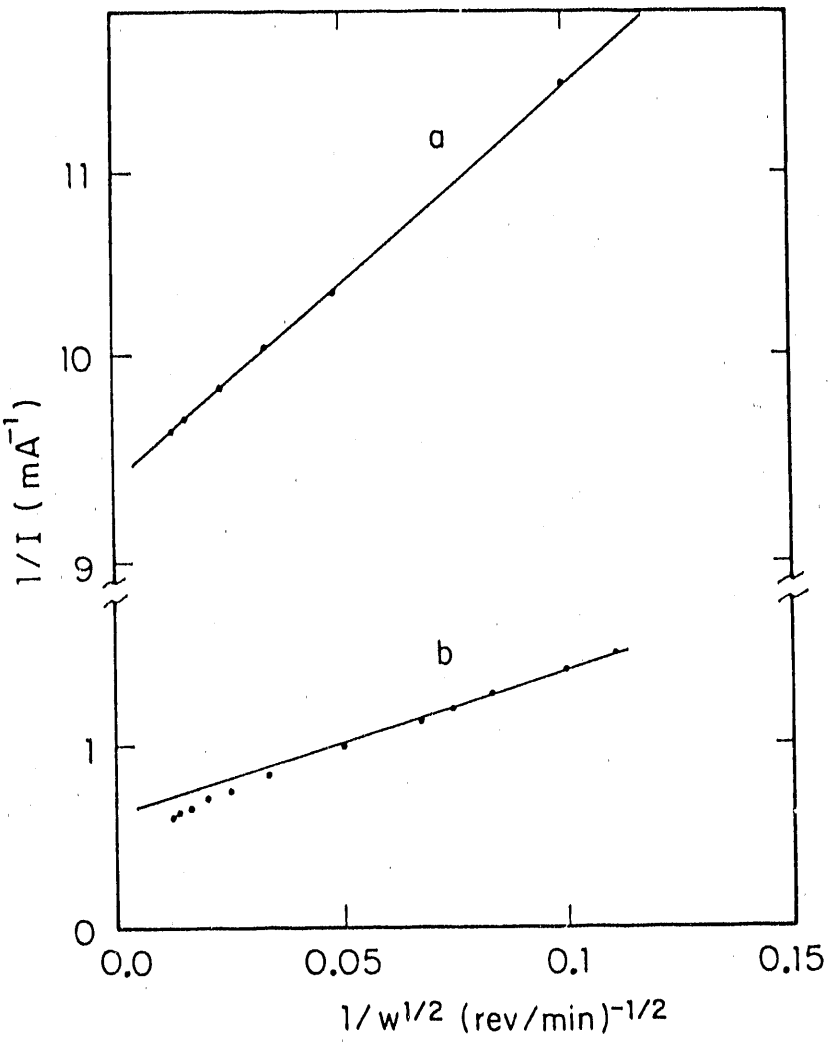

Figure 3B. Plot of 1/I *vs.* $1/w^{1/2}$ for the oxidation of 5 mM benzyl alcohol

Conditions: E = 1.7 V, 1 M H_2SO_4

Electrodes: (a) pure PbO_2 film on Au
(b) Cl-PbO_2 film on Au ($[Cl^-]/[Pb^{2+}]$ = 0.7)

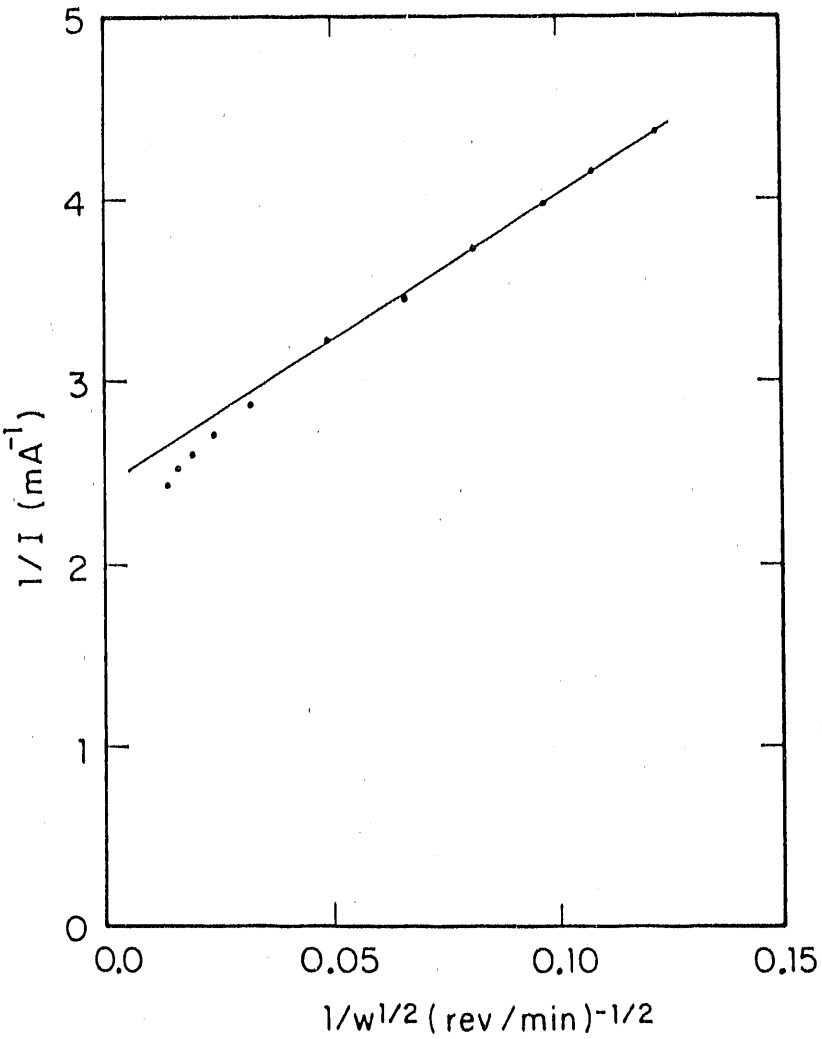

Figure 3C. Plot of 1/I *vs.* $1/w^{1/2}$ for the oxidation of 5 mM benzaldehyde

Conditions: E = 1.7 V, 1 M H_2SO_4

Electrode: Cl-PbO_2 film on Au ($[Cl^-]/[Pb^{2+}]$ = 0.7)

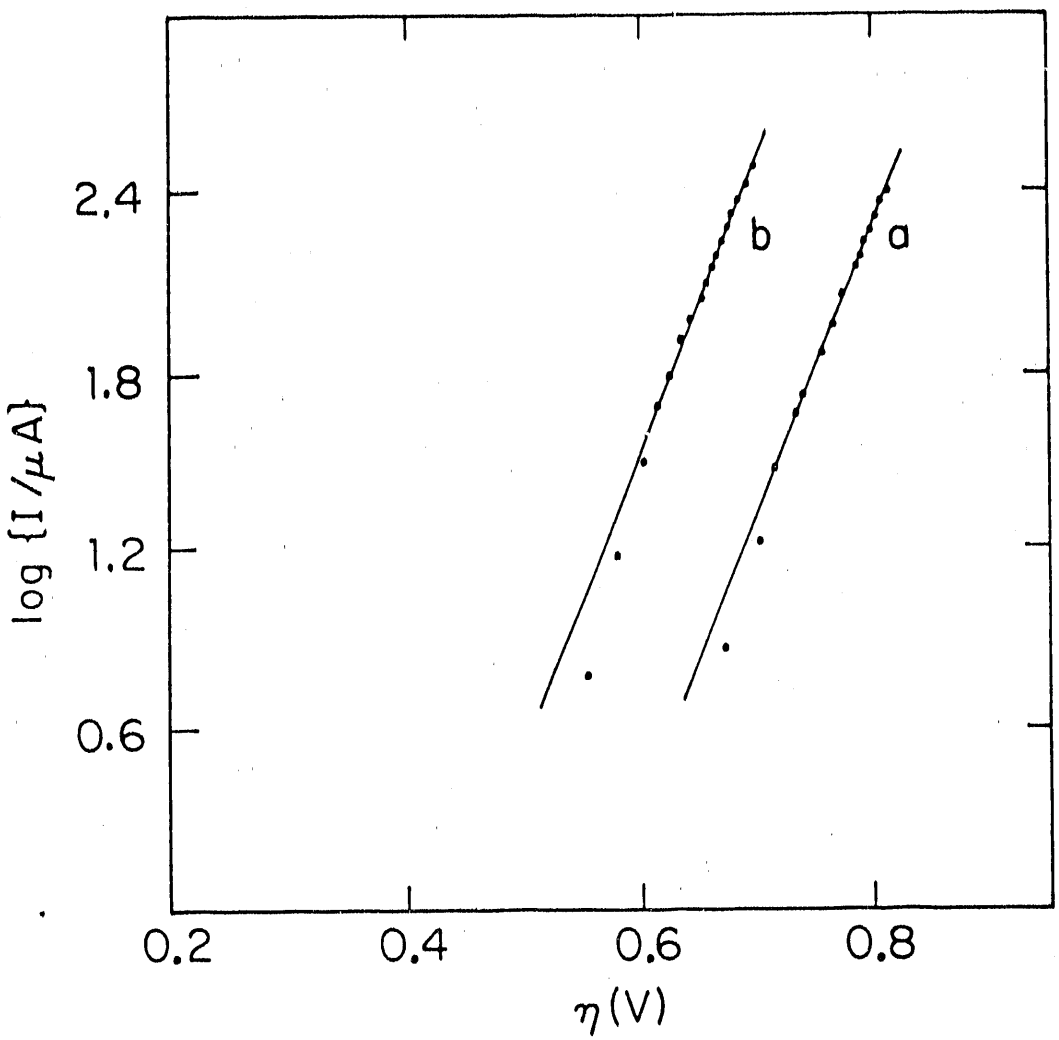

Figure 4. Plot of log(I) vs. η for O_2 evolution in 1 M $HClO_4$

Conditions: +10 mV s^{-1}, 1600 rev min^{-1}

Electrodes: (a) pure PbO_2 film on Au
(b) Cl-PbO_2 film on Au ($[Cl^-]/[Pb^{2+}]$ = 0.7)

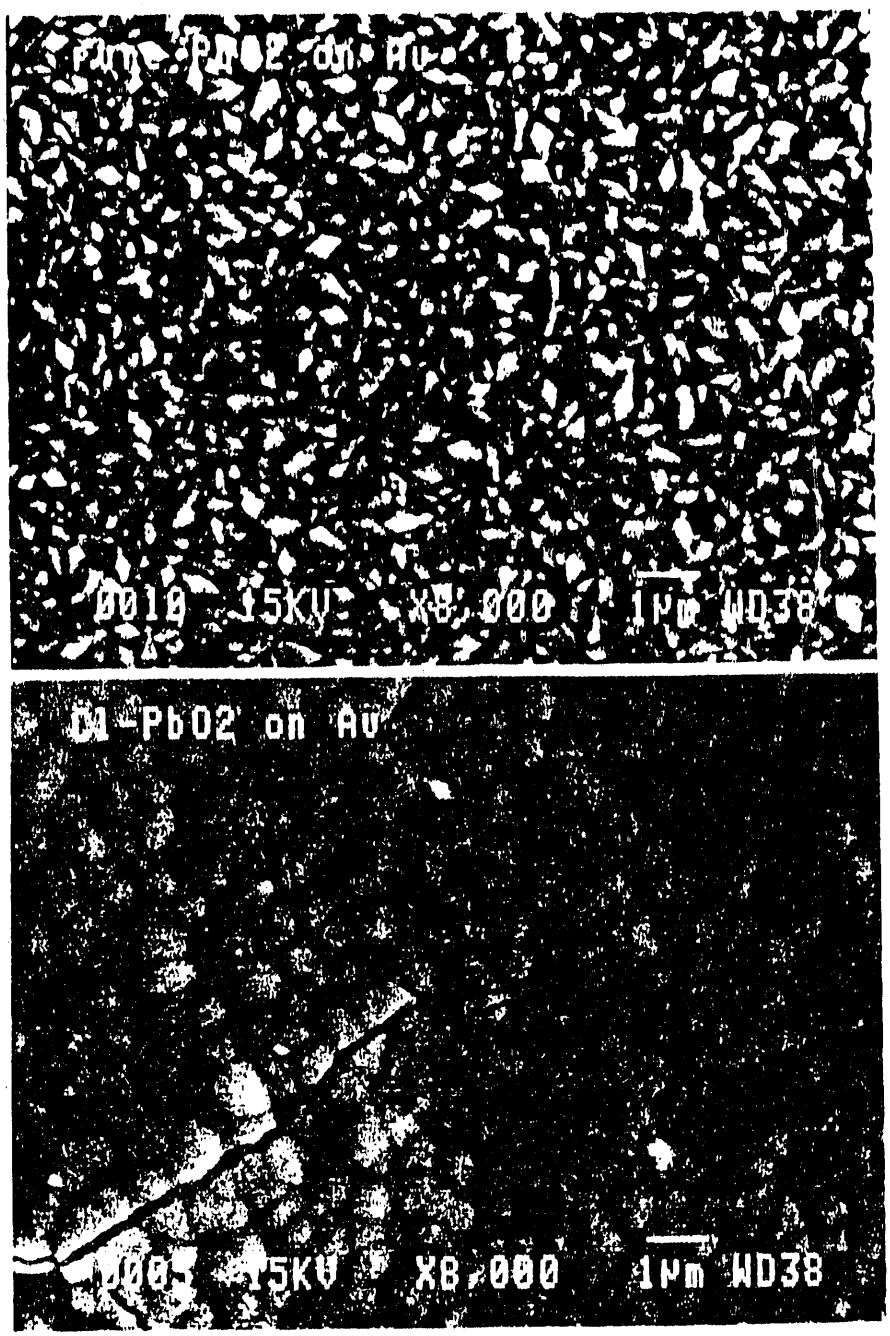

Figure 5. Scanning Electron Micrographs (X 8000) of a PbO_2 film (a) and a Cl-PbO_2 film (b) on a Au substrate

Conditions of deposition: E = 1.8 V, $[Pb^{2+}]$ = 0.7 mM

Films: (a) pure PbO_2 film on Au
(b) Cl-PbO_2 film on Au ($[Cl^-]/[Pb^{2+}]$ = 0.3)

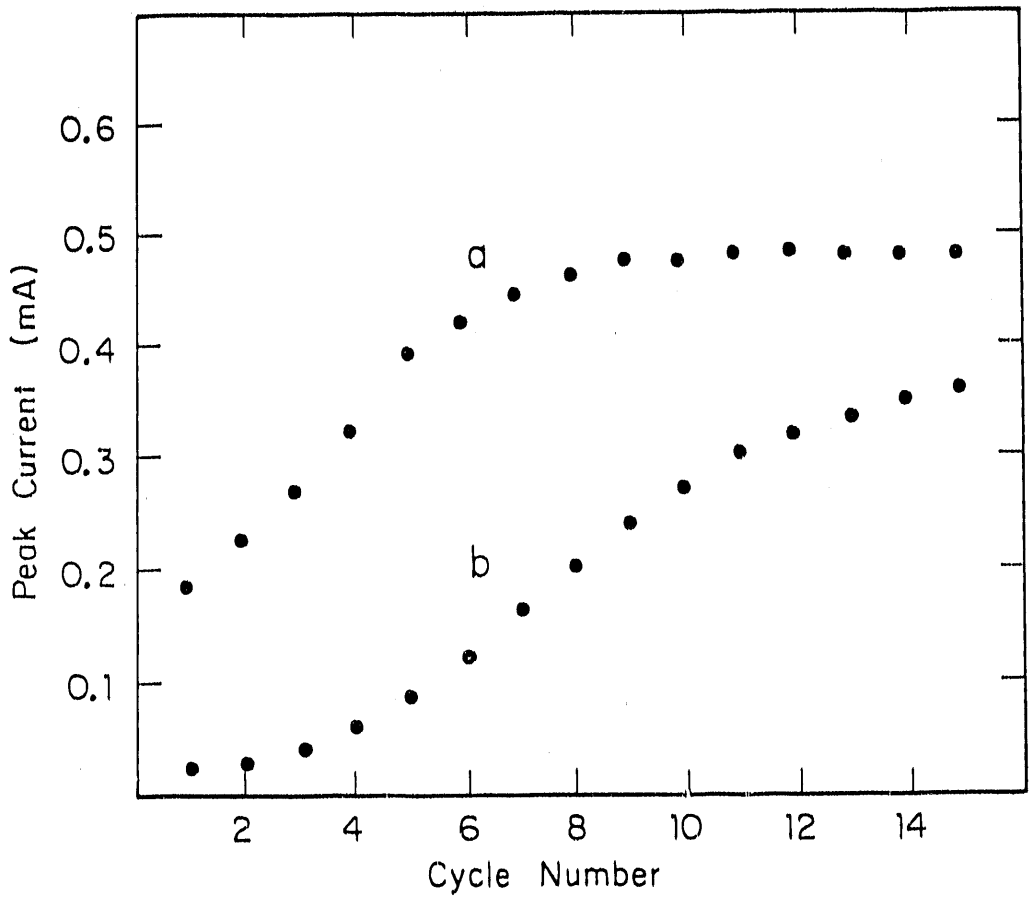

Figure 6. Plot of reduction peak currents vs. sequence of cycles at the Au RDE

Conditions: (a) 0.7 mM Pb^{2+},
(b) same as (a) with 28.5 uM NaCl
(i.e. $[Cl^-]/[Pb^{2+}] = 0.04$)

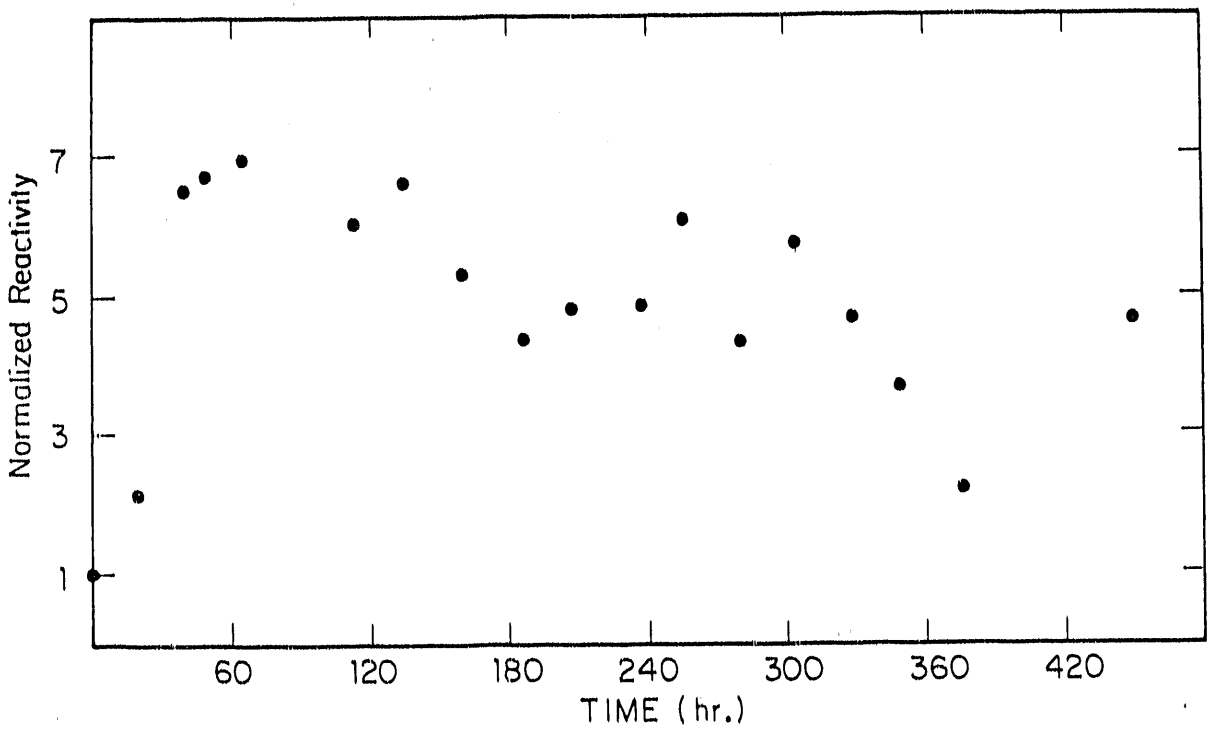

Figure 7. Normalized reactivity vs. time for Cl-PbO_2 film on a Pt-gauze electrode for oxidation of 5 mM DMSO

Conditions for Cl-PbO_2 deposition: $[Cl^-]/[Pb^{2+}] = 0.1$

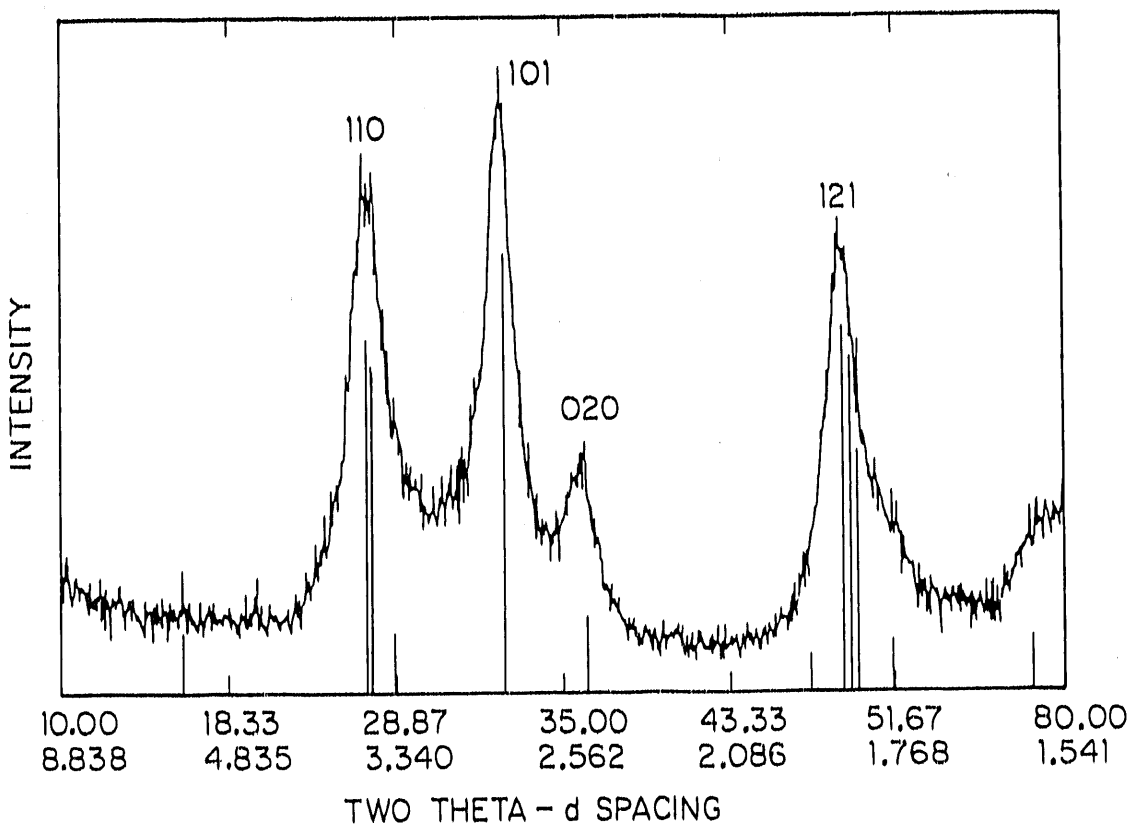

Figure 8A. X-ray diffraction powder patterns of Cl-PbO_2 removed and powdered after electrodeposition on a Au-wire substrate

Conditions for Cl-PbO_2 deposition: $[Cl^-]/[Pb^{2+}]$ = 0.3, E = 1.8 V

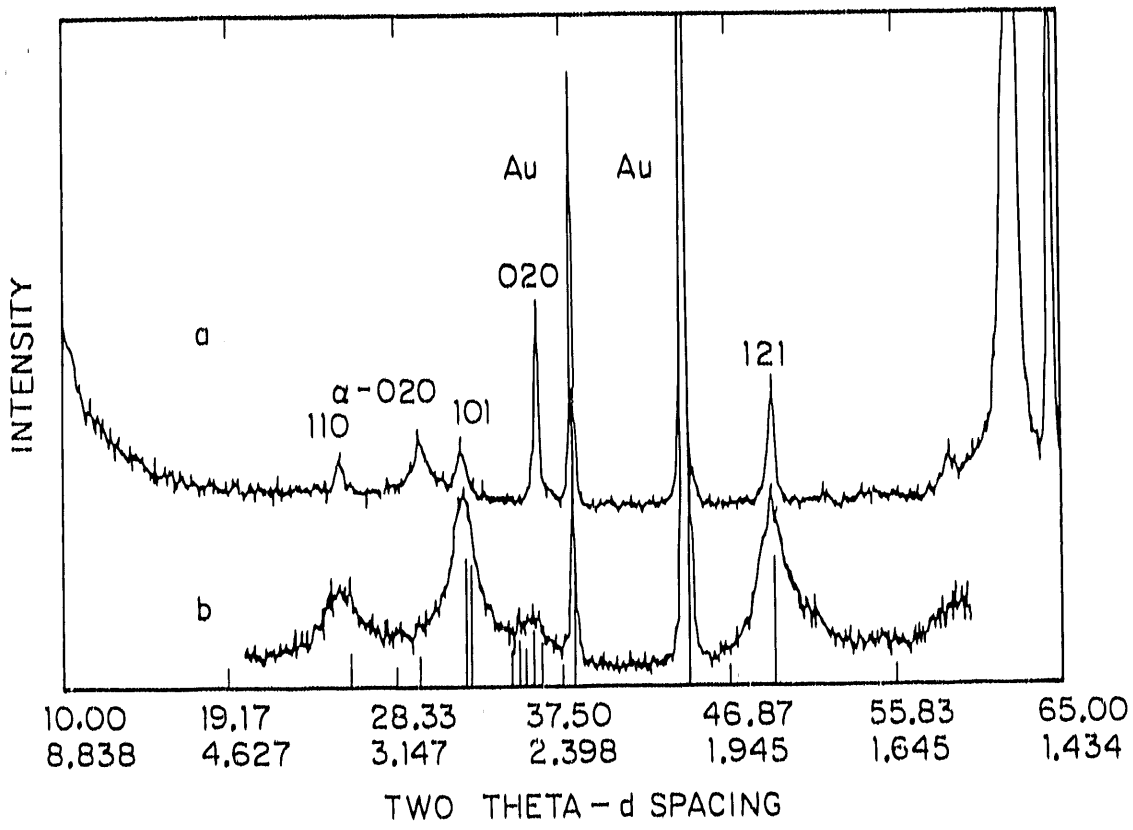

Figure 8B. X-ray diffraction patterns for a PbO_2 film (a) and a Cl-PbO_2 film (b) electrodeposited on the Au substrate

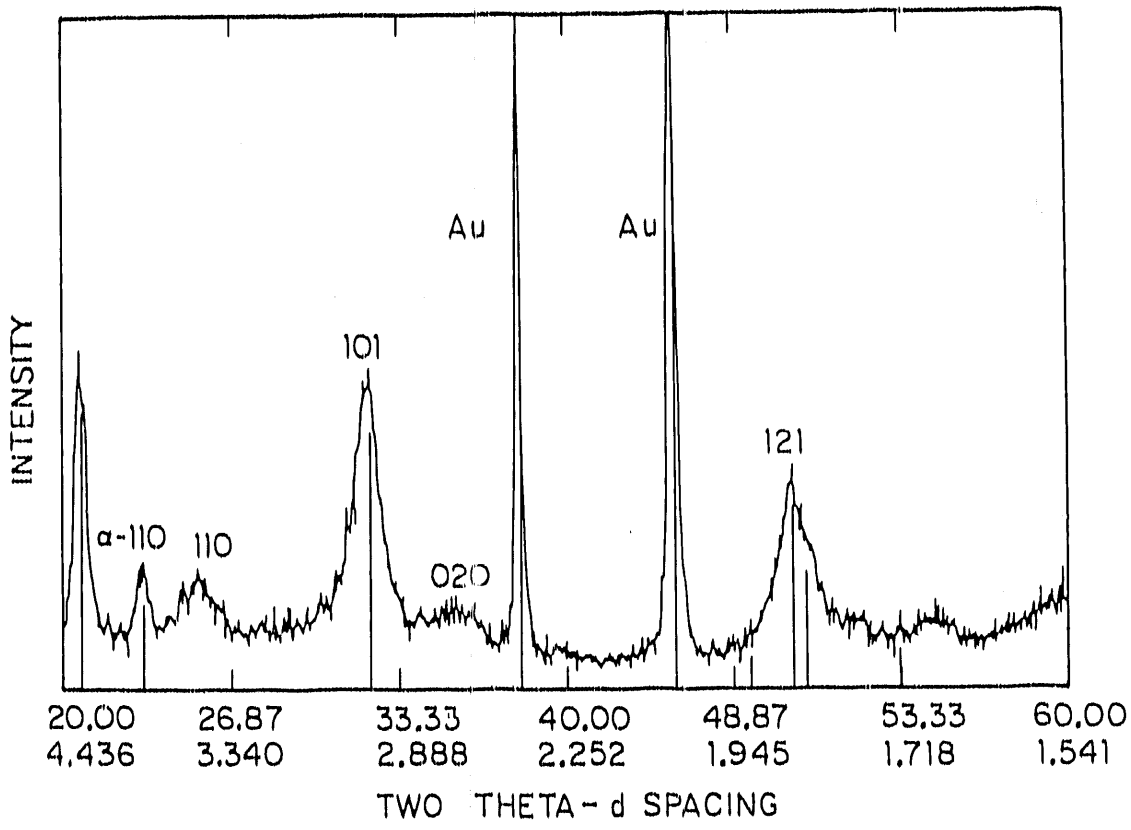

Figure 8C. X-ray diffraction pattern for a Cl-PbO_2 film on Au after storage for 4 hrs in 1.0 M $HClO_4$

CHAPTER III.

ELECTROCATALYSIS AT CHLORIDE-DOPED LEAD DIOXIDE FILMS IN SULFURIC ACID MEDIA[1]

Abstract

Reaction rates for the oxidations of DMSO and Mn^{2+} at the Cl-doped PbO_2 film-electrode (Cl-PbO_2) were determined to be significantly increased in 1 M H_2SO_4 as compared with that in 1 M $HClO_4$. The pure PbO_2 electrode which shows poor anodic reactivity for DMSO was gradually activated by exposure to 1 M $HClO_4$ containing 50 uM HSO_4^- or Cl^-. Examinations of mass change at the electrode surface during voltammetric scan were performed using an Electrochemical Quartz Crystal Microbalance (EQCM). Results revealed no mass change at the electrode surface during the oxidation of DMSO in 1 M $HClO_4$. However, a mass increase of ca. 210 ± 10 ng at the electrode surface (0.38 cm^2) was obtained when H_2SO_4 was added to the solution. This result indicated the possibility of adsorption of HSO_4^- at the surface of the Cl-PbO_2 electrode. The adsorption was speculated to occur via an anion-exchange mechanism which involved irreversible substitution of the solution anion (HSO_4^-)

---

[1] J. Electrochem. Soc. to be submitted.

for the surface anion (Cl^-). The adsorbed monohydrogen sulfate (HSO_4^-) was concluded to activate the neighboring Pb^{4+} sites which functioned as catalytic centers for the oxidation of DMSO and Mn^{2+}.

Introduction

Effort in the development of catalytic PbO_2-film electrodes for numerous anodic oxygen-transfer reactions has been the research interest in this group for recent years. Successful electrocatalysis has been applied for the oxidations of Mn^{2+} and phenol at Bi^{5+}-doped PbO_2 films (Bi-PbO_2) in acidic solution (1), and the oxidations of Mn^{2+} and DMSO (2) at the Bi^{5+}-adsorbed PbO_2 electrode in perchloric acid media. Catalytic results have also been obtained at Cu-doped (3) and Fe-doped (4) PbO_2-film anodes for the oxidation of CN^- in alkaline solution.

It has been reported that PbO_2 does not exist in a stoichiometric form (5a). The generally accepted composition lies within the limits indicated by the formula $PbO_{1.80\text{-}1.98}OH_{0.11\text{-}0.26}$ (5a). Nonstoichiometry is observed regardless of the method of preparation (5b-5d). Bagshaw and co-workers (5c) proposed an explanation for the deposition kinetics for PbO_2 based on both pH effects and anion effects. At low pH values, the concentration of OH^- is small, and there is a greater probability that anions, rather than OH^-, are incorporated within the coordination sphere around the Pb^{4+} (5c).

Recent work in this laboratory on co-deposition of various metal ions with PbO_2 has revealed an unexpected catalytic contribution

from Cl^- which was present as the counter ion of the metallic dopant ion (6-7). The oxidations of DMSO, Mn(II), benzyl alcohol, benzaldehyde, and toluene have been reported to be greatly catalyzed at the Cl-PbO_2 anodes (8). It was anticipated that the incorporated Cl^- which substituted for lattice O(II), provided partial charge compensation for Pb^{4+}, and resulted in disruption of the bond order of Pb^{4+}. Hence, at the surface of Cl-PbO_2 electrodes, there is a corresponding increase in the density of partially filled orbitals from the Pb^{4+} centers which are then available for adsorption of OH radicals (8).

Use of acetate ion (OAc^-) as dopant for PbO_2 deposition also resulted in a highly active and stable film for the oxidations of DMSO, toluene, and benzyl alcohol in 1 M H_2SO_4, as described in Chap. IV. In this chapter, a possible catalytic mechanism for the anodic oxygen-transfer reactions at Cl-PbO_2 electrodes in sulfuric acid media is discussed.

Experimental

Apparatus

A three-compartment electrolysis cell was used with the Pt-wire counter electrode separated from the working solution by a fritted-glass junction. The SCE reference contacted the working solution through a Harber-Luggin capillary. Heterogeneous rate constants and current potential curves were obtained by cyclic voltammetry at a Au rotated disc electrode (RDE, 0.1642 cm^2) covered with an electrochemically

deposited PbO_2 film. A PIR rotator with an RDE3 potentiostat (Pine Instrument) and a model 2000 X-Y recorder (Houston Instrument) were also used.

The X-ray fluorescence (XRF) signals were obtained using a model SRS 200 sequential spectrometer (SIEMENS) with PbO_2 films deposited on Au foils which were attached to detachable stainless steel discs with conductive silver paste. Germanium and LiF crystals were used as monochromators to disperse the K-α lines emitted from Cl and Pb, respectively. Values of 2d (as for $n = 2d\sin\theta$) are 6.532 Å and 4.02 Å for Ge and LiF, respectively. A data acquisition system linked to the spectrometer, programmed by SIEMENS Co. and translated to IBM-compatible software by Pfizer Pigments, Inc. (Easton Pennsylvania), was used for data collection. Measuring conditions were defined as code number 50113 and 20113, and signals were collected within the 2θ range of 92.25° - 93.45° for Cl, and 33.15° - 34.85° for Pb.

Instrumentation for the EQCM measurements has been previously described (9-12). Potentiostatic control, data acquisition, and data analysis were achieved by interfacing the instrument to an IBM-compatible PC/AT using a DT2801-A board (DATA Translation) which was driven from the ASYST programming environment (DATA Translation). Planar (2.5-cm diameter) overtone polished, AT-cut quartz crystals (Valpey-Fisher) were operated at the fundamental frequency of 5 MHz in all experiments. Gold electrodes (ca. 200-nm thick, 0.38-cm^2 area) were evaporated onto both sides of the crystals using a model E306A coating system (Edwards, West Sussex, England). Calibration of the

piezoelectrical and electrochemical response for each crystal have been described elsewhere (13-14). A coiled Pt wire (effective area = 2.8 cm^2) served as the counter electrode. All potentials were recorded and are reported versus a Ag/AgCl reference.

Reagents

All chemicals were Analytical Reagent Grade and solutions were prepared from water purified in a NANOpure-II deionizing system (SYBRON/Barnstead). The supporting electrolyte solutions were 1 M $HClO_4$ for electrodeposition of oxide films, and 1 M H_2SO_4 for kinetic testing and cyclic voltammetry.

Procedures

Prior to electrodeposition, the Au RDE was polished with 0.5-um alumina powder (Buehler Ltd.) followed by rinsing with deionized water. Then, the electrode potential was cycled between the scan limits of 0.5 V and 1.8 V in 1 M $HClO_4$ until a reproducible cyclic voltammogram was obtained which represented the clean Au surface. Preparation of the Cl-doped ß-PbO_2 films (Cl-PbO_2) was done using the exact conditions described in Chap. II. The electrodes were rinsed with deionized water after preparation and then used immediately.

The Au-coated quartz crystals were electrochemically activated prior to all measurements by the application of repeated cyclic potential scans, as described above, until no further changes were detected in the current-potential curves. The relationship between the change in the mechanical resonant frequency (df, Hz) of the quartz

crystal and the measurement of mass changes (Δm) at the electrode surface has been previously described for EQCM measurements (9-12, 14). The mass-to-charge ratio ($\Delta m/\Delta q$, mg coul^{-1}) for an electrochemically sorbed species is

$$\Delta m/\Delta q = -(A_e/K)(df/dq) \qquad [1]$$

In Equation [1], A_e is the electrochemically active area (cm^2), K is a proportionality constant with units of cm^2 Hz mg^{-1} (K is dependent upon the fundamental resonant frequency of the quartz crystal in the absence of the deposited mass, the shear modulous of quartz, and the density of quartz) (9), and Δq (coul) is the net charge passed by the electrosorption process. Note that an increase in mass corresponds with a negative frequency change at the quartz crystal. Values of A_e/K were determined experimentally to be 7.15 ng Hz^{-1} for the crystal from the values of df/dq obtained for the deposition of Pb based on the value $\Delta m/\Delta q$ = 1.07 mg coul^{-1} for the process of $Pb^{2+} + 2e \longrightarrow Pb$. Values of $\Delta m/\Delta q$ were then determined from values of df/dq for the electrodeposition of Cl-PbO_2 films and the electrosorption of HSO_4^- at the Cl-PbO_2 films.

Results and Discussion

Potentiostatic studies of the effect of sulfuric acid concentrations on the electrocatalytic activity of Cl-PbO_2 electrodes

The stability as well as the electrocatalytic activity of Cl-PbO_2 electrodes in 1 M $HClO_4$ were examined on the basis of the reaction rate obtained for DMSO oxidation. Figure 1 shows the kinetic result of DMSO oxidation at the Cl-PbO_2 film electrode. In this figure, curve a corresponds to the Cl-PbO_2 in 1 M H_2SO_4, and b to the Cl-PbO_2 in 1 M $HClO_4$. The heterogeneous rate constant for the oxidation of DMSO at a newly prepared Cl-PbO_2 film was determined to be 4.7×10^{-3} cm s^{-1} at 1.6 V. The rate constant was measured again in another fresh DMSO solution following 37 hr of continuous electrolysis, and determined to be 1.05×10^{-3} cm s^{-1}. This represented a 78% loss in the activity of the electrode (Fig. 1, curve b). Degradation in the catalytic property seems to be an inevitable situation for almost every catalytic electrode. The decrease in the catalytic efficiency of the Cl-PbO_2 film might have resulted from fouling of the electrode surface, or a possible dissolution of the surface Cl^-.

Different kinetic results were obtained when the electrolysis was performed in 1 M H_2SO_4. The heterogeneous rate constant of DMSO oxidation at a newly prepared Cl-PbO_2 film electrode was determined to be 1.20×10^{-2} cm s^{-1} in 1 M H_2SO_4, which was almost three times larger than that measured in 1 M $HClO_4$. Following a 54-hr period of continuous electrolysis, the electrode was transferred to a new solution and the

rate constant was determined to be 1.36×10^{-2} cm s^{-1}, 13% larger than the initial value (Fig. 1, curve a). It should be noted that in 1 M H_2SO_4 (k_{a2} = 0.012), 98.8% of sulfuric acid exists as HSO_4^- (988 mM), and only 1.2% as SO_4^{2-} (12 mM), and the concentration of H^+ is 1.012 M. Therefore, it was concluded that the pH value of 1 M H_2SO_4 was approximately the same as that of 1 M $HClO_4$. It was speculated, based on these results, that HSO_4^- promoted the catalytic oxidation of DMSO at Cl-PbO_2.

Voltammetric studies of the oxidation of DMSO

Voltammetric results of the oxidation of DMSO at the Cl-PbO_2 films were compared in 1 M $HClO_4$ and 1 M H_2SO_4. Figure 2A shows the cyclic voltammograms of DMSO at a Cl-PbO_2 film in 1 M $HClO_4$. The dashed curve represents the residual current measured in the absence of DMSO. Evolution of O_2 from the electrode surface became apparent at E > 1.7 V on the positive potential scan. Although oxidation of DMSO was thermodynamically allowed over the entire potential range shown (E° = 0.23 V vs. NHE), the voltammetric current for DMSO oxidation was not evident until E > 1.6 V on the positive scan. This observation indicated an extreme kinetic control mechanism for DMSO oxidation at the Cl-PbO_2 film in 1 M $HClO_4$.

It appears from the voltammograms that the oxidation of DMSO occurred with the concomitant evolution of O_2 from the electrode surface. Currents produced for DMSO oxidation increased with increasing concentrations of DMSO. However, net current obtained for DMSO

oxidation was indeed very small, as compared to the huge background signal produced for O_2 evolution. It was speculated that there was a lack of catalytic sites for DMSO adsorption at the electrode surface in 1 M $HClO_4$, thus the combination of adjacent $^{\cdot}OH_{ad}$ to produce O_2 became the favorable electrochemical process.

Cyclic voltammograms of DMSO shown in Fig. 2B at the Cl-PbO_2 electrode in 1 M H_2SO_4 appeared different from those in 1 M $HClO_4$ (Fig. 2A). Results in 1 M H_2SO_4 revealed an enhancement in the catalytic oxidation of DMSO and a suppressed production of O_2. The oxidation of DMSO became evident at $E > 1.4$ V on the positive scan with a half wave potential ($E_{1/2}$) of 1.6 V. The net current measured at 1.8 V was 7.3 mA for 25 mM DMSO. Beneficial consequences of the addition of H_2SO_4 were i) a decrease in the positive potential required for onset of DMSO oxidation and ii) an increase in the potential required for onset of the anodic oxidation of water.

It was speculated that the adsorption of HSO_4^- at Cl-PbO_2 occurred via an ion-exchange substitution with surface Cl^-. Furthermore, it was speculated that the substitution of HSO_4^- for surface Cl^- created active sites for DMSO adsorption during the catalytic oxidation. Shown in Figure 2C is the plot of anodic current for DMSO oxidation corrected for background at 1.6 V (curve a), 1.7 V (curve b), 1.8 V (curve c), and 1.9 V (curve d) as a function of DMSO concentrations. Based on examination of the slopes of the lines, current response at 1.8 V was the most sensitive. At a larger positive potential (1.9 V, curve d), a loss in current efficiency for DMSO oxidation was observed. Since the

number of $'OH_{ad}$ produced was assumed constant at a fixed potential value, the decrease in the observed current for DMSO oxidation was tentatively concluded to result from the severe evolution of O_2 from adjacant $'OH_{ad}$, which consequently caused a decreased number of $'OH_{ad}$ available for the anodic O-transfer reaction of DMSO.

Contrary to what was observed for Cl-PbO_2, the kinetic results for DMSO oxidation at the pure PbO_2-film electrode was not dependent on the identity of the electrolyte. Shown in Fig. 2D are the cyclic voltammograms for the oxidation of DMSO at a pure PbO_2-film electrode in 1 M H_2SO_4. Currents of DMSO oxidation increased with increasing concentrations of DMSO. However, current values did not substantially vary with the rotation speed of the disc electrode. It is apparent that the reaction rate was very slow for the oxidation of DMSO at the pure PbO_2 film in 1 M H_2SO_4. The net current obtained at 1.8 V was only 1.36 mA for 25 mM DMSO, which was only 15% that at Cl-PbO_2 in 1 M H_2SO_4 (9 mA).

Voltammetric results for DMSO oxidation at the pure PbO_2 in 1 M $HClO_4$ showed very small current value with little rotation speed dependence. The cyclic voltammograms (not shown) resembled those shown in Fig. 2D.

The observation that the H_2SO_4 solution did not contribute significantly to the catalytic activity of the pure PbO_2-film electrode led to the conclusion that surface Cl^- was required for HSO_4^- to activate the electrode for the oxidation of DMSO.

Voltammetric studies of Mn^{2+} oxidation

The oxidation of Mn^{2+} to MnO_4^- has been an interesting goal of the electrocatalysis project because of the possible usage of MnO_4^- as a strong oxidizing agent for a variety of purposes. Being the intermediate product of the anodic oxidation of Mn^{2+} to MnO_4^-, MnO_2 tends to foul the electrode surface by blocking the catalytic sites as barrier layers. Therefore, the most important goal in the electrosynthetic production of MnO_4^- is to achieve a one-step oxidation to prevent the catalytic electrode from being fouled by the intermediate product of insoluble MnO_2 (13, 15-16).

As described in the previous sections, sulfuric acid contributed unique catalytic effects to Cl-PbO_2 electrodes for DMSO oxidation. The catalytic effect was also expected to occur for the oxidation of Mn^{2+} at the Cl-PbO_2 electrode in sulfuric acid media. Figure 3A shows the cyclic voltammogram of 5 mM Mn^{2+} at a Cl-PbO_2 electrode in 1 M $HClO_4$. The dashed curve represents the background current measured in the absence of Mn^{2+}. An anodic peak was obtained at E = 1.68 V on the positive potential scan, which was concluded to result from the formation of insoluble MnO_2 at the electrode surface. The MnO_2 film resulted in fouling of the electrode, and inhibited the O_2 evolution process. Evidence for the loss of electrode activity by the formation of MnO_2 was revealed by the negative net current obtained at E > 1.75 V on the positive scan. Clearly, the MnO_2-covered electrode was a poor anode for further oxidation of Mn^{2+}.

Figure 3B shows the cyclic voltammetric results of Mn^{2+} at the Cl-PbO_2 film in 1 M H_2SO_4. Residual current was shown by the dashed curve. The oxidation of Mn^{2+} became evident at E > 1.6 V on the positive potential scan. A well defined current plateau, rather than a current peak, was obtained at E > 1.75 V on the positive scan as compared with that in 1 M $HClO_4$ (Fig. 3A). On the succeeding negative scan, the current was observed to decrease from its limiting value at 300 mV more negative (1.45 V) than that for the positive scan (1.75 V). It is apparent from that within the potential region of 1.5 V to 1.73 V, anodic current on the negative scan was larger than that on the positive scan. This hysteresis observation was not obtained for DMSO oxidation (Fig. 2B); hence, the identity of the reactant was speculated to account for this unusual phenomenon. This hysteresis result was reproducible, and only occurred at rotation speeds of the disc electrode ≥ 900 rev min^{-1} (7b). The anodic O-transfer reaction of Mn^{2+} involved the transfer of $^{\cdot}OH_{ad}$ to the neighboring $Mn^{2+}{}_{ad}$. It was tentatively concluded that the electrosorption of Mn^{2+} at Cl-PbO_2 was irreversible. In other words, Mn^{2+} began to substantially adsorb at the electrode surface for E > 1.6 V on the positive scan; however, the desorption of Mn^{2+} required more activation energy, which only became significant for E < 1.6 V on the negative scan.

Catalytic current of DMSO oxidation as a function of sulfuric acid concentrations

There was virtually no anodic activity observed for the oxidations of DMSO and Mn^{2+} at the pure PbO_2-film electrode, even in 1 M H_2SO_4. Thus, it was expected that HSO_4^- undergoes ion exchange with the incorporated Cl^- at the Cl-PbO_2 surface and functioned catalytically during the oxidations of DMSO and Mn^{2+}. Correlation between the electrode activity and H_2SO_4 concentrations was examined.

The Cl-PbO_2 film was electrochemically deposited on Au RDE using a concentration ratio of $[Cl^-]/[Pb^{2+}] = 0.7$ in 1 M $HClO_4$, as described in the Experimental Section. Figure 4A shows the voltammetric response of DMSO at the Cl-PbO_2 film electrode. The dashed curve represents the background current obtained in the absence of DMSO. A 60-mL mixture of 1 M $HClO_4$ and 1 M H_2SO_4 was used as the electrolyte with varying fractions of H_2SO_4. Currents were recorded at a potential scan rate of 10 mV s^{-1} and a rotation speed of 900 rev min^{-1} for the disc electrode.

Since the concentration of H^+ in 1 M H_2SO_4 (1.012 M) is approximately equal to that in 1 M $HClO_4$ (1.0 M); therefore, mixing any aliquot of 1 M H_2SO_4 with 1 M $HClO_4$ will not result in substantial change in pH value and ionic strength of the electrolyte.

Apparently, increases in the anodic current for DMSO oxidation in 1 M $HClO_4$ were observed following each addition of H_2SO_4. The current at 1.65 V was 0.1 mA in 1 M $HClO_4$ (solid curve a). The current was 2.0 mA in 1 M H_2SO_4 (solid curve d), which was an increase of 20x that for 1 M $HClO_4$.

Conversely, decreases in the current for O_2 evolution were observed with increasing concentrations of added H_2SO_4 (dashed curves a-d in Fig. 4A). It was anticipated that HSO_4^- substituted for surface Cl^-, which resulted in active sites for DMSO adsorption. However, this substitution decreased the number density of adjacent $'OH_{ad}$, and resulted in a decreased rate of O_2 evolution.

Curve a in Fig. 4B shows the current values for DMSO oxidation at the Cl-PbO_2 film at 1.7 V as a function of H_2SO_4 concentrations (data taken from Fig. 4A). Current increased with increasing concentrations of H_2SO_4, and reached a limiting value for $[H_2SO_4] > 0.2$ M. Experimentation was repeated at a Cl-PbO_2 film deposited at the ratio $[Cl^-]/[Pb^{2+}] = 0.3$ and a pure PbO_2 electrode, according to the exact conditions described for Fig. 4A; results were plotted in Fig. 4B curve b and c, respectively.

It is apparent from this figure that the initial current for DMSO oxidation at zero concentration of H_2SO_4 as well as the limiting current obtained at $[H_2SO_4] > 0.2$ M increased with increasing ratio of $[Cl^-]/[Pb^{2+}]$ for the deposition of Cl-PbO_2.

It was concluded that the level of incorporated Cl^- in the Cl-PbO_2 film increased with increasing concentration ratio of $[Cl^-]/[Pb^{2+}]$ in the deposition solution (data were shown in the following section). Therefore, the fraction of the surface Cl^- replaced by HSO_4^- was expected increase with increasing concentrations of H_2SO_4 in the solution. Thus, for the same concentration of H_2SO_4, the Cl-PbO_2 with higher Cl^- level exhibited better activity than that with lower Cl^-

level. A complete substitution of HSO_4^- for surface Cl^- was tentatively concluded to occur at $[H_2SO_4] > 0.2$ M. The slight increase in the current for DMSO oxidation at the pure PbO_2 electrode was tentatively concluded to result from the trace defect sites occurred naturally for all crystals (17).

X-ray fluorescence data

The Cl^- level in Cl-PbO_2 was determined using X-ray fluorescence spectrometry (XRF). The Cl-PbO_2 film was electrodeposited on the Au RDE according to the conditions described in the experimental section. The prepared film was washed thoroughly with copious amount of deionized H_2O before being transferred to the sample holder for analysis. Standard spectra were obtained to identify the peak maximum of Cl^-. Signals from a blank specimen were collected as backgroumd intensity for sample-intensity correction. Signal-to-noise ratio was larger than 45 for the data reported here.

Figure 5 shows the fluorescence intensities of Cl^- of Cl-PbO_2 films as a function of concentration ratio of $[Cl^-]/[Pb^{2+}]$ in the deposition solution. It is apparent that the amount of incorporated Cl^- increased with increasing ratio of $[Cl^-]/[Pb^{2+}]$.

Catalytic oxidation of DMSO at pure PbO_2 in $HClO_4$ with the presence of Cl^- and HSO_4^-

The defect sites at the doped-PbO_2 surface were anticipated to result from co-deposition with anion dopants, including OAc^-, Cl^-, and HSO_4^-. The electrocatalytic activities of the anion-doped PbO_2-film

electrodes for the oxidation of DMSO were shown to be greatly enhanced, as compared with that for the pure PbO_2.

Figure 6 shows the effect of Cl^- and HSO_4^- on the catalytic I-t curves of DMSO at the pure PbO_2-film electrode in 1 M $HClO_4$ at 1.7 V. The anodic I-t response of DMSO in 1 M $HClO_4$ is shown in this figure (curve a) for comparison. It is shown that a steady state current of approximately 115 μA was maintained in 1 M $HClO_4$ throughout the entire electrolysis over the 105-min period. However, significant increases in the anodic current of DMSO were observed in 1 M $HClO_4$ following the addition of Cl^- (curve b) and HSO_4^- (curve c). Starting at 115 μA, the current of DMSO oxidation in 50 μM Cl^- increased with the increasing time value for the first 45 min, and reached a nearly constant value of 210 μA thereafter.

In 1 M $HClO_4$ containing 50 μM HSO_4^-, current of DMSO oxidation was also observed to gradually increase with time value over the 110-min period. An increase of 283% in anodic current was obtained at t = 110 min (440 μA).

It was speculated that Cl^- and HSO_4^- were gradually incorporated into the matrix of PbO_2 during the long-term electrolysis process. This incorporation activated the electrode during the catalytic oxidation of DMSO.

Applications of the electrochemical quartz crystal microbalance (EQCM)

Experimentation was done with the Cl-PbO_2 film electrodeposited on Au-coated quartz crystal (Au/QC) in an EQCM to investigate the mass change at the electrode surface produced by ion exchange. The Cl-PbO_2 film was electrodeposited from 1 M $HClO_4$ containing 1.67 mM $Pb(NO_3)_2$ at a ratio of $[Cl^-]/[Pb^{2+}] = 0.7$. The electrode potential was stepped from 1.5 V to 1.7 V for 60 sec with N_2 purging. This process was repeated three times to achieve a uniform brown color of Cl-PbO_2 at the Au/QC.

Any mass change occurring at the electrode surface resulted in a frequency change in the EQCM. The mass change (Δm) was related to the frequency change (df) according to Equation [1]. It was assumed that HSO_4^- replaced the surface Cl^- of Cl-PbO_2 folllowing the exposure to 1 M H_2SO_4. This substitution was predicted to result in a negative frequency change at the EQCM following the addition of H_2SO_4 because the mass of HSO_4^- is greater than that of Cl^-. The substitution was tentatively concluded to occur via an anion-exchange mechanism and the amount of surface Cl^- replaced was dependent on H_2SO_4 concentration but not the applied potential.

Figure 7A shows the current-time (I-t) and frequency-time (f-t) responses obtained simultaneously at the Cl-PbO_2 film deposited on the Au/QC in 1 M $HClO_4$. The electrode potential was held at 1.5 V for 5 sec, then stepped to 1.7 V for 120 sec followed by stepping back to 1.5 V for another 5 sec. Nitrogen gas was bubbled to the solution throughout the entire 130-sec oxidation period. There was virtually no

significant frequency change obtained for this blank solution. The slight increase of frequency change for $t < 30$ sec was speculated to result from desorption of specifically adsorbed species following the potential step.

Figure 7B shows the I-t and f-t responses obtained simultaneously at the Cl-PbO_2 film deposited on Au/QC in 1 M $HClO_4$. Experimental conditions were exactly the same as those described for Fig. 7A, except for adding 5 mM DMSO to the solution at $t = 10$ sec. The DMSO needed time to move to the electrode surface; therefore, no instantaneous current response was detected; however, a sudden decrease of frequency change was observed following DMSO addition at $t = 10$ sec. This frequency change did not result from mass change at the electrode surface but was due to the sudden agitation of solution caused by the quickly added DMSO, and, therefore, resulted in perturbation of the quartz-crystal vibration. The current increase observed at $t > 65$ sec was concluded to correspond to DMSO oxidation, which, however, did not result in substantial frequency change. In fact, this f-t response appeared similar to that obtained for the blank solution (Fig. 6A).

Figure 7C shows the I-t and f-t responses obtained simultaneously at the Cl-PbO_2 film deposited on Au/QC in 1 M $HClO_4$ containing 15 mM DMSO. This experiment was done according to the conditions described for Fig. 7B, except that 200 mM H_2SO_4 was added to the solution at $t = 10$ sec. The increase in the anodic current of DMSO at $t > 20$ sec was concluded to result from the activated Cl-PbO_2 by HSO_4^- modification.

The up-and-down current response for t > 35 sec was caused by irregular bubbling of N_2, which also produced the peak-and-valley response in frequency change at the quartz crystal. The sudden decrease of frequency change at t = 10 sec was due to the same reason described for Fig. 7B. It is apparent from this f-t response that frequency decreased (df < 0) following the addition of HSO_4^- at t = 10, which corresponed to a positive mass change ($\Delta m > 0$) at the electrode surface. This positive mass change was an indication of the substitution of HSO_4^- for surface Cl^- ($\Delta m = 61.5$ g mol^{-1}). A total frequency change of 30 Hz was obtained, which was equivalent to a mass increase of 210 ± 10 ng at the electrode surface.

Conclusion

Significant enhancement in the reaction rate of the oxidation of DMSO and Mn^{2+} were observed at Cl-PbO_2 in 1 M H_2SO_4 as compared with that obtained in 1 M $HClO_4$. The catalytic results were concluded to occur as a result of HSO_4^- modification. A mass increase of 210 ± 10 ng was obtained at the Cl-PbO_2 film following the addition of 200 mM HSO_4^-, as studied with EQCM. The HSO_4^- ions were speculated to modify the Cl-PbO_2 surface by replacing the incorporated Cl^- following an anion-exchange reaction. It was proposed that one Cl^- of Cl-PbO_2 is substituted for one HSO_4^- based on the examination of the effective ionic radii of HSO_4^- (r = 4 Å), and Cl^- (r = 3 Å) (18). This substitution may cause distortion as well as interruption of the crystal

lattice, which in return results in defect sites for the catalytic adsorption of solution reactants.

The formation of adsorbed OH radicals ($^{\cdot}OH_{ad}$) is the prerequisite for both O-transfer and O_2-evolution processes. Results showed that increases of k_{app} as well as a decrease of the current of O_2-evolution at the Cl-PbO_2 electrode, for $E < 1.75$ V, was obtained in 1 M H_2SO_4 as compared with those in 1 M $HClO_4$. The adsorption of HSO_4^- was concluded to create active sites for reactant adsorption, while suppressed the combination of $^{\cdot}OH_{ad}$ to form O_2.

The application of Cl-PbO_2 film as anode material with 1 M H_2SO_4 as supporting electrolyte satisfied the premise for the modification of a selectively catalytic electrode for anodic O-t reaction. Increases in the rate of the oxidation of solution reactant were obtained without a severe concomitant evolution of O_2 at the electrode surface.

References

1. Yeo, I-Y; Johnson, D. C. J. Electrochem. Soc. 1987, 134, 1973.
2. Chang H.; Johnson, D. C. J. Electrochem. Soc. submitted for publication.
3. Wels, B. R.; Johnson, D. C. J. Electrochem. Soc. submitted for publication.
4. Feng, J.; Johnson, D. C. J. Electrochem. Soc. 1990, 137, 507.
5. (a) Burbank, J. N.R.L. Report 6859; Naval Research Laboratory: Washington, D.C., 1978. (b) Ruetschi, P.; Cahan, B. D. J. Electrochem. Soc. 1958, 105, 369. (c) Bagshaw, N. E.; Clarke, R. L.; Halliwell, B. J. Appl. Chem. (London), 1966, 16, 180. (d) Duisman, J. A.; Giauque, W. F. J. Phys. Chem. 1968, 72, 562.

6. Feng, J.; Johnson, D. C. unpublished results, Chemistry Dept., Iowa State University, Ames, Iowa, 1987.

7. Feng, J.; Johnson, D. C. unpublished results, Chemistry Dept., Iowa State University, Ames, Iowa, 1990.

8. Hsiao, Y.-L.; Johnson, D. C. J. Electrochem. Soc. 1989, 136, 3704.

9. Ostrom, G. S.; Buttry, D. A. J. Electroanal. Chem. 1988, 256, 411.

10. Orata, D.; Buttry, D. A. J. Am. Chem. Soc. 1987, 109, 3574.

11. Varineau, P. T.; Buttry, D. A. J. Phys. Chem. 1987, 91, 1292.

12. Melory, O.; Kanazawa, K.; Gordon II, J. G.; Buttry, D. A. Langmuir 1986, 2, 697.

13. Larew, L. A.; Gordon, J. S.; Hsiao, Y.-L.; Buttry, D. A.; Johnson, D. C. J. Electrochem. Soc. 1990, 137, 3701.

14. Bruckenstein, S.; Shay, M. Electrochim. Acta 1989, 30, 1295.

15. LaCourse, W. R.; Hsiao, Y.-L.; Johnson, D. C.; Weber, W. H. J. Electrochem. Soc. 1989, 136, 3714.

16. Chang, H. Ph.D. Dissertation, Iowa State University, Ames, Iowa, 1989.

17. Madou, M. J.; Morrison, S. R. Chemical Sensing With Solid State Devices; Academic Press, Inc.: New York, 1989.

18. Dean, J. A. Lange's Handbook of Chemistry; McGraw Hill: New York, 1985, section 5, p. 5.

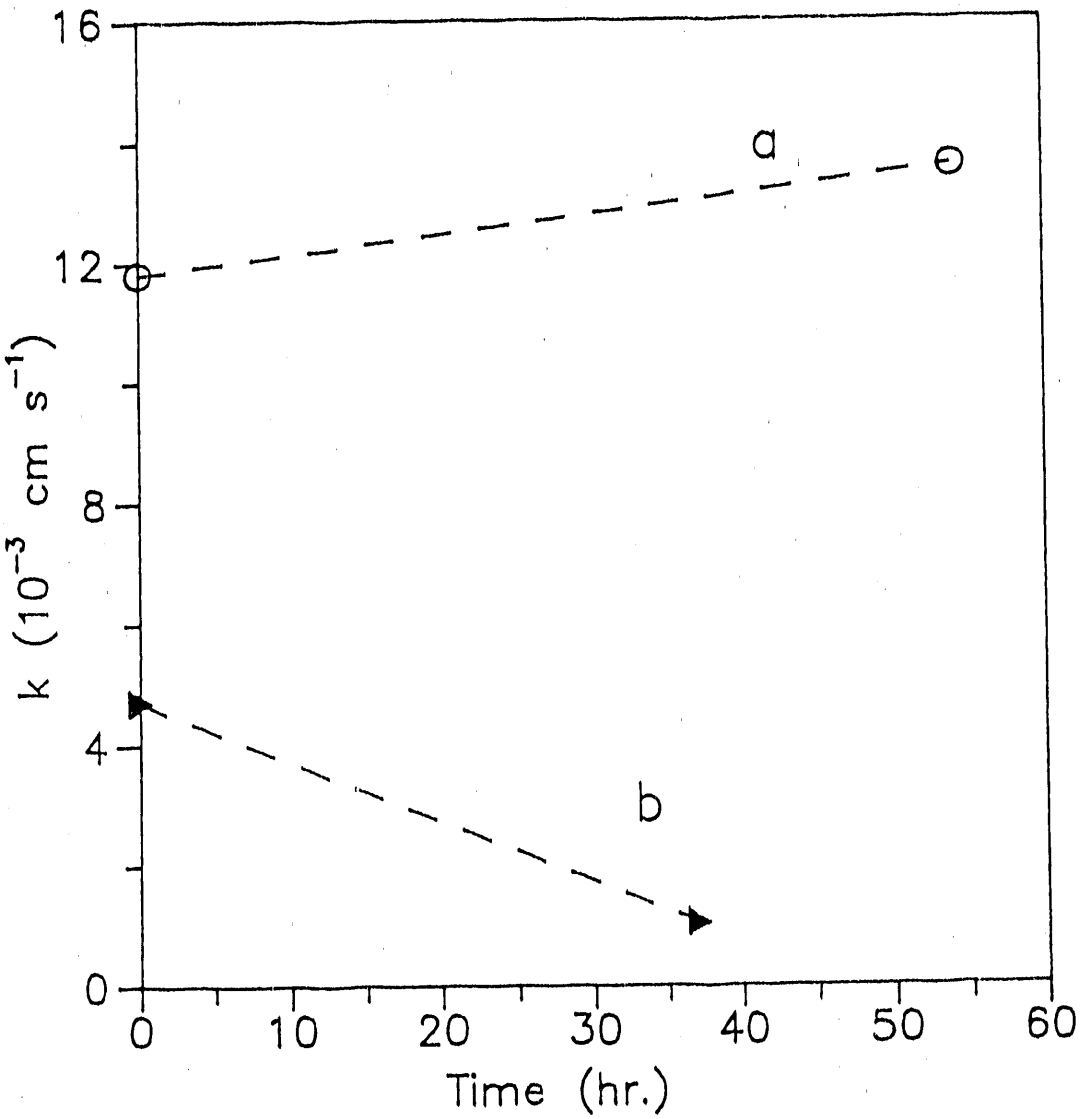

Figure 1. Plot of the heterogeneous rate constant *vs.* time for DMSO oxidation at the Cl-PbO_2 film on the Au RDE

Conditions: 5 mM DMSO, E = 1.6 V

Electrolytes: (a) 1 M H_2SO_4, (b) 1 M $HClO_4$

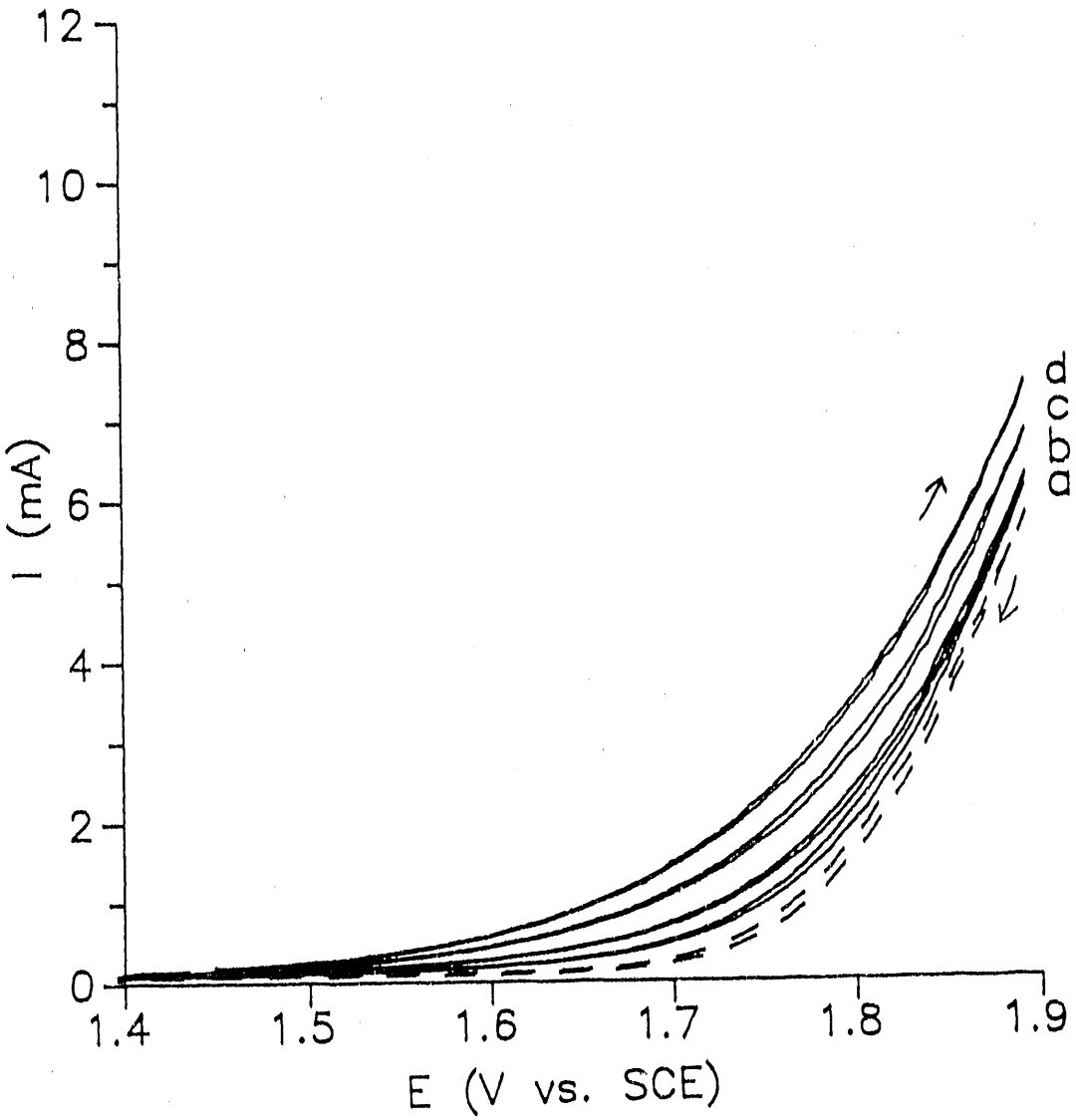

Figure 2A. Cyclic voltammograms for DMSO at the Cl-PbO_2 film on a Au RDE

Conditions: 20 mV s^{-1}, 2500 rev min^{-1}

Electrolyte: 1 M $HClO_4$

DMSO concentrations (mM): (---) 0, (a) 10, (b) 15, (c) 20, (d) 25

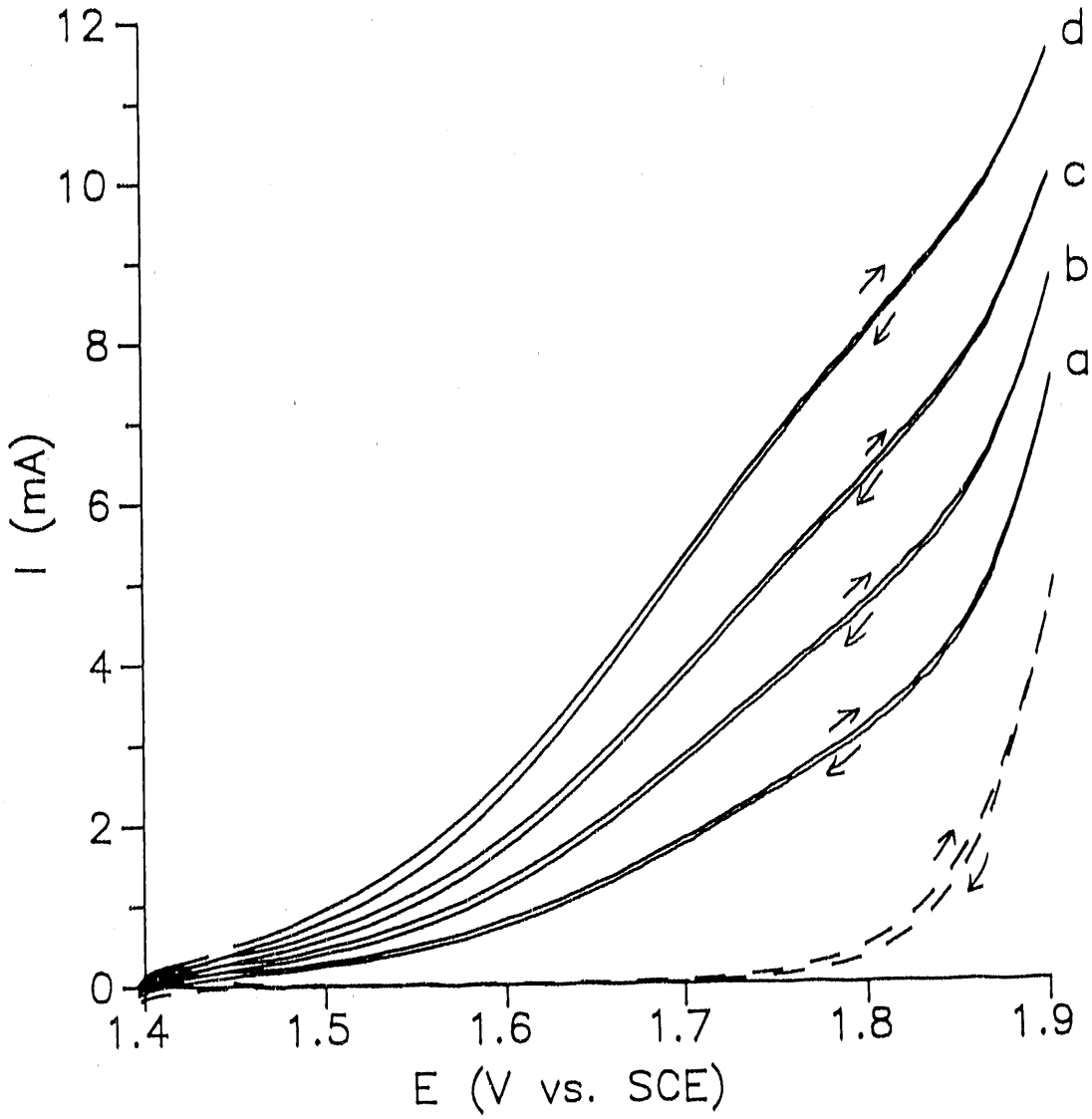

Figure 2B. Cyclic voltammograms for DMSO at the Cl-PbO_2 film on a Au RDE

Conditions: same as Fig. 2A

Electrolyte: 1 M H_2SO_4

DMSO concentrations (mM): same as Fig. 2A

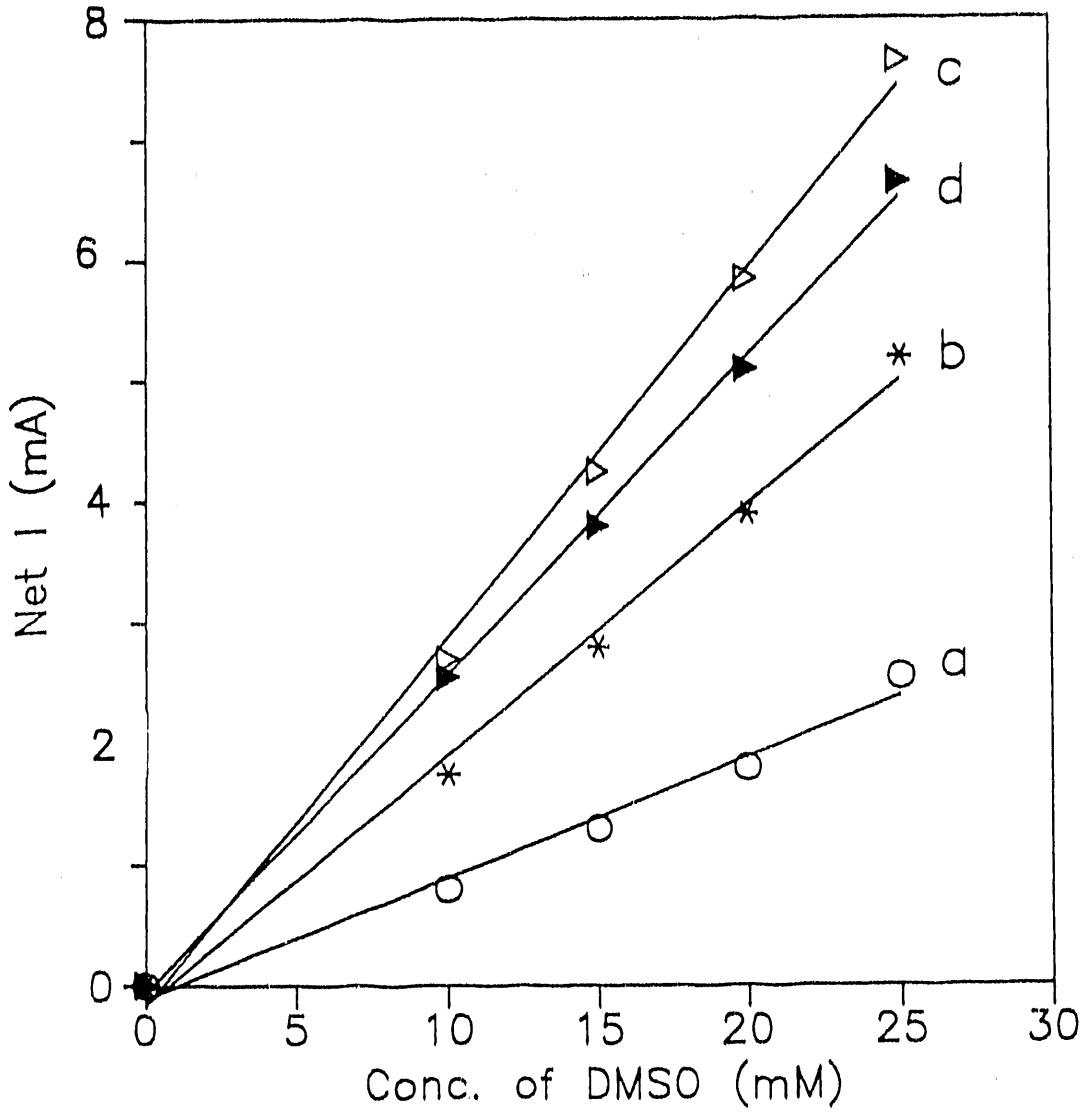

Figure 2C. Plot of net current (I), produced from DMSO oxidation at the Cl-PbO_2 film on Au RDE, *vs.* DMSO concentration

Conditions: 2500 rev min^{-1}, 1 M H_2SO_4

Electrode potential (V): (a) 1.6, (b) 1.7, (c) 1.8, (d) 1.9

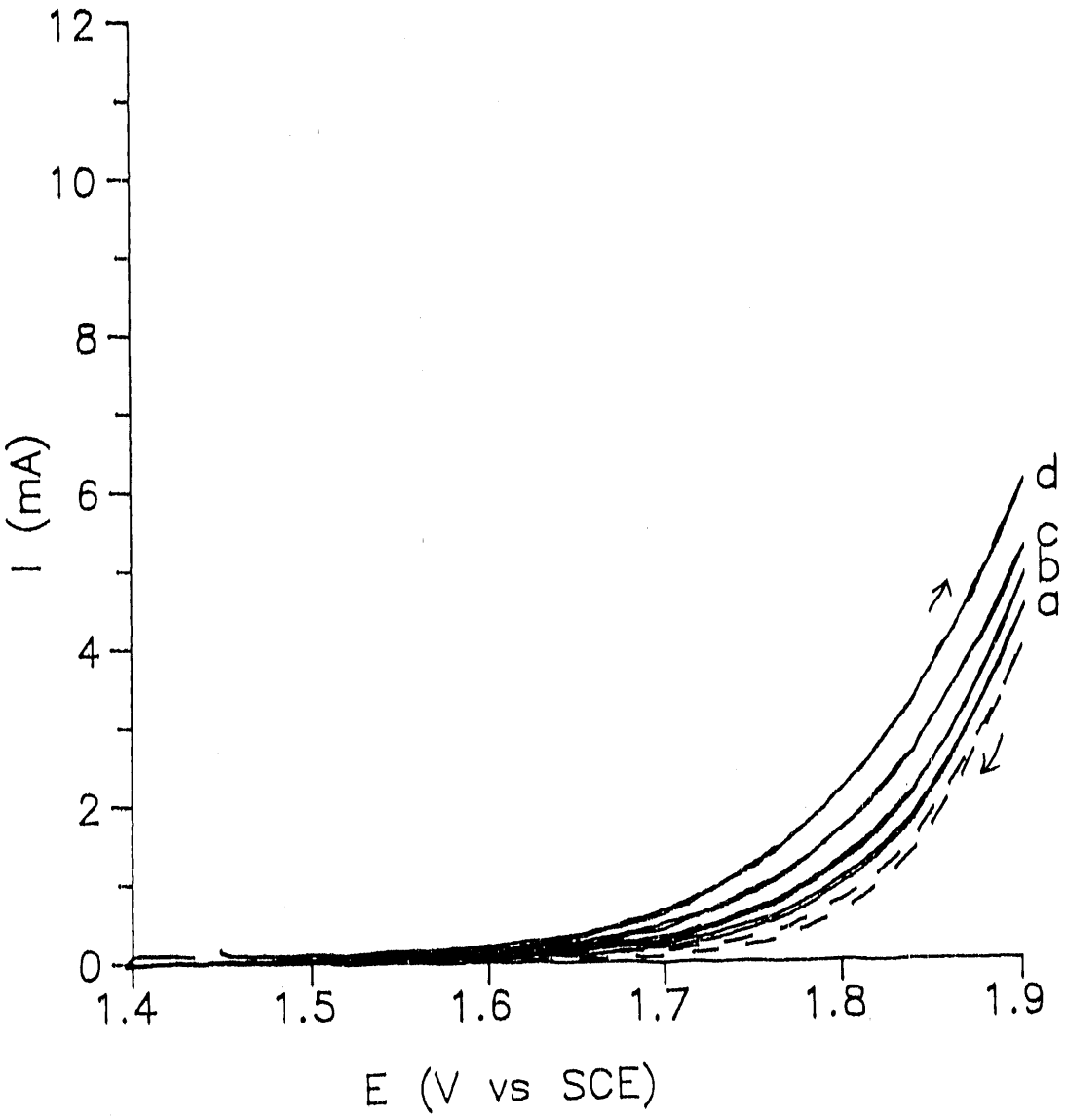

Figure 2D. Cyclic voltammograms for DMSO at a pure PbO_2 film on Au RDE

Conditions: 20 mV s^{-1}, 2500 rev min^{-1}

Electrolyte: 1 M H_2SO_4

DMSO concentrations (mM): (---) 0, (a) 10, (b) 15, (c) 20, (d) 25

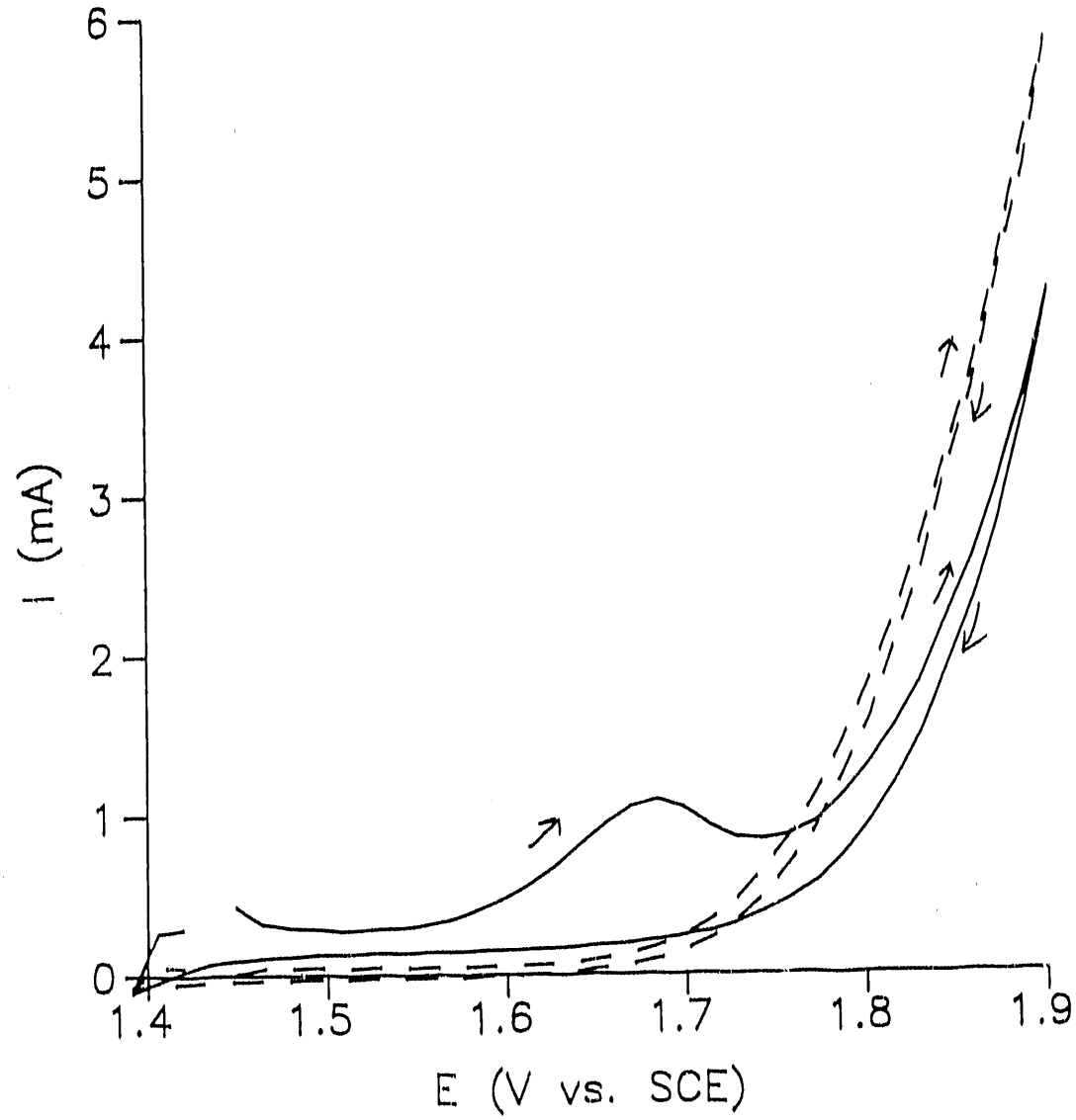

Figure 3A. Cyclic voltammograms for Mn^{2+} at the Cl-PbO_2 film on Au RDE

Conditions: 1 M $HClO_4$, 50 mV s^{-1}, 900 rev min^{-1}

Curves: (---) residual
(——) 5 mM Mn^{2+}

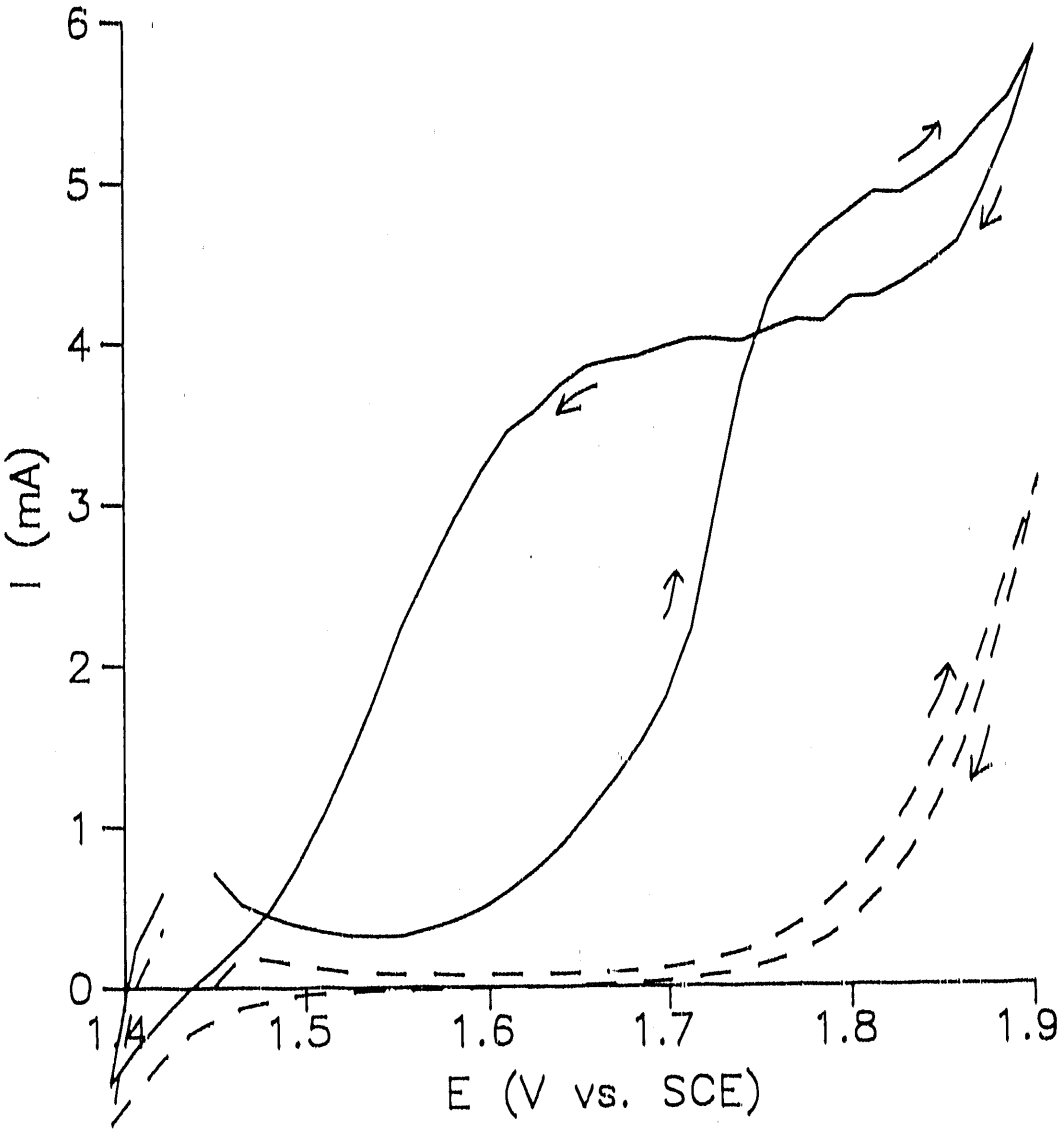

Figure 3B. Cyclic voltammograms for Mn^{2+} at a Cl-PbO_2 film on Au RDE

Conditions: 50 mV s^{-1}, 900 rev min^{-1}, 1 M H_2SO_4

Curves: (---) residual
(——) 5 mM Mn^{2+}

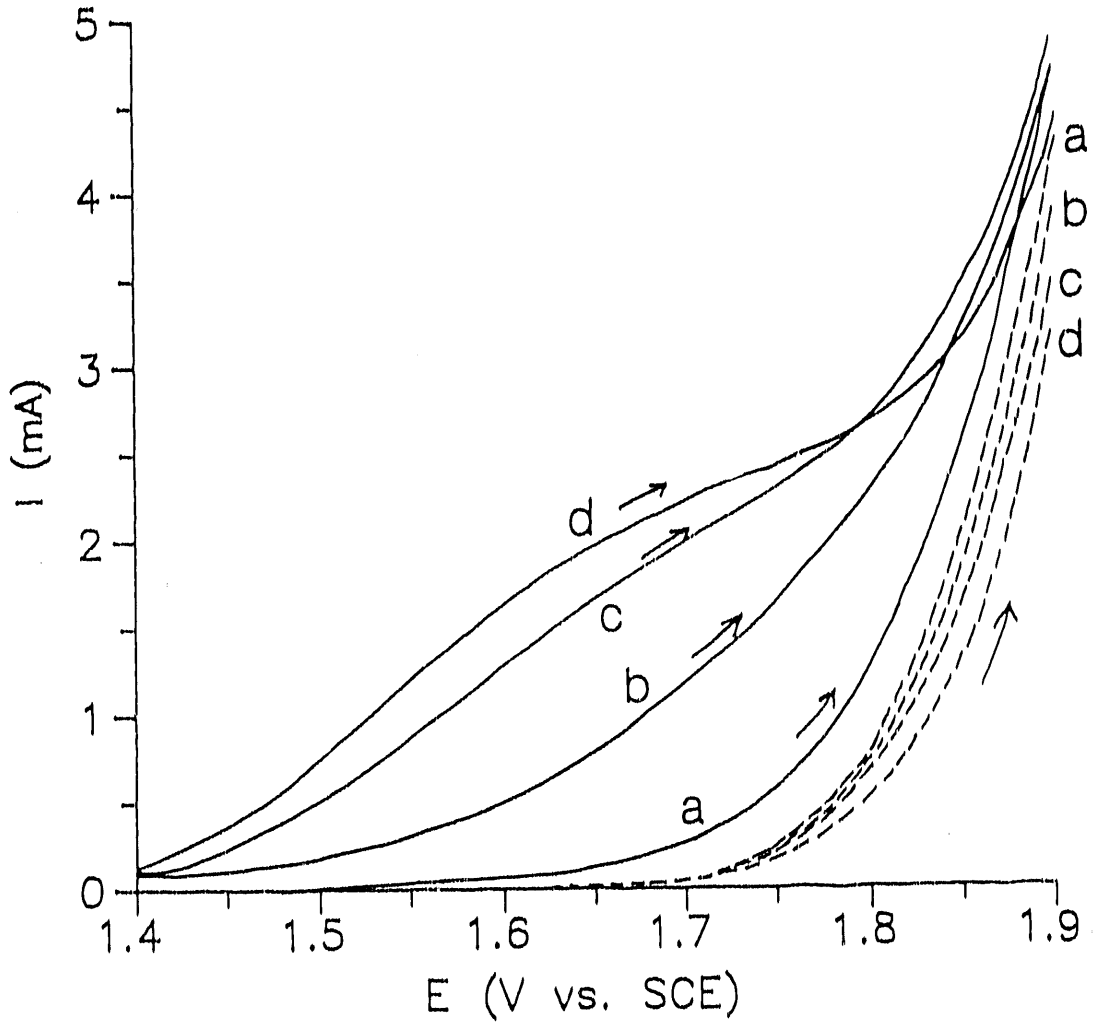

Figure 4A. Cyclic voltammograms for DMSO at a Cl-PbO_2 film on Au RDE

Conditions: 10 mV s^{-1}, 900 rev min^{-1}

Curves: (---) residual (positive scan),
(——) 10 mM DMSO (positive scan)

H_2SO_4 concentrations (mM): (a) 0, (b) 83,
(c) 250, (d) 1000

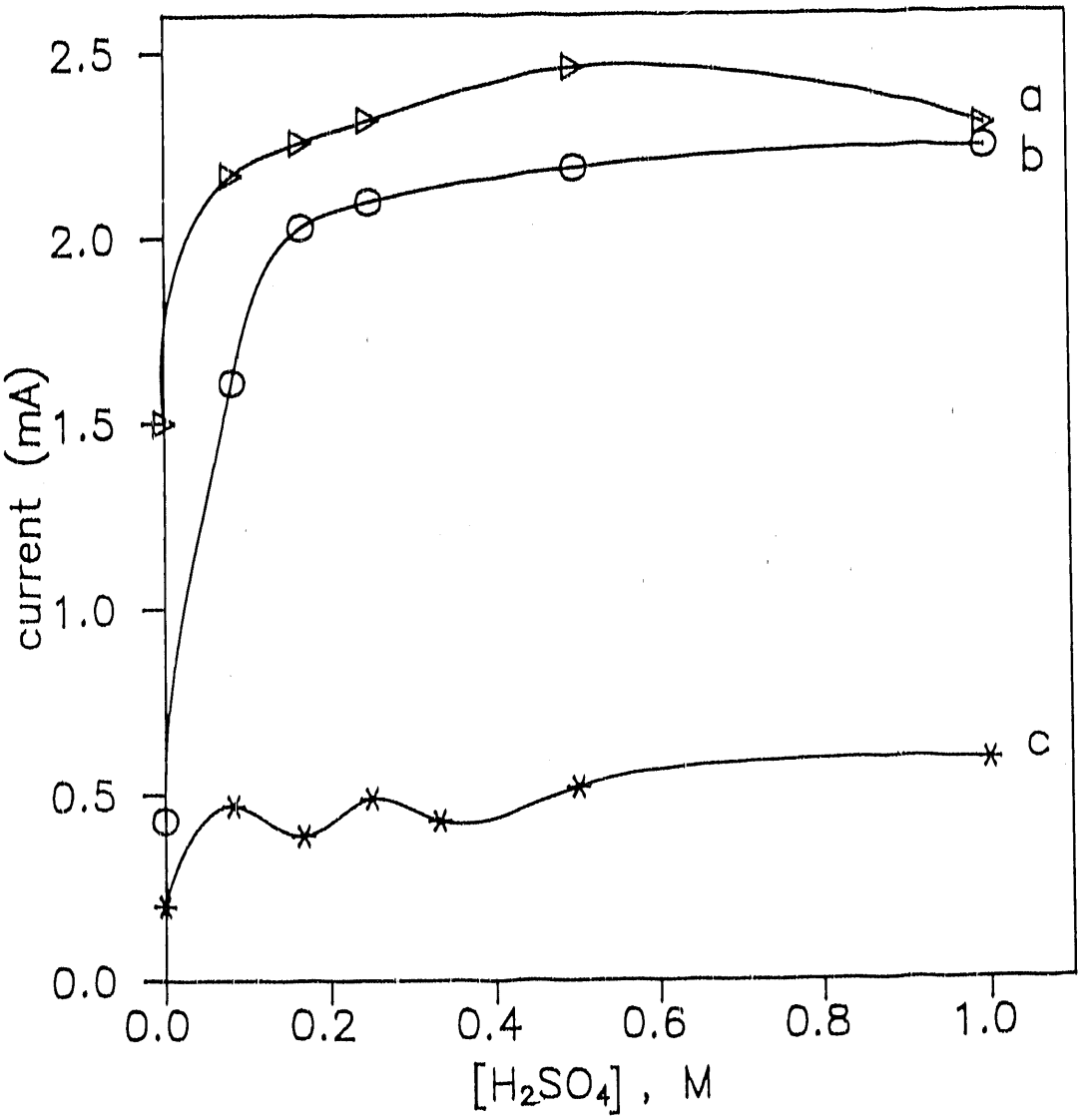

Fogure 4B. Plot of current for DMSO oxidation *vs*. H_2SO_4 concentrations

Conditions: 10 mM DMSO,
900 rev min^{-1}, E = 1.7 V

Electrodes: (a) Cl-PbO_2 film on Au ($[Cl^-]/[Pb^{2+}]$ = 0.7),
(b) Cl-PbO_2 film on Au ($[Cl^-]/[Pb^{2+}]$ = 0.3),
(c) pure PbO_2 film on Au

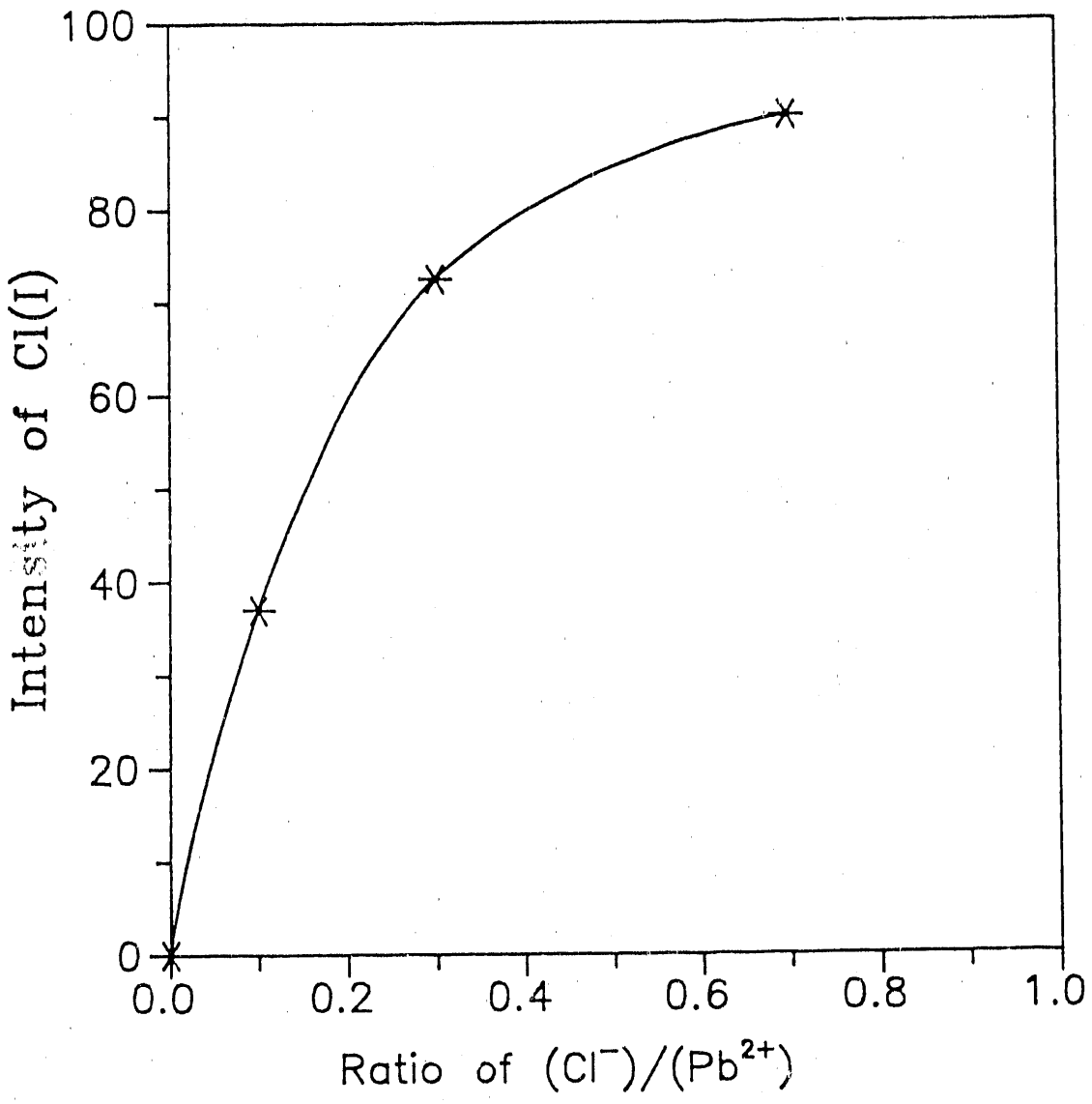

Figure 5. Plot of the X-ray fluorescence intensity for Cl^- at the Cl-PbO_2 film *vs.* concentration ratio of $[Cl^-]/[Pb^{2+}]$ in the deposition solution

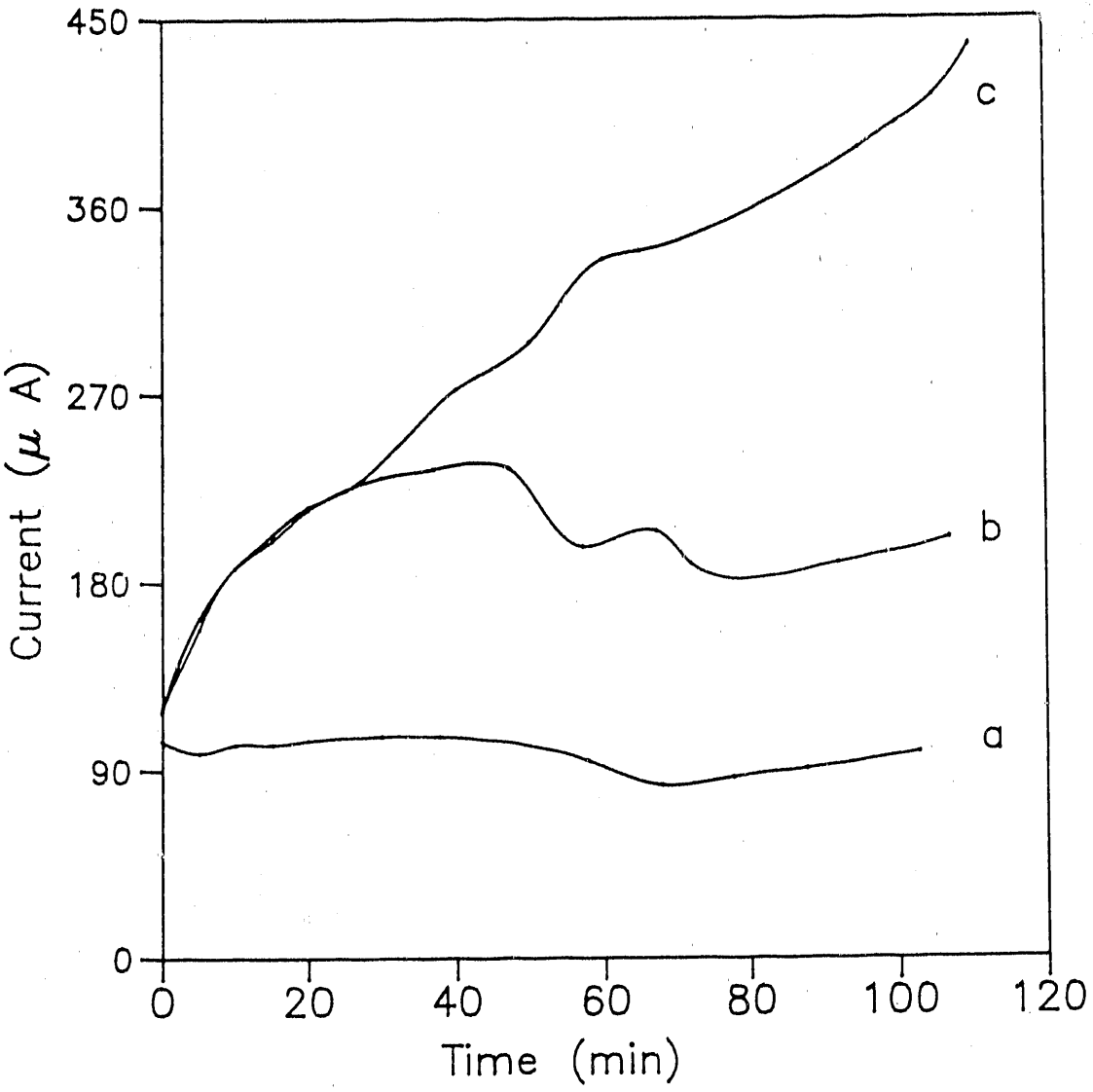

Figure 6. Current-time response for the oxidation of DMSO at a pure PbO_2 film on Au RDE

Conditions: 1 M $HClO_4$,
1600 rev min^{-1}, E = 1.7 V

Curves: (a) 10 mM DMSO,
(b) 10 mM DMSO + 50 μM Cl^-,
(c) 10 mM DMSO + 50 μM HSO_4^-

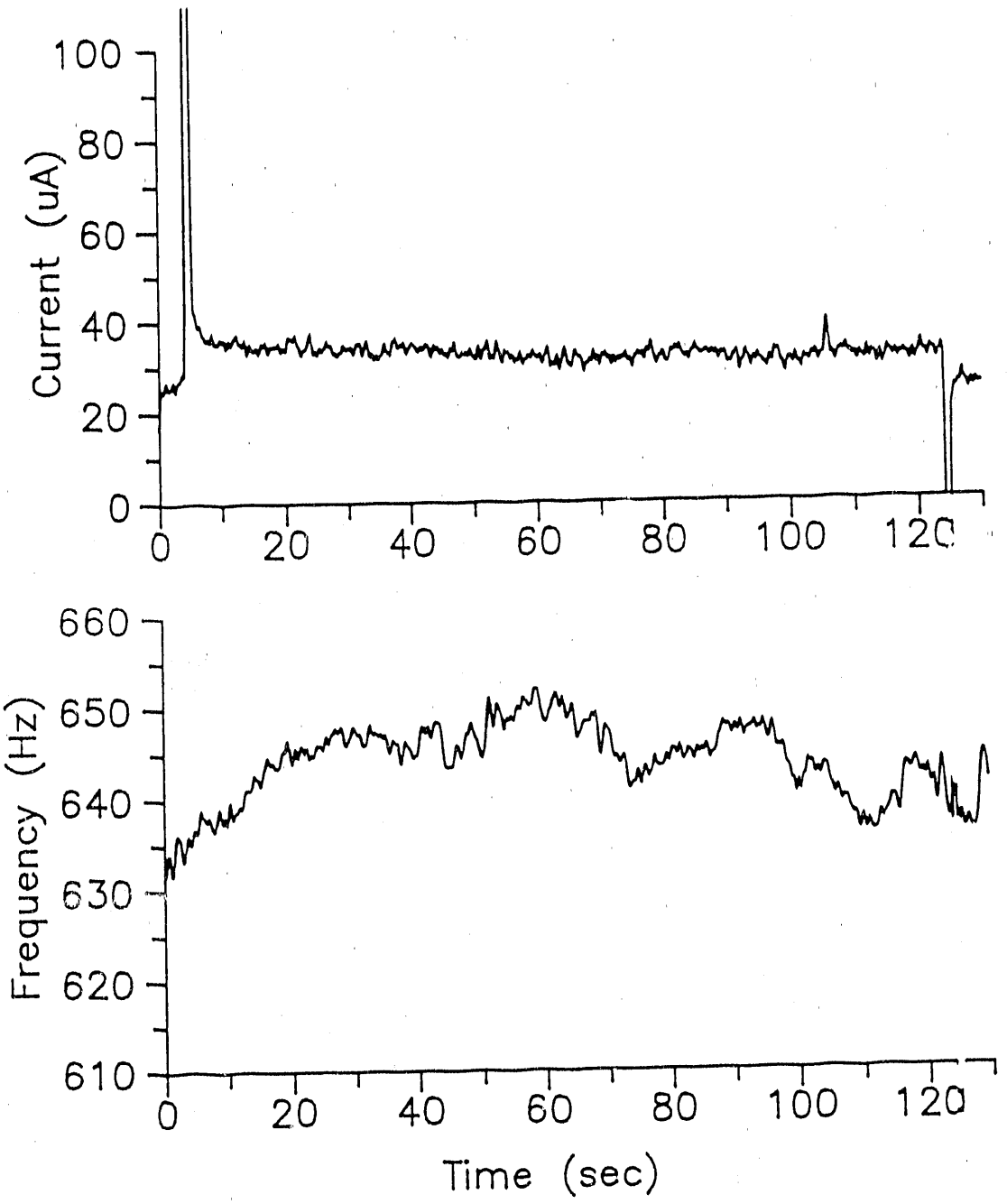

Figure 7A. Current-time and frequency-time responses at the Cl-PbO_2 film deposited on Au/QC in 1 M $HClO_4$

Conditions: 1 M $HClO_4$, N_2 purging

Potential step = from 1.5 V (t = 0 - 5 sec)
to 1.7 V (t = 6 - 125 sec)
back to 1.5 V (t = 126 - 130 sec)

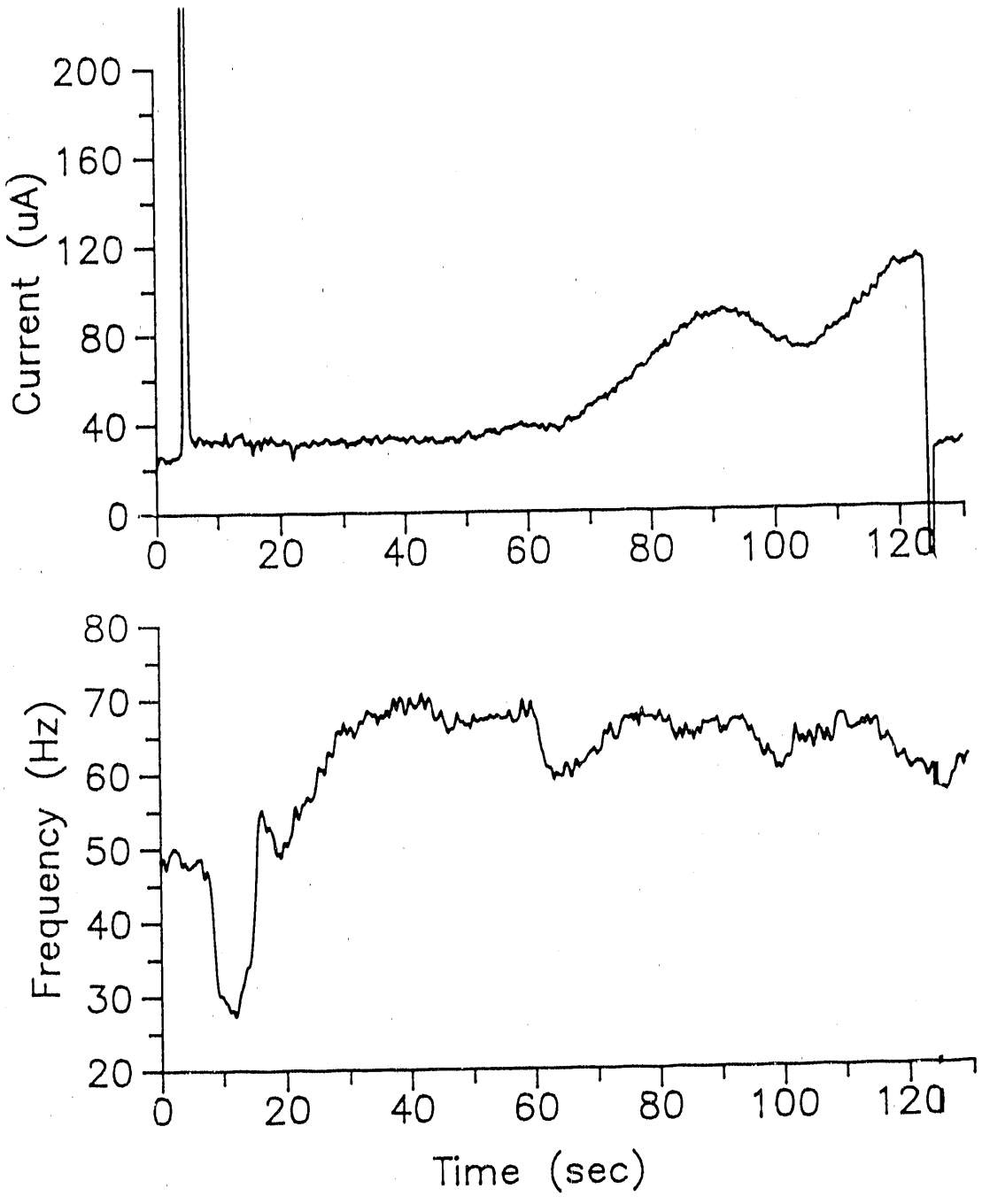

Figure 7B. Current-time and frequency-time responses at the Cl-PbO_2 film deposited on Au/QC in 1 M $HClO_4$

Conditions & potential step: Same as Fig. 7A

DMSO concentration: 5 mM (at t = 10 sec)

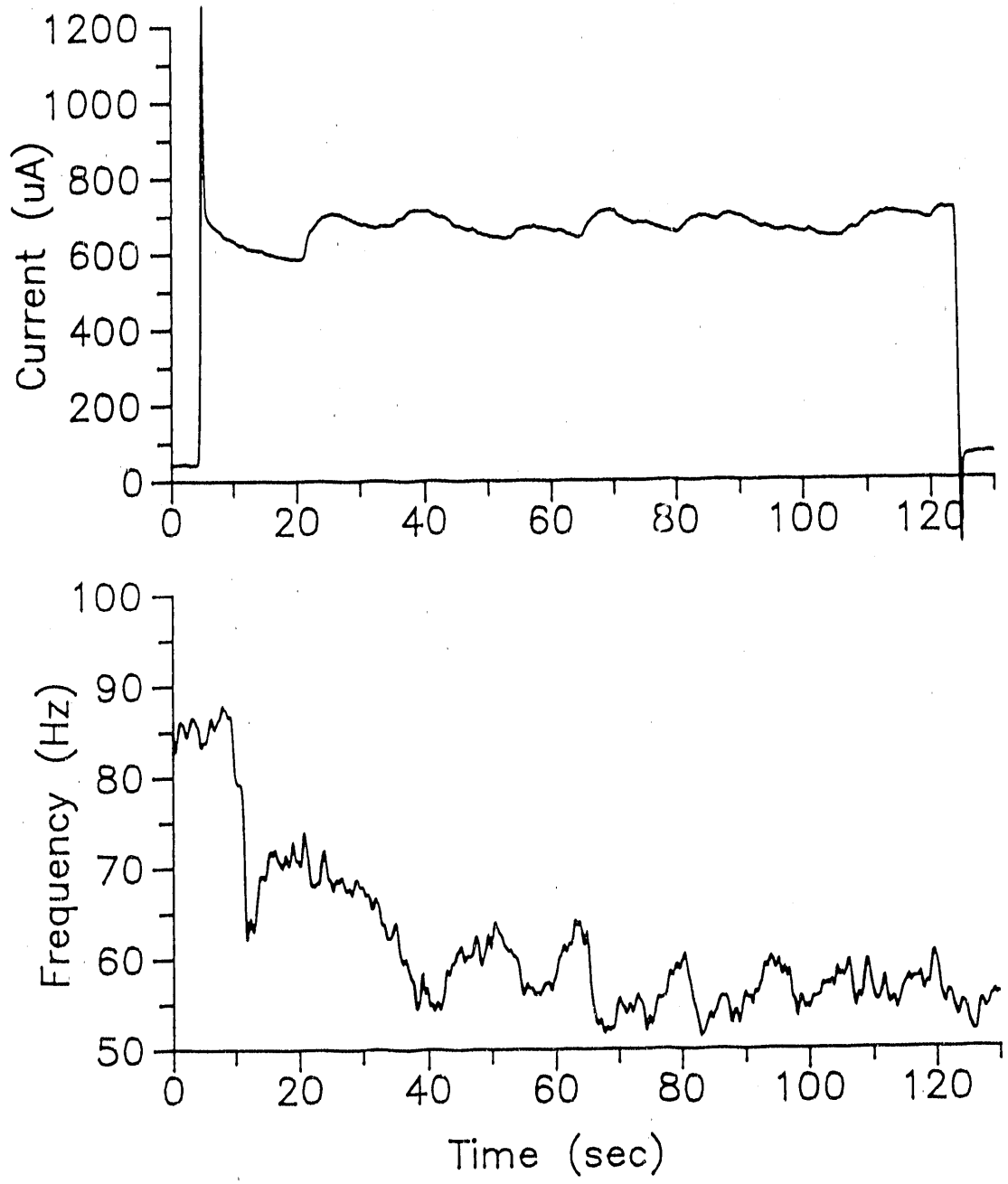

Figure 7C. Current-time and frequency-time responses at the Cl-PbO_2 film deposited on Au/QC in 1 M $HClO_4$

Conditions & potential step: Same as Fig. 7A

[DMSO] = 15 mM (t = 0 sec)

[H_2SO_4] = 200 mM (t = 10 sec)

CHAPTER IV.

ELECTROCATALYSIS AT ACETATE-DOPED LEAD DIOXIDE ELECTRODES

"Very interesting, but very confusing."

A. Johnson, "Laugh In",
National Broadcasting Company

Abstract

Oxidations of DMSO, toluene, and *p*-xylene at pure PbO_2-film electrodes were shown to be under extreme kinetic control with values of the heterogeneous rate constant << 0.001 cm s^{-1}. However, a significant increase in the rate constant was observed at the acetate-doped PbO_2 film (OAc-PbO_2) electrodes. Rate increases were *ca.* 26x for toluene, *ca.* 80x for DMSO, and over 100x for *p*-xylene in sulfuric acid media.

Investigations of the preferential crystalline orientations, and studies of surface morphologies of OAc-doped PbO_2 films were performed using X-ray diffraction spectrometry (XRD) and scanning electron microscopy (SEM). Results indicated that both pure and OAc-doped PbO_2 retained the ß-form pure PbO_2 which has a slightly distorted rutile structures. However, changes in the preferred crystal orientations were apparent from changes in the relative intensities of diffraction peaks corresponding to the (301), (310), and (202) crystal planes. Surface morphology of the OAc-PbO_2 film were substantially different from that

for the pure PbO_2 film. A catalyzed process for O_2 evolution was observed at the OAc-PbO_2 as compared for the pure PbO_2. The value of Tafel slope obtained for O_2 evolution at OAc-PbO_2 films was larger than that for the pure PbO_2 electrodes.

Introduction

The application of the Cl-PbO_2 film electrode for the catalytic oxidations of DMSO and Mn^{2+} in sulfuric acid media has been discussed previously (1). Increases in the rate constant were *ca.* 80x and 28x, for DMSO and Mn^{2+}, respectively, in comparison with those measured at the pure PbO_2-film electrode.

It was concluded that HSO_4^- substituted for the surface Cl^-, and created active sites for DMSO adsorption during the catalytic oxidation. However, this substitution suppressed the process of O_2 evolution at the electrode surface. The catalytic effect of doping PbO_2 films with OAc^- will be described.

Experimental

Reagents

Acetate buffer solutions (pH 3.74) were prepared from solutions of 0.1 M NaOAc and 0.01 M HOAc prepared with deionized water. All other chemicals have been described previously (2-3).

Instrumentation

The apparatus for hydrodynamic voltammetry, chronoamperometry, scanning electron microscopy, and X-ray diffractometry have been described before (3).

Procedures

Prior to electrodeposition, the Au RDE was polished and cleaned according to procedures described in Chap. II. The plating solution contained 1.67 mM $Pb(NO_3)_2$ in an acetate buffer (pH 3.74), and the deposition of OAc-doped PbO_2 was done at a constant potential of 1.36 V vs. SCE, on a disc electrode rotated at 900 rev min^{-1}. A uniform brown film appeared during the 20-min deposition period.

Heterogeneous rate constants were calculated from the intercepts of plots of 1/I *vs.* $1/w^{1/2}$ according to the Levich-Koutecky equation (see Chap. II, Equation 7).

Results and Discussion

Voltammetric studies of the deposition of PbO_2 in acetate solution

Figure 1 shows typical voltammograms recorded at the Au RDE in NaOAc buffer solution (pH 3.74) before (---) and after (——) the addition of 0.42 mM Pb^{2+}. The numbers correspond to the cyclic scan number for the deposition of OAc-PbO_2. Gold oxide was formed at E > 1.0 V on the positive potential scan and was reduced at E < 0.78 V on the following negative scan. The formation of PbO_2 became evident at E > 1.18 V on the first positive scan, and a well defined wave developed

with a current plateau of 0.8 mA and a half-wave potential ($E_{1/2}$) of 1.44 V. The deposition of OAc-PbO_2 continued on the succeeding negative scan and stopped at 1.08 V. Cathodic peaks at E = 0.88 V on the negative scans corresponded to the reductive stripping of OAc-PbO_2. Results showed that the production of Au oxide was affected by the OAc-PbO_2 formation. This effect caused the peak potential for the cathodic stripping of Au oxide to shift slightly toward more negative values (0.65 V), and appear as a broader peak, as compared to that measured in the absence of Pb^{2+} (curve ---).

The subsequent 2nd, 3rd, 8th, and 10th potential scans also are shown in Fig. 1. The value of $E_{1/2}$ for the anodic wave shifted from 1.40 V for the 1st positive scan to 1.26 V for the 3rd and following positive scans. However, not much change in $E_{1/2}$ (1.15 V) was observed for the succeeding negative potential scans.

It has been reported that a residue of PbO which existed at the electrode surface after the first cathodic stripping of PbO_2 provided nucleation sites for PbO_2 deposition in the following positive scan (4). Negative shifts in the value of $E_{1/2}$ for the anodic formation of PbO_2 indicated higher rate of PbO_2 deposition on the pre-existing PbO residue than at the Au-oxide surface. In other words, PbO catalyzed the process of PbO_2 formation. A full surface coverage by PbO was tentatively concluded to have formed following the 3rd cathodic scan. This full surface coverage terminated the negative shift in $E_{1/2}$ on the positive scan.

The cathodic peak height at 0.88 V for the reductive stripping of OAc-PbO_2 films was observed to vary with voltammetric scan number. The cathodic peak current increased for the first two scans and then decayed during the following scans. Results of cathodic peak current are shown in Fig. 2 as a function of scan number.

It should be noted that although the peak current for OAc-PbO_2 reduction decreased with increasing scan number following the 2nd potential scan, values of the limiting current (0.8 mA) and $E_{1/2}$ (1.26 V) for the deposition of OAc-PbO_2 remained the same. In other words, the amount of OAc-PbO_2 reduced was getting less and less than what was formed during the 3rd and 10th scans. It was speculated that once a full surface coverage by PbO_2 was achieved, the oxide film became more stable and more difficult to be removed.

X-ray diffraction data (XRD) and scanning electron micrographs (SEM)

The ß-form of PbO_2, having a slightly distorted rutile structure, can be electrochemically deposited from 1 M $HClO_4$ containing Pb^{2+} (5, 6b). On the other hand, the a-form of PbO_2, with an orthorhombic structure, can be deposited from alkaline solutions of Pb^{2+} (6). The structural information of OAc-PbO_2 deposited from an acetate buffer (pH 3.74) was obtained using X-ray powder diffractometry.

Figure 3 shows the X-ray diffraction patterns for an OAc-PbO_2 (pattern a) and a pure PbO_2 (pattern b) films deposited on Au. Both oxides were identified to be in the ß-form, according to peak assignments given in reference (7). Strong intensities for the

diffraction peaks corresponding to (110), (101), (020), and (211) crystal planes were observed for both pure and OAc-doped PbO_2 films. However, those of (202), (310), and (301) crystal planes observed at the pure PbO_2 were substantially diminished for the OAc-PbO_2 film.

In addition, diffraction peaks observed for the OAc-PbO_2 film appear broader than that for the pure PbO_2 film. Since the width of the X-ray diffraction peaks are inversely related to grain sizes of the crystal, this observation was concluded to be an indication of reduced grain sizes of the PbO_2 by co-deposition with OAc^-.

Figure 4 shows the scanning electron micrograph (SEM) of the surface of an OAc-PbO_2 film deposited on Au substrate. The surface morphology appeared to be substantially different from that of a pure PbO_2 film (Chap. I, Fig. 5a). Crystals of the OAc-PbO_2 film are clearly shaped as ne..les and an increase in the roughness factor is apparent from the micrograph.

Certainly, the observed catalytic effect could be a possible result from an incease in surface roughness. However, experimental results indicated that the electrocatalytic properties of OAc-PbO_2 film electrodes were better in H_2SO_4 than in $HClO_4$ media. Therefore, it is not likely that increases in surface roughness will have this kind of effect on the catalytic mechanism. Therefore, it was concluded that the factor of surface roughness was not the only cause for the enhanced catalytic results at OAc-PbO_2.

Oxidation of DMSO The anodic O-transfer product of DMSO has been determined to be $DMSO_2$ by coulometry (3) and mass spectrometry (4). The oxidation of DMSO, which involves one oxygen transferred from H_2O to the final product ($DMSO_2$), was selected as the model reaction to demonstrate the reactivities of pure and doped PbO_2-film electrodes. Furthermore, both DMSO and $DMSO_2$ are neutral species, and, therefore, the heterogeneous rate constant was expected to have relatively little dependence on ionic changes in the compact double-layer region.

Figure 5 shows the plot of $1/I$ *vs.* $1/w^{1/2}$ for the oxidation of DMSO at OAc-PbO_2 films in 1 M $HClO_4$ (line a) and 1 M H_2SO_4 (line b). According to the Koutecky-Levich Equation shown in Chap. II (Equation [3]), heterogeneous rate constants are shown to be inversely related to values of the intercepts of plots of $1/I$ *vs.* $1/w^{1/2}$. It is apparent that sulfuric acid had a greater catalytic effect on the oxidation of DMSO at OAc-PbO_2 than perchloric acid. Heterogeneous rate constants were calculated to be 6×10^{-3} cm s^{-1} and 2.96×10^{-2} cm s^{-1} for 1 M $HClO_4$ and 1 M H_2SO_4, respectively. In comparison with that obtained for the pure PbO_2, the increase in rate constant was ca. 100x.

For electrocatalysis at Cl-PbO_2 in 1 M H_2SO_4, it was proposed that HSO_4^- in the solution replaced the incorporated Cl^- according to an anion-exchange reaction (3). This ion-exchange mechanism for HSO_4^- with surface anion was also assumed to occur at OAc-PbO_2 for the incorporated OAc^-. This ion-exchange resulted in surface sites for DMSO adsorption during the anodic oxidation. Results for the catalytic adsorption activated by HSO_4^- at the Cl-PbO_2 surface have been discussed in

Chap. III. It was also concluded that in 1 M H_2SO_4, the inhibited oxidation of water occurred as the result of decreased number of adsorbed 'OH.

Figure 6 shows typical cyclic voltammograms obtained at an OAc-PbO_2 electrode in 1 M H_2SO_4 before (-.-.-.) and after (curves a-d) the addition of 5 mM DMSO. Anodic currents measured on the negative scans are shown as the dashed curves for DMSO oxidation (---). Oxidation of DMSO at the OAc-PbO_2 film began at E > 1.4 V in 1 M H_2SO_4 (curves a-d). Voltammetric currents varied substantially with rotation speed of the RDE. Half wave potential ($E_{1/2}$), was measured at *ca.* 1.55 V for DMSO oxidation on the positive scans.

The maximum catalytic efficiency at OAc-PbO_2 was obtained in 1 M H_2SO_4, for which small current of O_2 evolution and large current of DMSO oxidation were obtained. It was observed, however, severe O_2 evolution with virtually no anodic activity of DMSO occurred at the OAc-PbO_2 film in "1 M $HClO_4$" (result not shown). It was apparent that H_2SO_4 had an catalytic effect on the electrode reactivity of the OAc-PbO_2 film electrode.

In the absence of DMSO, there was virtually no faradic current detected within the potential region 1.4 to 1.7 V (curve -.-.-, Fig. 6). Evolution of O_2 became apparent at E > 1.75 V on the positive scan. In comparison, the potential observed for apparent O_2 evolution was more positive at the OAc-PbO_2 film-electrode than that for the pure PbO_2 (1.7 V), Au (1.6 V), and Pt (1.45 V) anodes. This observation suggested a possibility of a longer lifetime of $'OH_{ad}$ at OAc-PbO_2 at E $\leq$ 1.75 V,

before they formed O_2, than that for the pure PbO_2, Au, and Pt electrodes. Therefore, larger probability was obtained for $^{\cdot}OH_{ad}$ to transfer to the neighboring $DMSO_{ad}$ to produce the final product of $DMSO_2$.

Oxidations of toluene and *p*-xylene

Figure 7 shows the plots of 1/I *vs.* $1/w^{1/2}$ for the oxidation of toluene at 1.7 V at a pure (curve a) and OAc-doped (curve b) PbO_2-film electrode in 1 M H_2SO_4. Curve a for pure PbO_2 is linear over the entire range of $1/w^{1/2}$ values, whereas curve b for OAc-PbO_2 exhibits a distinct change in slope at intermediate values of $1/w^{1/2}$ to produce the two linear segments labeled b1 and b2. According to the Koutecky-Levich equation (Chap. II, Equation 3), the number of electrons transferred in an electrode reaction is inversely related to the slope of the plot. Therefore, the change of slope in curve b is concluded to be a consequence of a change in n_{eff} with decreasing *w* values for the better catalyzed reaction at the OAc-PbO_2 surface.

The consideration of a step-wise oxidation according to a simple *ee* mechanism was described in Chap. II. The value of n_{eff} for pure PbO_2 (curve a) was calculated to be *ca.* 2, assuming the diffusion coefficient $D = 10^{-5}$ cm^2 s^{-1} for toluene. Since the value of n_{eff} is inversely related to the slope in the plot of 1/I *vs.* $1/w^{1/2}$, the slope of the two linear segments in curve b (*i.e.*, b1/b2) was calculated to be 1.83 ($\simeq$ 2), indicating a value of $n_{eff} = 4$ eq mol^{-1} was obtained at low *w* values at the OAc-PbO_2 electrode. Values of $n_{eff} = 2$ and 4 were predicted to

correspond to reactions [1] and [2], respectively.

$$C_6H_5\text{-}CH_3 + H_2O \longrightarrow C_6H_5\text{-}CH_2OH + 2H^+ + 2e \quad [1]$$

$$C_6H_5\text{-}CH_3 + H_2O \longrightarrow C_6H_5\text{-}CHO + 2H^+ + 4e \quad [2]$$

At the pure PbO_2 electrode, the oxidation of toluene terminated with the production of benzyl alcohol (n = 2) with a heterogeneous rate constant of $k = 1.9 \times 10^{-3}$ cm s^{-1}. Whereas, the rate constant was increased by a factor of 26 at the OAc-PbO_2 surface, $k = 5.1 \times 10^{-2}$ cm s^{-1}. Furthermore, toluene can be catalytically oxidized to benzaldehyde at the highly active OAc-PbO_2 surface at low values of *w* according to reaction [2] shown above.

There was virtually no anodic activity detected for *p*-xylene at the pure PbO_2-film electrode. For OAc-PbO_2, significant anodic reactivity was observed and the anodic current showed rotation speed dependence for the entire range of *w* values. Figure 8 shows the plot of 1/I *vs.* $1/w^{1/2}$ for the oxidation of *p*-xylene at an OAc-PbO_2 film in 1 M H_2SO_4. The observation described above for the oxidation of toluene led to the consideration of possible step-wise oxidation for *p*-xylene at the OAc-PbO_2.

Based on the examination of the slope in the linear portion of the 1/I *vs.* $1/w^{1/2}$ plot in Fig. 8, n_{eff} for *p*-xylene oxidation was determined to be ca. 12, assuming value of $D = 10^{-5}$ cm^2 s^{-1} for *p*-xylene. Therefore, the oxidation of *p*-xylene at low values of *w* was tentatively concluded to correspond to reaction [3] with terephthalic acid as the product.

$$CH_3\text{-}C_6H_4\text{-}CH_3 + 4H_2O \longrightarrow\longrightarrow HOOC\text{-}C_6H_4\text{-}COOH + 12H^+ + 12e \qquad [3]$$

At large values of w (i.e., $w > 4900$ rev min^{-1}), anodic current of *p*-xylene at 1.7 V was observed to gradually decay to virtually zero value within a 45-min period electrolysis. However, based on the examination of charge corresponded to the area under this I-t curve, only 10% of *p*-xylene was oxidized. This observation suggested that surface fouling occurred at the OAc-PbO_2 electorde at values of w higher than 4900 rev min^{-1} (i.e., $1/w^{1/2} = 0.014$) in 1 M H_2SO_4 containing 5 mM *p*-xylene. The fouling process was speculated to occur via the formation of radicals which were strongly adsorbed at the electrode surface. These adsorbed radicals blocked the surface sites initially available for *p*-xylene adsorption, and resulted in retardation of the electrode reaction, and therefore, current decayed. Because of this fouling process, no attempt was made to investigate the n_{eff} value for *p*-xylene oxidation at regions of large values of w (i.e., small $1/w^{1/2}$) in Fig. 8.

Tafel plot for oxygen evolution

Both O_2 evolution and anodic O-transfer reactions (e.g., DMSO, toluene, and *p*-xylene) share one common reaction step. This step has been proposed to be the anodic discharge of water to produce adsorbed ·OH (4). Detailed description of this mechanism was presented in Chap. II.

The distinct enhancement of electrocatalytic reactivity of the PbO_2-film electrode from OAc^- doping, can signal a change of mechanisms

of O_2 evolution for these two electrodes. Experimentation was done to evaluate the kinetic parameters based on a plot of log(I) *vs.* overpotential, known as the *Tafel Plot* (8). Figure 9 shows the Tafel plots for the O_2 evolution process in 1 M H_2SO_4. Tafel plots are interpreted on the basis of Equation [4],

$$\log(I) = \log(I_o) + \frac{ßnF}{RT} \cdot \eta \qquad [4]$$

where η is the overpotential, I_o is the exchange current at $\eta = 0$, ß is the transfer coefficient, and n is the number of electrons transferred for the kinetically limited step (8). Curve a corresponds to a pure PbO_2 film, and curve b to an OAc-PbO_2 film, both of which were electrochemically deposited on the Au RDE. The data were taken from voltammetric curves recorded during the positive potential scan (20 mV s^{-1}). The overpotential η was measured relative to the standard reduction potential for the reaction: $H_2O \longrightarrow 1/2O_2 + 2H^+$ (1.23 V *vs.* NHE, or 0.99 V *vs.* SCE).

Kinetic results obtained from the Tafel plot for the pure and the OAc-PbO_2 electrodes are summarized in Table I. Values of the Tafel slopes obtained for O_2 evolution at OAc-PbO_2 (18.7 ± 0.9) and at pure PbO_2 (7.82 ± 0.05) corresponded to 53 mV/decade, and 128 mV/decade, respectively.

The anodic discharge of H_2O molecules has been concluded as rate determining for O_2 evolution with a Tafel slope of 2RT/F (118 mV/decade) (9). Therefore, it was concluded that the Tafel slope obtained for O_2

evolution at the pure PbO_2 film (122 ± 0.8 mV/decade) was considered to be characteristic of this limiting step. The Tafel slope obtained for OAc-PbO_2 (54.8 ± 1.4 mV/decade) was considered to be in good consistency with the value of RT/F (59 mV/decade). The different Tafel slopes for O_2 evolution at the pure PbO_2 and OAc-PbO_2 film electrodes could imply a change in rate-limiting step.

Based on the evaluation of Tafel slope and the expression RT/ßnF, the transfer coefficient (ß) for O_2 evolution was calculated to be 0.48 (n = 1 eq mol^{-1}), for which the formation of $.OH_{ad}$ at the pure PbO_2-film electrode was rate limiting. The nß value for OAc-PbO_2 was calculated to be 1.08, for which, reaction [6] was proposed as rate limiting.

$$S[\ ] + H_2O \longrightarrow S[.OH] + H^+ + e \quad \text{(slow at pure } PbO_2\text{)} \quad [5]$$

$$S[.OH] + OH^- \longrightarrow S[O] + H_2O + e \quad \text{(slow at OAc-}PbO_2\text{)} \quad [6]$$

$$2S[O] \longrightarrow 2S[\ ] + O_2 + 4e \quad [7]$$

where S[ ] represents the vacant surface site. Reaction [5] is the so-called "anodic discharge of water". This step was no longer rate limiting for O_2 evolution at the OAc-PbO_2 film electrodes. Therefore, it was concluded that the OAc-doped PbO_2 film was more active than the pure PbO_2 film for DMSO oxidation in terms of the formation of $\cdot OH_{ad}$ (reaction 5).

The exchange current (I_o) for O_2 evolution at the OAc-PbO_2 film was extremely small (1.15×10^{-12} µA), as compared with that for the pure

PbO_2 (2.45×10^{-4} μA). Exchange current reflects magnitude of the equilibrium rate constant (k_o) for the electrode reaction (10-12). Therefore, it was concluded that O_2-evolution process was suppressed at the OAc-PbO_2 film, as compared with that at the pure PbO_2-film electrode.

Conclusion

Distinct enhancement in the catalytic activity of the OAc-PbO_2 electrode for numerous anodic O-transfer reactions led to the consideration of possible changes in the catalytic mechanism for O_2 evolution process. Results obtained from Tafel plots (Fig. 9) indicated that doping OAc^- with PbO_2 could imply a change in rate determining step, for O_2 evolution, from the discharge of H_2O (120 mV/decade) to the deprotonation of $\cdot OH_{ad}$ (59 mV/decade). The formation of $\cdot OH_{ad}$ was promoted at the OAc-doped PbO_2 films, which favored the O-transfer reactions. However, the overall process of H_2O oxidation to from O_2 was suppressed as observed experimentally and revealed by the small exchange current ($I_o = 1.15 \times 10^{-12}$ μA) in comparison with the undoped films ($I_o = 2.45 \times 10^{-4}$ μA).

It is speculated that enhancement in the electrocatalytic property of OAc-PbO_2 in sulfuric acid, as compared with that in perchloric acid media, is a result of ion-exchange reaction between the surface OAc^- and solution HSO_4^-, as was observed for Cl-PbO_2 in H_2SO_4. The substitution of HSO_4^- for the surface OAc^- might cause interruption of the crystal

lattice as well as the electron density around Pb(IV), which in return result in catalytically active sites for reactants adsorption during the electrode reactions.

References

1. Hsiao, Y.-L.; Johnson, D. C. J. Electrochem. Soc. 1989, 136, 3704.
2. This dissertation, Chap. III.
3. This dissertation, Chap. II.
4. (a) Chang, H. Ph.D. Dissertation, Iowa State University, Ames, Iowa, 1987. (b) Yeo, I.-H. Ph.D. Dissertation, Iowa State University, Ames, Iowa, 1987. (c) Larew, L. A.; Gordon, J. S.; Hsiao, Y.-L.; Buttry, D. A.; Johnson, D. C. J. Electrochem. Soc. 1990, 137, 3701.
5. Sharpe, T. F. Encyclopedia of Electrochemistry of the Elements; Marcel Dekker; New York, 1975; vol I.
6. (a) Mindt, W. J. Electrochem. Soc. 1969, 116, 1076. (b) Carr, J. P.; Hampson, N. A. Chem. Rev. 1972, 72, 679.
7. Harada, H. J. Appl. Crystallogr. 1981, 13, 141.
8. Tafel, J. Z. Physik. Chem. 1905, 50A, 641.
9. Bockris, J. O'M. J. Chem. Phys. 1956, 24, 817.
10. Bard, A. J.; Faulkner, L. R. Electrochemical Methods, Fundamentals and Applications; John Wiley & Sons: New York, 1980; Chap. 3.
11 Bockris, J. O'M.; Reddy, A. K. N. Modern Electrochemistry; Plenum: New York, 1970; vol. 2, chap. 9.
12. Kiss, L. Kinetics of Electrochemical Metal Dissolution; Elsevier Science Publishing Co., Inc.: New York, 1988, p. 60.

Table I. Kinetic data obtained from the Tafel plot in Fig. 9 for the O_2 evolution process in 1 M H_2SO_4

Film	slope (mV/decade)	I_o (uA)[a]	nß
pure PbO_2	122.3 ± 0.8	(2.45 ± 0.06) x 10^{-4}	0.48
OAc-PbO_2	54.8 ± 1.4	(1.15 ± 0.13) x 10^{-12}	1.08

[a]Exchange current at overpotential (η) = 0.

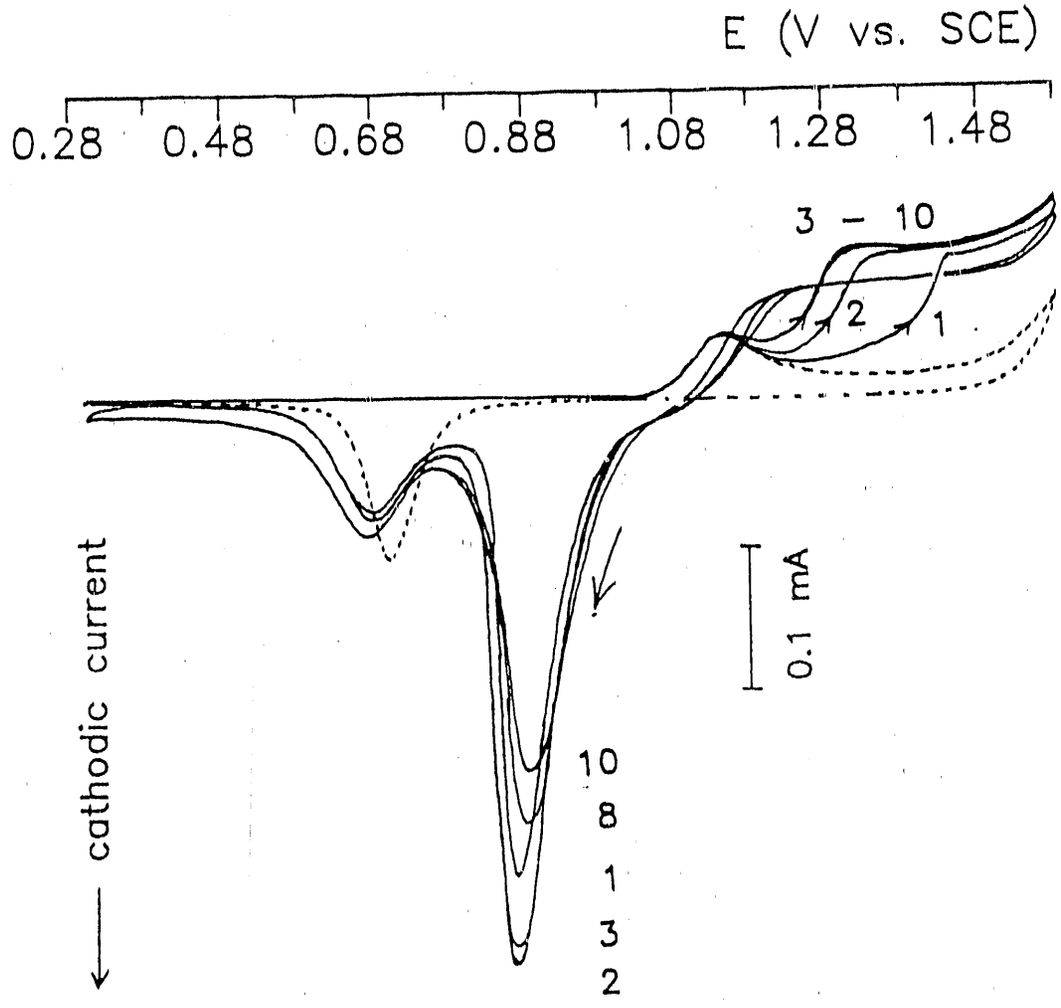

Figure 1. Cyclic voltammograms for the deposition of OAc-PbO_2 film at the Au RDE

Conditions: 50 mV s^{-1}, 900 rev min^{-1}, NaOAc buffer (pH 3.74)

Curves: (.....) residual,
(———) 0.42 mM Pb^{2+}

(Numbers indicate the order of potential scans)

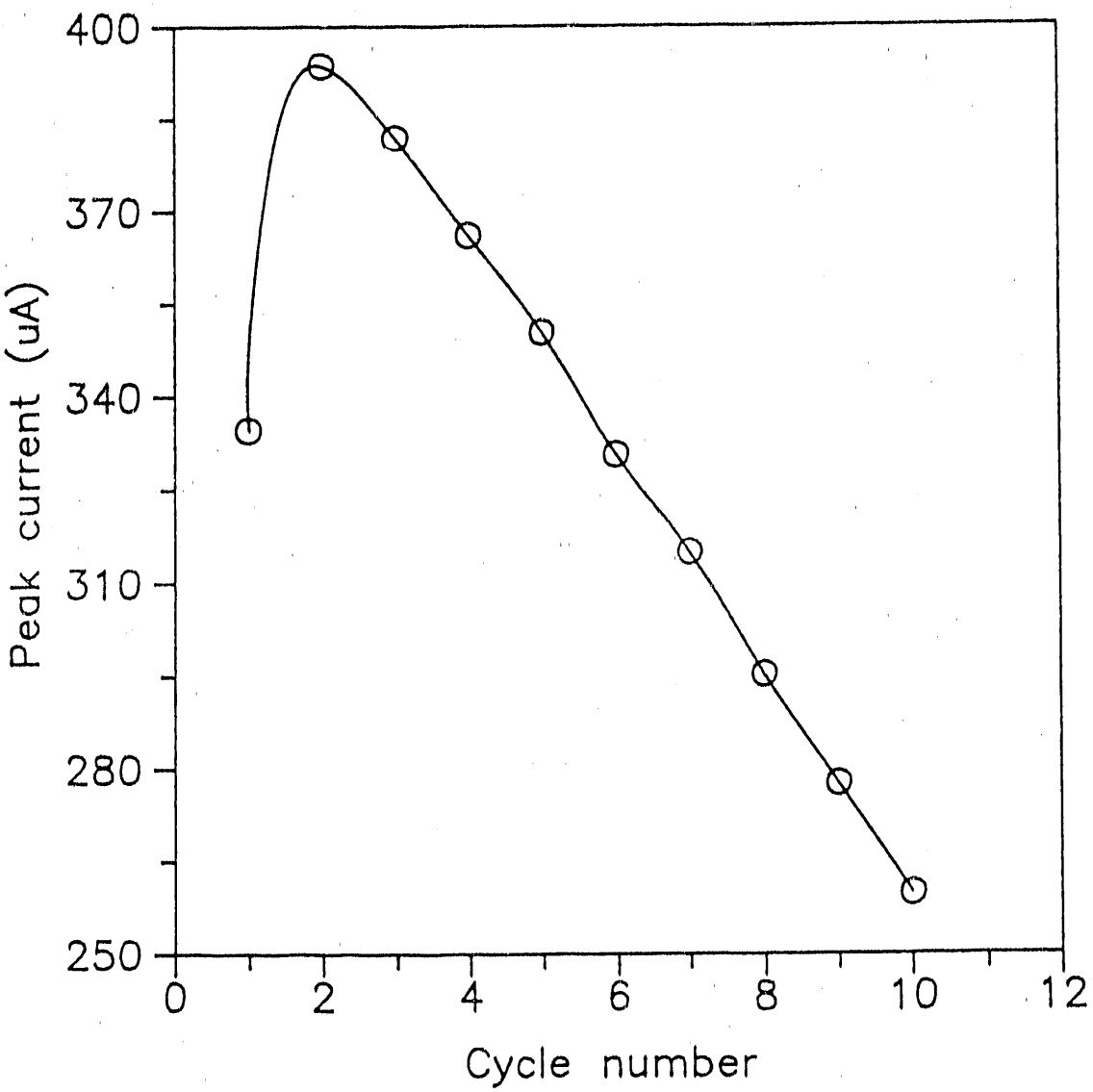

Figure 2. Plot of peak current for the reduction of PbO_2 at E = 0.8 V (data taken from figure 1) *vs.* scan number for the electrodeposition of PbO_2 at the Au RDE

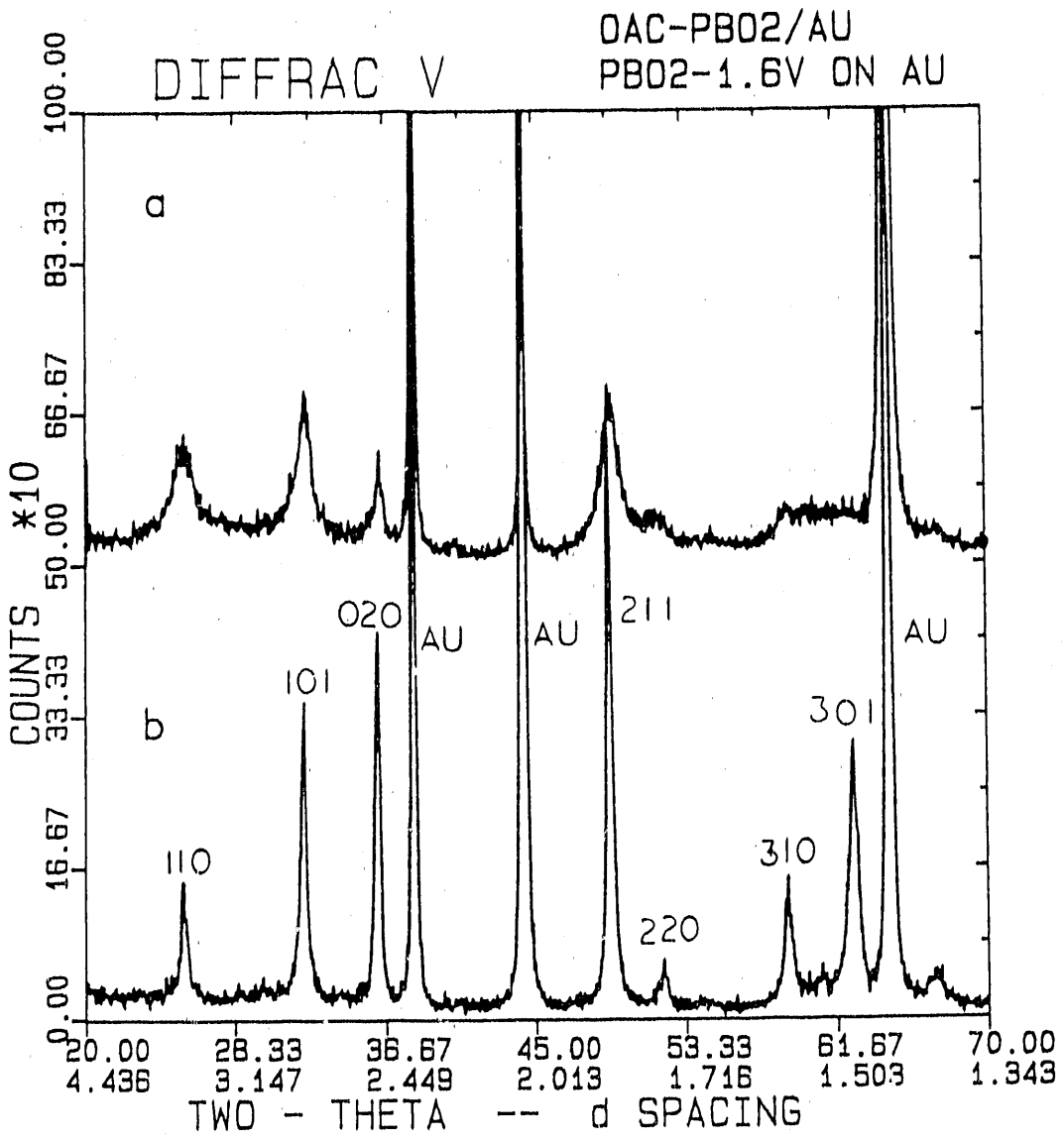

Figure 3. X-ray diffraction patterns of PbO_2 films deposited on Au RDE

(a) OAc-doped PbO_2 film on Au,
(b) pure PbO_2 film on Au

(Numbers indicate the specified crystal planes)

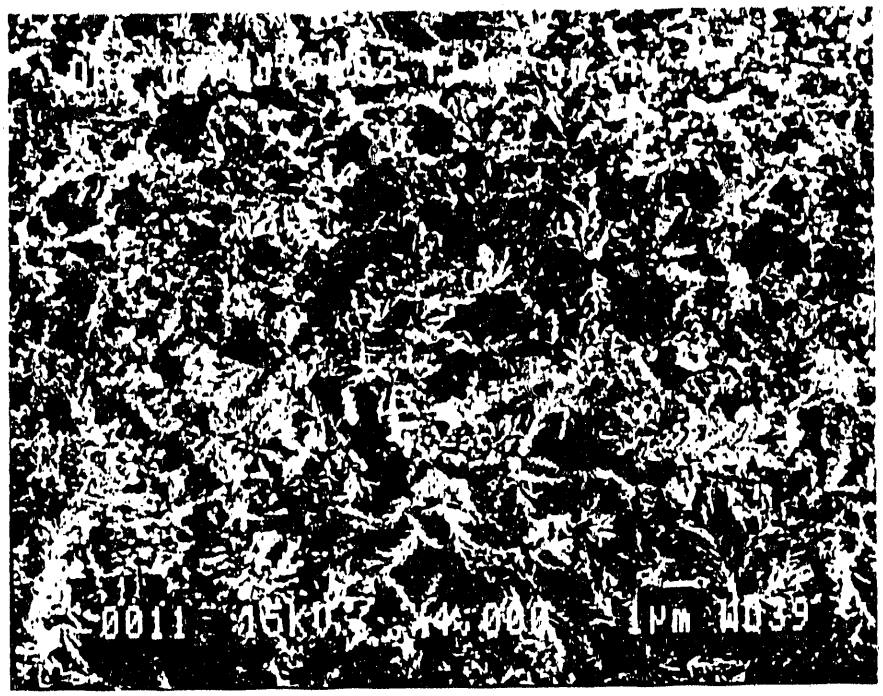

Figure 4. Scanning electron micrograph (X 4000) of the surface of the OAc-PbO_2 film deposited on Au

Deposition conditions: 1.4 mM Pb^{2+}, 1.36 V, 900 rev min^{-1}, 20 min, NaOAc buffer (pH 3.74)

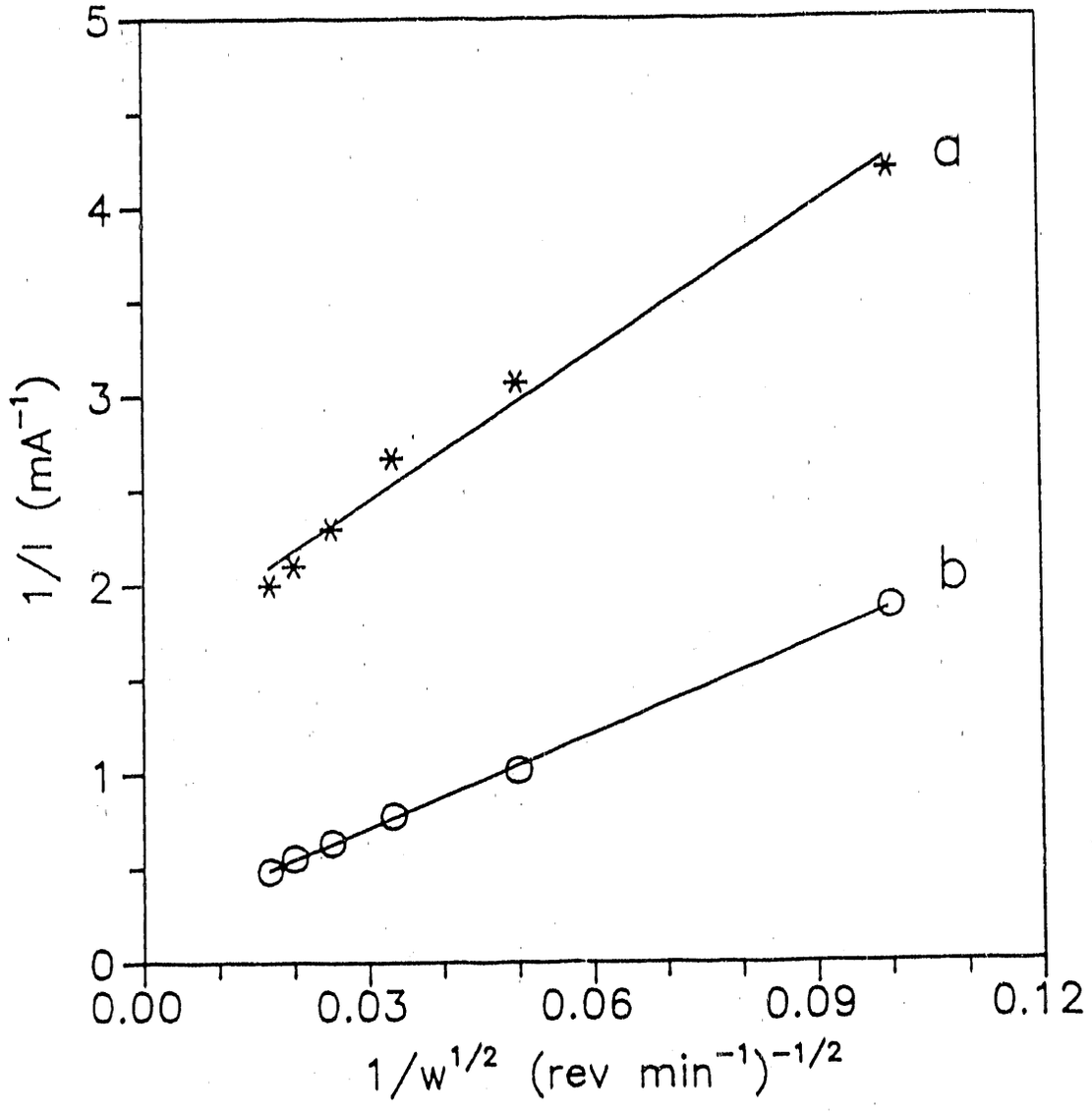

Figure 5. Plot of 1/I *vs.* $1/w^{1/2}$ for the oxidation of DMSO at the OAc-PbO_2 films on Au RDEs

Conditions: 5 mM DMSO, E = 1.7 V

Electrolyte: (a) 1 M $HClO_4$,
(b) 1 M H_2SO_4

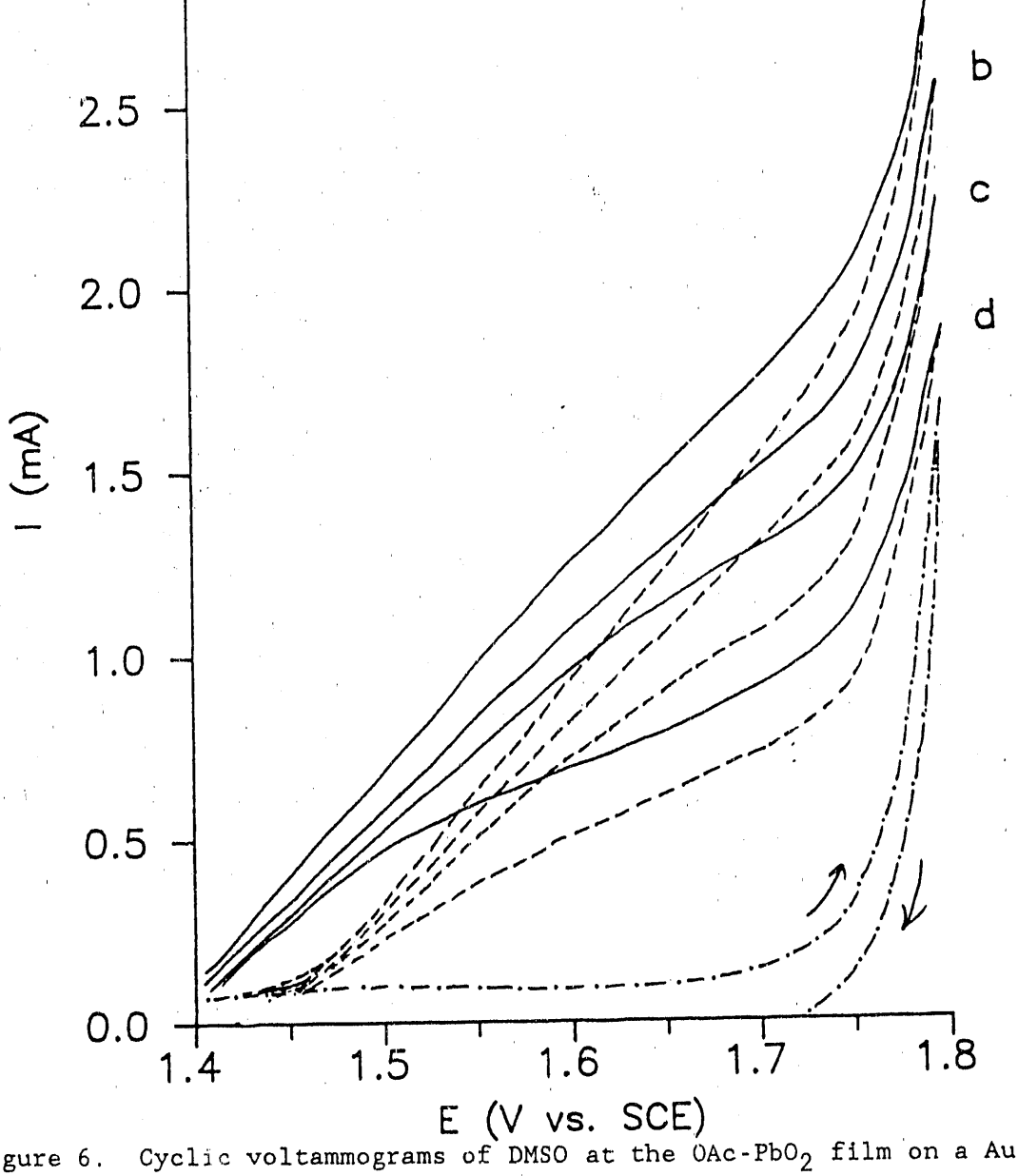

Figure 6. Cyclic voltammograms of DMSO at the OAc-PbO_2 film on a Au RDE

Conditions: 1 M H_2SO_4, 20 mV s^{-1}.

Curves: (-.-.-) residual,
(———) 5 mM DMSO (positive scan),
(-----) 5 mM DMSO (negative scan)

Rotation speed (rev min^{-1}): (a) 2500, (b) 1600, (c) 900, (d) 400

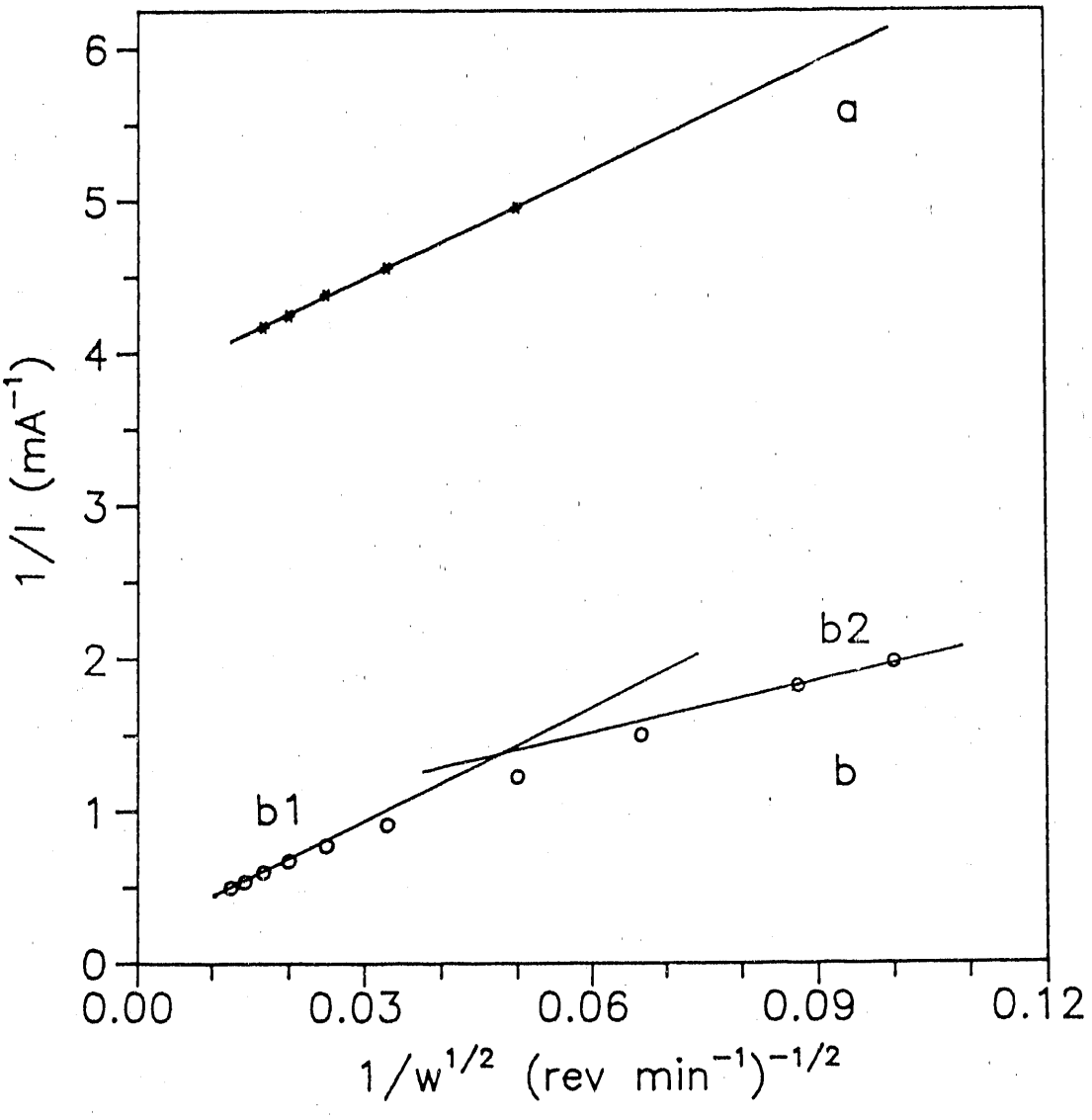

Figure 7. Plot of 1/I *vs.* $1/w^{1/2}$ for the oxidation of toluene in 1 M H_2SO_4

Conditions: 5 mM toluene, 1 M H_2SO_4, E = 1.7 V

Electrodes: (a) pure PbO_2 film on Au RDE,
(b) OAc-PbO_2 film on Au RDE

Values of n_{eff} (eq mol^{-1}): (a) 2, (b1) 2, (b2) 4

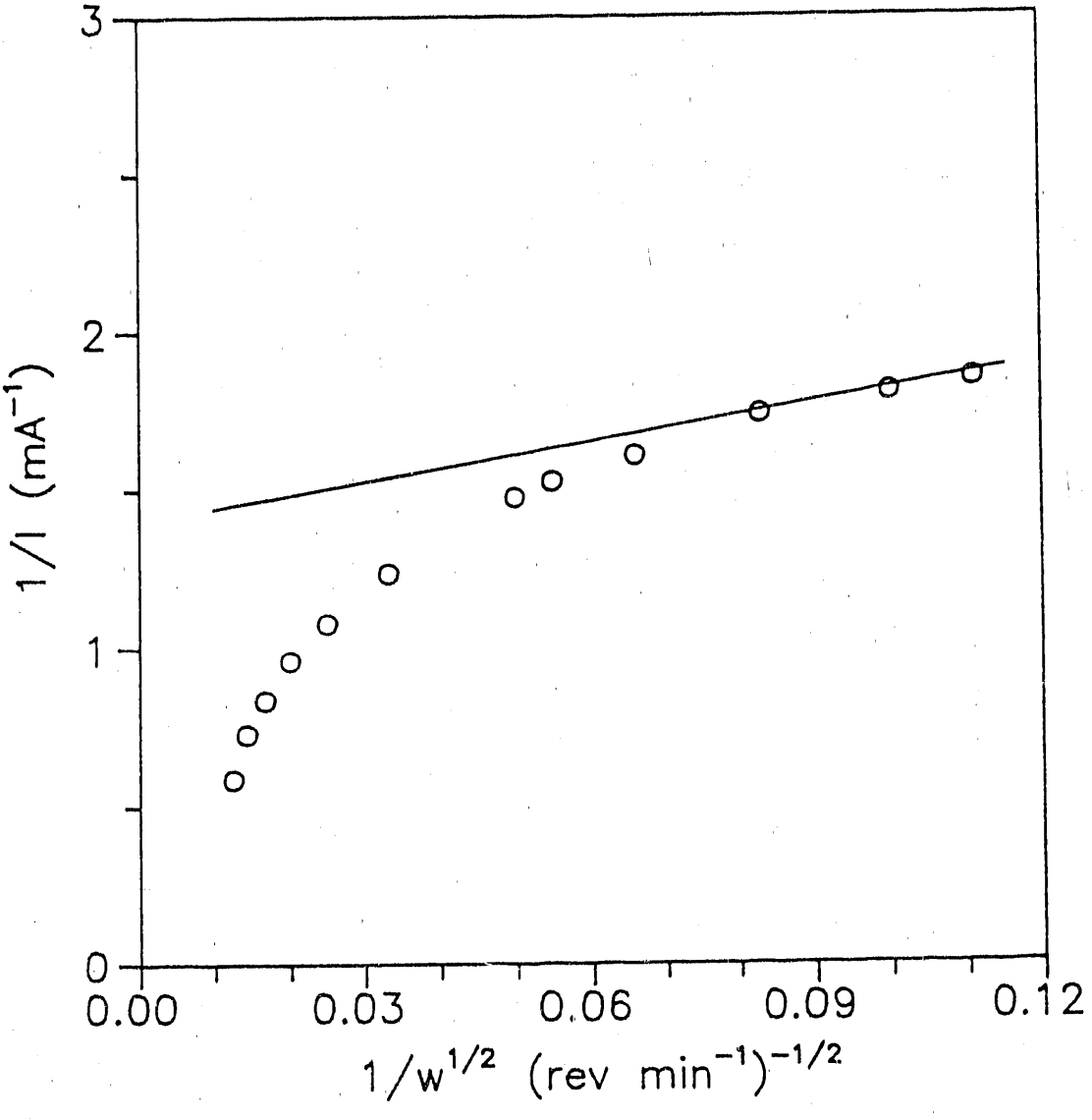

Figure 8. Plot of 1/I *vs.* $1/w^{1/2}$ for the oxidation of *p*-xylene in 1 M H_2SO_4

Conditions: 5 mM *p*-xylene, 1 M H_2SO_4, E = 1.7 V

Electrode: OAc-PbO_2 film on Au RDE

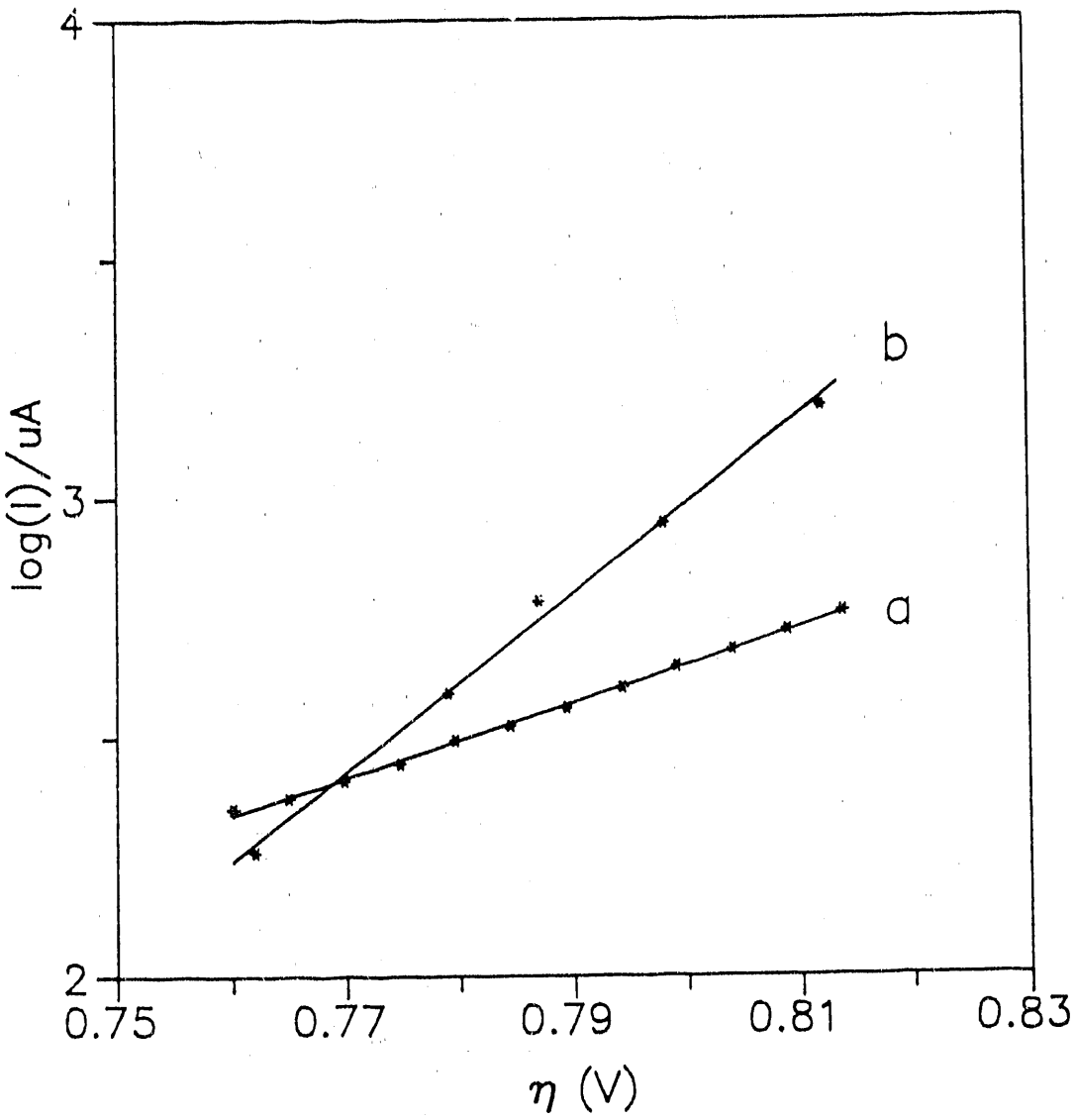

Figure 9. Tafel plot for O_2 evolution process in 1 M H_2SO_4

Conditions: 20 mV s^{-1}, 900 rev min^{-1}

Electrodes: (a) pure PbO_2 film on Au RDE,
(b) OAc-PbO_2 film on Au RDE

CHAPTER V.

STUDIES OF ELECTROCHEMICAL BEHAVIOR OF LEAD DIOXIDE ELECTRODES ACTIVATED BY CYCLIC VOLTAMMETRIC SCANS IN SULFURIC ACID SOLUTION

Abstract

Anodes comprised of electrochemically deposited ß-PbO_2 films on solid conducting substrates were shown to exhibit enhanced electrocatalytic reactivity for the oxidations of benzyl alcohol and dimethyl sulfoxide (DMSO) following repeated cyclic voltammetric scans in 1 M H_2SO_4. Linear sweep voltammetry and an Electrochemical Quartz Crystal Microbalance (EQCM) were used to study the electrochemical behavior of PbO_2-film electrodes. Examinations on surface morophology and exposed crystallite orientations of the PbO_2 films were performed using scanning electron microscopy (SEM), and X-ray diffractometry (XRD), respectively. Multiple layers of $PbSO_4$ were formed as reduction product of PbO_2 during the negative potential scans in 1 M H_2SO_4. However, the rate of reoxidation of $PbSO_4$ back to PbO_2 was slow, which resulted in the gradual accumulation of $PbSO_4$ in the matrix of PbO_2 during the repeated voltammetric scans. The PbO_2 matrix was expanded by the incorporated $PbSO_4$ because of a larger value of the molecular size for $PbSO_4$ than that for PbO_2. However, the size of the matrix did not resume its initial value during the succeeding positive scan (1). A

porous structure and an increase in the true surface area was obtained as a result of the expanding mitrix.

Introduction

As was described earlier (Chap. III), the Cl-doped PbO_2-film electrodes (Cl-PbO_2) were more active in 1 M H_2SO_4 than in 1 M $HClO_4$ for the oxidations of DMSO and Mn^{2+} (2). That observation led to the consideration of catalytic modification of PbO_2 films by co-deposition of SO_4^{2-} simultaneously with PbO_2. However, this was not possible because of the low solubility of $PbSO_2$.

An alternate procedure for incorporation of SO_4^{2-} into the matrix of PbO_2 will be described. This process involves cyclic voltammetry between the potential limits of 0.5 and 1.8 V with the PbO_2-film electrode immersed in 1 M H_2SO_4. This procedure has obvious similarilities to the charge/discharge processes for lead-acid batteries.

The charge/discharge process for the lead-acid battery in H_2SO_4 solution has been investigated by many workers (1, 3-9). Due to the difference in molecular sizes for $PbSO_4$ and PbO_2, increases in the size of the matrix occur during the discharge process (PbO_2 to $PbSO_4$). A "breathing" model has been established for this process to explain the irreversible swelling of the positive plate after several repeated cyclings (1). It has also been reporterd that there was $PbSO_4$ deposited at the electrode surface as well as at the interface of PbO_2 film and Au

substrate if the PbO_2 was discharged at a temperature higher than room value (e.g., 50°C) (9). The relative intensities of diffraction peaks corresponding to (002) and (020) crystal planes of $PbSO_4$ were different for that at the surface and the interface. A conclusion was made that the $PbSO_4$ growth at the interface may be limited in the direction parallel to the substrate, and, therefore, it is difficult to oxidize such orientated $PbSO_4$ (9).

For the studies reported here, the amount of SO_4^{2-} incorporated in PbO_2 was controlled by changing experimental parameters such as scan rate, scan limits, and number of the potential scans. Electrocatalytic properties of the cycled PbO_2-film electrodes were studied based on the kinetic data obtained for the oxidations of DMSO and benzyl alcohol.

Experimental

Apparatus

A three-compartment electrolysis cell was used with the Pt-wire counter electrode separated from the working solution by a fritted-glass junction. The SCE reference contacted the working solution through a Harber-Luggin capillary. Current potential curves were obtained by cyclic voltammetry at a Au rotated disc electrode (RDE, 0.1642 cm^2) in a PIR rotator with an RDE3 potentiostat (Pine Instrument) and a model 2000 X-Y recorder (Houston Instrument).

Surface morphologies of the ß-PbO_2 film electrodes before and after the consecutive potential scans in 1 M H_2SO_4 were examined using a model

JSM-840A scanning electron microscopy (SEM) (Jeol). X-ray diffraction data were obtained with a model D500 diffractometer and crystal monochromatized Cu Kα (λ = 1.54184 Å) radiation (Siemens). Value of the film thickness of PbO_2 was 0.3um, as determined by an α-step surface profile (Tencor).

Reagents

All chemicals were analytical reagent grade and solutions were prepared from distilled water purified in a NANOpure-II deionized system (SYBRON/Barnstead). The supporting electrolytes were 1.0 M $HClO_4$ for electrodeposition of the oxide films, and 1.0 M H_2SO_4 for kinetic testing and cyclic voltammetry.

Procedure

Prior to electrodeposition, the Au RDE was polished with 0.5-um alumina powder (Buehler Ltd.) followed by rinsing with copious amount of deionized water. Then, the electrode potential was cycled between the scan limits of 0.5 V and 1.8 V in 1.0 M $HClO_4$ until a reproducible cyclic voltammogram was obtained which represents the clean Au surface.

The ß-form PbO_2, having a slightly distorted rutile structure, was electrochemically deposited on the Au RDE (900 rev min^{-1}) at 1.6 V, 1.7 V or 1.8 V in a deposition solution of 1 M $HClO_4$ containing 1.67 mM $Pb(NO_3)_2$. The electrodes were rinsed with deionized water after preparation and were used immediately, unless specified to the contrary. A uniformly black oxide film was achieved during a 20-min deposition period. The PbO_2 mentioned in the rest of this paper denotes to the ß-

form structure unless otherwise specified.

Cycling process for the pre-deposited PbO_2-film electrode was achieved by scanning the electrode potential between the potential limits of 0.5 V and 1.8 V (50 mV s^{-1}) in 1 M H_2SO_4 at 1600 rev min^{-1} for the rotated disc electrode. All kinetic measurements were obtained in 1 M H_2SO_4.

Studies of the mass change at electrode surface was performed by using an Electrochemical Quartz Crystal Microbalance (EQCM) with PbO_2 film deposited on the Au-coated quartz crystal (Au/QC). Preparation of the PbO_2 film was done by potential step from 1.5 V to 1.7 V in 1 M $HClO_4$ containing 1.67 mM $Pb(NO_3)_2$ for 120 sec with N_2 purging. This procedure was repeated for three times to achieve a uniform brown color of PbO_2 film.

Current-potential (I-E) and frequency-potential (f-E) responses at the Cl-PbO_2 film on Au/QC were obtained simultaneously during the cyclic voltammetric scan. Values of potential quoted for EQCM measurements were measured *vs.* Ag/AgCl reference. Preparations and general operation theory for the EQCM have been previously described (2).

Reactions under mixed transport-kinetic control at the rotated electrode were assumed to be consistent with the Koutecky-Levich equation as follows (10-13).

$$\frac{1}{I} = \frac{1}{n_{eff}FAK_{app}C^b} + \frac{1}{0.62n_{eff}FAD^{2/3}\nu^{-1/6}C^b}\left[\frac{1}{w^{1/2}}\right] \qquad [1]$$

The significances of this equation were discussed in Chap. II. Values of heterogeneous rate constants were calculated from the intercepts of plots of $1/I$ *vs.* $1/w^{1/2}$ according to the Koutecky-Levich equation. All values of I were corrected for the background current measured in the absence of solution reactants.

Results and Discussion

Cyclic voltammetry of ß-PbO_2 in sulfuric acid

Cyclic voltammetric response is shown in Fig. 1A for the pre-deposited PbO_2 film in 1 M H_2SO_4. The oxide film was electrodeposited at a constant potential of 1.7 V (20 min) and the I-E curves were obtained starting at 1.8 V. Numbers indicate the order of the cyclic voltammetric scans. It should be noted that Pb^{2+} was NOT present in the solution. Therefore, any voltammetric responses shown in this figure was due to the electrochemical reactions between the PbO_2-film electrode and the H_2SO_4/H_2O electrolyte.

The cathodic peak at 1.13 V on the first potential scan was anticipated to correspond to the reduction of PbO_2 to $PbSO_4$ at the electrode surface. Reoxidation of the surface $PbSO_4$ to PbO_2 was observed at $E > 1.2$ V on the succeeding positive scan. The wave obtained at $E > 1.55$ V was concluded to result from O_2 evolution.

Based on the examination of the charge corresponded to the areas under the anodic and cathodic peaks, it is apparent that the $PbSO_4$ produced during the negative potential scan was not completely

reoxidized on the following positive scan. It has been reported that the oxidation of $PbSO_4$ to PbO_2 is a slow reaction involving a nucleation process with a long induction period (14). Therefore, only a relatively small amount of $PbSO_4$ was reoxidized (11%) during the succeeding positive scan (Fig. 1A, curve 1).

Interesting phenomena were observed for the second voltammetric scan. The peak potential for the reduction of PbO_2 shifted to a more positive value and two peaks were resolved within the potential region of 1.2 V to 1.4 V. In addition, the height of the anodic peak for the oxidation of $PbSO_4$ at 1.4 V, and the magnitude of the current wave obtained for O_2 evolution were larger than those for the first scan.

Subsequently, the peak currents for the cathodic production of $PbSO_4$ continued to increase. However, on the positive scans, the anodic peak currents produced for the reoxidation of $PbSO_4$ to PbO_2 at 1.4 V did not vary substantially with cycle number for 30 scans. This observation indicated that an increasing amount of $PbSO_4$ was incorporated into the matrix of PbO_2 following every cycle. This incorporation was expected to result in a sulfate-doped PbO_2 film-electrode (SO_4^{2-}-PbO_2).

The O_2-evolution process at $E > 1.55$ V became more and more apparent as scan number increased (Fig. 1A, curves 10-30), with an increase of 4.7x (from 1.6 mA to 7.5 mA) for the current at 1.8 V during the the first 30 cycles. It was speculated that the electrode was activated by the incorporated $PbSO_4$ during the cyclic potential scans. These results were indicative of an apparent catalytic production of O_2 at SO_4^{2-}-PbO_2, as compared with that for the pure PbO_2.

Cyclic voltammetry was also performed at a pure PbO_2-film electrode according to the exact conditions described for Fig. 1A, except for using 1 M $HClO_4$ as the electrolyte. The current-potential curves (results not shown) were different in many aspects from those obtained in 1 M H_2SO_4. On the 1st negative potential scan, the reduction of PbO_2 in 1 M $HClO_4$ produced a cathodic peak current 12.5 times larger than that obtained in 1 M H_2SO_4. Also, there was virtually no cathodic current detected for the reduction of PbO_2 subsequent to the 1st potential scan. These observations indicated that the cathodic reduction of PbO_2 in 1 M $HClO_4$ produced soluble Pb^{2+} which was quickly transported away from the rotated disc electrode. It was concluded that almost all of the oxide film was reductively dissolved during the first negative scan in 1 M $HClO_4$.

The uncycled PbO_2 film was 0.3 μm thick, as determined by the a-step surface profile. The concentration of Pb^{2+}, as dissolved from this ultra thin film, was too low ($\simeq$ 20 μM) for the redeposition of PbO_2 to be efficient during the proceeding positive scan (25 sec). Thereby, no PbO_2 will be available to produce any cathodic current after the first scan in 1 M $HClO_4$. In fact, the Au substrate became visible thereafter.

Conversely, formation of $PbSO_4$ occurred in 1 M H_2SO_4 containing Pb^{2+}, which stabilized the reduction product of PbO_2 (Pb^{2+}) during the negative scan. Cathodic currents produced for the reduction of PbO_2 continued to be measured subsequently (Fig. 1A, curves 2-30). It is evident that $PbSO_4$ remained at the electrode surface.

It has been noted that the electrocatalytic properties of the PbO_2-film electrodes were dependent of the potential applied during the deposition process (15). Interestingly, the cyclic voltammograms of the PbO_2 film (pre-deposited at 1.8 V) in 1 M H_2SO_4 were different in many aspects from those for the PbO_2 film deposited at 1.7 V. Typical voltammetric results are shown in Fig. 1B.

The PbO_2 film deposited at 1.8 V showed the following features, in comparison with that deposited at 1.7 V.

1. The cathodic peak potential in scan 1 was measured at 70 mV more positive (1.20 V *vs.* 1.13V).
2. The cathodic peak current for the reduction of PbO_2 were larger for the corresponding scans.
3. The average current value of the anodic peak for $PbSO_4$ oxidation measured at 1.4 V was 6.6 times larger (4.38 mA *vs.* 0.58 mA).
4. The rate of increase in the current for O_2 evolution was much significant at E > 1.55 V.
5. Additional anodic peaks were observed in the O_2 evolution region (1.6 V and 1.75 V) subsequent to the 29th scans.

Since larger amounts of $PbSO_4$ were reoxidized during the succeeding positive scans, the reduction of PbO_2 to $PbSO_4$ was concluded to be more reversible at the PbO_2 deposited at 1.8 V than that deposited at 1.7 V. Results also indicated possible formation of lead dioxide in a higher oxide state, as shown by additional anodic peaks for E > 1.55 V. It has been reported that the varying crystal structure on the Au surface or changes in the packing of Pb atoms on the surface resulted in cathodic peaks measured at different potentials during the underpotential

deposition (UPD) of Pb (16). Therefore, the results obtained in Figs. 1A-1B indicated possible dependence of the crystal planes exposed at the PbO_2 film and the potential applied during the deposition process. Therefore, different shapes of the cyclic voltammograms were obtained at PbO_2 film deposited at different potential because of the different crystal planes exposed.

X-ray diffraction patterns

Figure 2A shows the X-ray diffraction patterns of the PbO_2 films deposited at 1.6 V (pattern a) and 1.8 V (pattern b). It is apparent from this figure that the deposition potential affected the preferential orientations of the crystallite plane exposed at the PbO_2 surface. The intensities for diffraction peaks corresponding to the (101), (020), (211), and (310) planes observed at the PbO_2 deposited at 1.6 V disappeared when the PbO_2 was deposited at 1.8 V. A summary of the peak intensities for the specified crystal planes is shown in Table I.

As was described before, gradual accumulation of $PbSO_4$ in PbO_2 matrix occurred during the repeated cyclic potential scans in 1 M H_2SO_4. The X-ray diffractometer was used to analyze this accumulation. The X-ray diffraction patterns are shown in Fig. 2B for a pre-deposited ß-PbO_2 film on Au substrate before (pattern a) and after (pattern b) 50 cyclic potential scans in 1 M H_2SO_4. Intensities of the diffraction peaks corresponding to $PbSO_4$ (open circles) were observed in addition to those for PbO_2 (filled circles) after 50 cycles. It has been reported that both $PbSO_4$ and PbO were reduction products of PbO_2 during the discharge

process for lead-acid battery (8, 17). However, since most of the diffraction peaks corresponding to PbO overlay with those of PbO_2 (18), it is difficult to assign the intensities for PbO among those of PbO_2 in this pattern.

It is apparent from Fig. 2B that the ß-form of rutile structure of PbO_2 was retained even after 50 consecutive potential cycles. However, the relative intensity for the diffraction peaks corresponding to (301) ($2\theta = 62.5$) and (310) ($2\theta = 60$) crystal planes was stronger for the PbO_2 after 50 cycles.

Figure 2C shows the X-ray diffraction patterns for the pre-deposited PbO_2 after 50 (pattern a) and 150 (pattern b) cyclic potential scans in 1 M H_2SO_4. It is apparent that the relative intensity for the diffraction peaks $(PbSO_4)/(PbO_2)$ is stronger after 150 cycles. A summary is presented in Table II for the relative intensity of the diffraction peaks corresponding to the specified crystal planes of PbO_2 and $PbSO_4$, before and after the cyclic potential scans. It was concluded that accumulation of $PbSO_4$ occurred at the PbO_2 surface during the cyclic potential scans in 1 M H_2SO_4. This accumulation is consistent with an increased intensity ratio $(PbSO_4)/(PbO_2)$ for the X-ray diffraction peaks with increasing cycle numbers.

Scanning electron micrographs

Figure 3 shows scanning electron micrographs (SEM) of the surface of PbO_2 films after 50 (a), and 150 (b) cyclic potential scans in 1 M H_2SO_4. The effect of scan number on the sizes and shapes of the

crystals are very apparent in thses micrographs. These big crystals were speculated to be $PbSO_4$. It is clear that these crystals are shaped as cubes. The crystal size of $PbSO_4$ increased with increasing cycle numbers of the voltammetric scans.

It was reported that $PbSO_4$ crystals grow via the "dissolution-precipitation" process in sulfuric acid solution (19). Larger $PbSO_4$ crystals are formed at the latter potentiostatic discharge process (19, 20). Since the rate of oxidation of $PbSO_4$ is inversely related to the crystal size (20); therefore, it becomes more and more difficult for the oxidation of $PbSO_4$ to occur after several potential scans due to the increased crystal sizes (Figs. 3a-b).

Studies with the electrochemical quartz crystal microbalance

Experimentation was done to investigate mass changes at the surface of a PbO_2 film during the cyclic potential scan. Measurements with the electrochemical quartz crystal microbalance (EQCM) were performed with a PbO_2 film electrochemically deposited on the Au-coated quartz crystal (Au/QC). Figure 4A shows the current-potential (I-E) response obtained during the cyclic scan in 1 M H_2SO_4. Cathodic reduction of PbO_2 film began at $E < 1.3$ V on the negative potential scan followed by the cathodic stripping of Au oxide at 0.9 V. Since the film thickness of PbO_2 on the Au-coated quartz crystal was much less than that on the Au RDE, the relative peak height for the reduction of Au oxide to that of PbO_2 reduction was much larger than that deposited at the Au RDE (Fig. 1A).

A positive frequency change ($df > 0$) indicates a loss of mass ($\Delta m < 0$). The reduction of 1 mole of PbO_2 to 1 mole of $PbSO_4$ corresponds to a mass increase of 1 mole of SO_2, which consequently resulted in a negative frequency change. Figure 4B shows the frequency-potential (f-E) response obtained simultaneously with Fig. 4A at the PbO_2 film deposited on Au/QC. An increase in the frequency response detected at $E < 1.3$ V on the negative potential scan was concluded to result from the cathodic reduction of PbO_2 to $PbSO_4$. Whereas, there was virtually no frequency change detected during the succeeding positive scan.

The frequency response shown in Fig. 4B was divided into four labeled regions: (a) an increase; (b) a sharp decrease; (c) a gradual decrease, and (d) a slight increase regions. These frequency changes corresponded to a mass decrease (region a), mass increases (regions b-c), and a mass decrease (region d) at the electrode surface during the negative potential scan. The experimental values of $\Delta m/\Delta q$ were calculated from the slopes of plots of frequency-charge shown in Fig. 4C for the cyclic potential scan. The letters, a, b, c, and d correspond to the lettered regions shown in Fig. 4B.

Region a As was mentioned before, the formation of $PbSO_4$ proceeds via the "dissolution-precipitation" process (19). The loss of mass at the electrode surface for region a was anticipated to correspond to the "reductive dissolution" of PbO_2 to Pb^{2+}, and the experimental value of $\Delta m/\Delta q$ (1.35 mg $coul^{-1}$) was considered to be in good agreement

with the theoretical value (1.24 mg $coul^{-1}$) for the following reaction.

$$PbO_{2(s)} + 4H^+ + 2e \longrightarrow Pb^{2+} + 2H_2O \quad [2]$$

Region b The sharp decrease in frequency of the quartz crystal for region b was ascribed to the reduction of PbO_2 to $PbSO_4$ (reaction [3]) plus the "precipitation" of Pb^{2+}, from reaction [2], with HSO_4^- to form the insoluble $PbSO_4$ at the electrode surface (reaction [4]).

$$PbO_{2(s)} + 3H^+ + HSO_4^- + 2e \longrightarrow PbSO_{4(s)} + 2H_2O \quad [3]$$

$$Pb^{2+} + HSO_4^- \longrightarrow PbSO_{4(s)} + H^+ \quad [4]$$

The experimental value of $\Delta m/\Delta q$ = 1.80 mg $coul^{-1}$ was in good consistency with the theoretical value ($\Delta m/\Delta q$ = 1.90 mg $coul^{-1}$) obtained for the combination of reactions [3] and [4].

Region c For this region (E = 1.1 to 0.7 V), the majority of charge was concluded to come from the reduction of Au oxide. This process should result in a "positive" frequency change as a result of negative mass change (Δm = -16 g mol^{-1}) at the electrode surface according to the reaction: $AuO_{(s)} + 2H^+ + 2e \longrightarrow Au_{(s)} + H_2O$, for which $\Delta m/\Delta q$ = 0.083 mg $coul^{-1}$. However, Fig. 4B showed a "negative" frequency change with $\Delta m/\Delta q$ = 0.35 mg $coul^{-1}$. Therefore, the formation of insoluble $PbSO_4$ via reaction [4], (Δm = 303 g mol^{-1}) was concluded to accompany the reduction of AuO in this region.

Region d There was no significant frequency change at the quartz crystal during the succeeding positive scan. A slight increase of frequency at E > 1.6 V (region d) was accounted for the loss of SO_2 at the electrode surface via the oxidation of $PbSO_4$ to PbO_2 (reversed reaction [3]). Both O_2 evolution and the formation of Au oxide contributed charges to the measurement, which made it difficult to determine the charge quantity produced solely for $PbSO_4$ oxidation. Therefore, no attempt was made to elucidate the $\Delta m/\Delta q$ values for this region.

Catalytic oxidation of DMSO

Figure 5A shows typical voltammograms obtained at the PbO_2-film electrode in 1 M H_2SO_4 before (---) and after (——) the addition of 125 mM DMSO. In the absence of DMSO, the cathodic reduction of PbO_2 was measured at peak potential (E_p) = 1.2 V on the negative scan. The reoxidation of surface $PbSO_4$ to PbO_2 occurred at E > 1.4 V with E_p = 1.5 V on the succeeding positive scan followed by O_2 evolution at E > 1.6 V.

The apparent onset of DMSO-oxidation wave occurred concomitantly with O_2 evolution, and stopped before the reduction of PbO_2 commensed (E = 1.4 V). The anodic currents showed apparent rotation speeds dependence. On the other hand, the reduction of PbO_2 was affected by the presence of DMSO, as shown by slight shift of the cathodic peak to a more positive potential.

Figure 5B shows cyclic voltammograms of DMSO at the PbO_2-film electrode in 1 M H_2SO_4. The dashed curve represents the residual current measured in the absence of DMSO. The solid waves a-d show the anodic current of DMSO at various concentrations from 125 mM to 400 mM.

Experimentations were also done at the Cl-doped PbO_2-film electrode (Cl-PbO_2) according to the exact conditions described for Figs. 5A-B. The Cl-PbO_2 film was electrodeposited on Au RDE at concentration ratio of $[Cl^-]/[Pb^{2+}]$ = 0.3. Figure 6A shows cyclic voltammograms at Cl-PbO_2 in 1 M H_2SO_4 before (---) and after (——) the addition of 200 mM DMSO. efore the addition of DMSO, the cathodic peak for Cl-PbO_2 reduction was measured at E_p = 1.25 V on the negative scan. The reoxidation of $PbSO_4$ was measured at potentials more positive than that for the pure PbO_2 (Fig. 5A, curve ---), and the anodic peaks measured were a sharp (E_p = 1.6 V), and a broad (1.7 V) peaks. It was speculated that this sharp peak which was not observed for the pure PbO_2 was related to the oxidation of Pb^{2+} neighboring the incorporated Cl^-.

The currents of DMSO oxidation varied with rotation speeds of the disc electrode as well as DMSO concentrations from 125 to 400 mM (Fig. 6B, curves a-d). In comparison with Figs 5A-5B, the potential values for the apparent onset of DMSO oxidation at both Cl-PbO_2 and pure PbO_2 films occurred at 1.6 V on the positive scans. However, the cessation of DMSO oxidation at pure PbO_2 (1.4 V) was measured at 50 mV more positive than that for Cl-PbO_2 (1.35 V) during the negative scans. This result indicated that Cl-PbO_2 was more

catalytically active than PbO_2 toward the oxidation of DMSO in 1 M H_2SO_4.

Figure 7 shows the plot of anodic current (I) of DMSO, measured at 1.9 V, as a function of DMSO concentration in 1 M H_2SO_4. Curve a corresponds to the Cl-PbO_2 and b to the PbO_2 film. Both curves show deviation from the linearity at large concentrations of DMSO. Based on the examination of slopes on the linear portion of the curves as well as the quantity of current obtained, it is apparent that the Cl-PbO_2 film was the more active anode material than PbO_2 for the oxidation of DMSO.

Catalytic oxidation of DMSO and benzyl alcohol

As were shown in Figs. 1A and 1B, a distinct enhancement of O_2 evolution was obtained at the pure PbO_2-film electrode after several repeated cyclic potential scans in 1 M H_2SO_4. Since the anodic discharge of water has been concluded as the rate limiting step for O_2 evolution (21), the catalytic phenomena shown in Figs. 1A-1B were speculated to result from the catalyzed production of $\cdot OH_{ad}$. The anodic oxygen-transfer reactions, which also involve the formation of $\cdot OH_{ad}$ as the limiting step, were also expected to have catalytic benefit at the cycled PbO_2-film electrode. Oxidations of DMSO and benzyl alcohol in aqueous solutions are typical anodic O-transfer reactions, and their kinetic results were examined.

Figure 8 shows the plot of heterogeneous rate constant (k) of DMSO oxidation at the PbO_2-film electrode, measured at 1.6 V, as a function of cycle number of the potential scans in 1 M H_2SO_4. The pure PbO_2-film

electrode was deposited on Au RDE at 1.7 V. Values of k were calculated from the intercepts of plots of 1/I *vs.* $1/w^{1/2}$ according to the Levich-Koutecky equation, Equation [1].

It is apparent from this figure that a positive correlation was obtained for k and cycle number. The significant increase of rate constant was observed for the first 20 scans. The rate constant obtained after 120 cycles (1.7×10^{-2} cm s^{-1}) was 100X larger than that for the uncycled electrode (1.68×10^{-4} cm s^{-1}). Kinetic results of DMSO oxidation are summarized in Table III.

Experimentation was repeated according to the exact conditions described for Fig. 8 except for using benzyl alcohol as the reactant. Kinetic results ($n_{eff}k$) were plotted in Fig. 9 as a function of cycle number. The value of $n_{eff}k$ was observed to increase for the first 41 cycles and remained nearly constant for the following to 101 cycles. An increase of 37x in the reaction rate was obtained after 41 cycles ($n_{eff}k = 5.04 \times 10^{-2}$ eq mol^{-1} cm s^{-1}), as compared with that for the uncycled PbO_2 film ($n_{eff}k = 1.35 \times 10^{-3}$ eq mol^{-1} cm s^{-1}). Kinetic data for the oxidation of benzyl alcohol are summarized in Table IV.

Conclusion

The repeated cyclic potential scans at the PbO_2-film electrode in 1 M H_2SO_4 produces $PbSO_4$ as the reduction product on the negative potential scans, as determined by X-ray diffractometry. Because of the slow rate of reoxidation of $PbSO_4$, this cycling process resulted in the

gradual acummulation of $PbSO_4$ in the PbO_2 matrix. The electric conductivity of $PbSO_4$ is much less than that for PbO_2, and, therefore, it is expected that formation of the resistive layers of $PbSO_4$ will result in retardation of the electron transfer at the electrode-electrolyte interface. However, results showed significant enhancement rather than decrease in the electrocatalytic reactivities for the $PbSO_4$ incorporated PbO_2-film electrode. The rates of O_2 evolution and O-transfer reactions were both observed to increase during the repetitive potential scans.

The catalytic discharge of H_2O to produce $'OH_{ad}$ was speculated to occur at the active Pb^{4+} centers of the PbO_2 surface (22). The incorporated $PbSO_4$ was concluded to activate the neighboring Pb^{4+} during the repetitive potential scans in 1 M H_2SO_4. While the results reported here do not provide enough information for a clear understanding of the detailed catalytic mechanism, it seems that the incorporated SO_4^{2-} can change the electron density of the neighboring Pb^{4+}, which in return affects the tendency for the catalytic adsorption of 'OH.

References

1. Pavlov, D.; Bashtavelova, E. J. Electrochem. Soc. 1986, 133, 241.
2. Chapter III in this dissertation.
3. Pavlov, P.; Bashtavelova, E. J. Electrochem. Soc. 1984, 131, 1468.
4. Simon, A. C.; Caulder, S. M.; Stemmle, J. T. J. Electrochem. Soc. 1975, 122, 461.
5. Caulder, S. M.; Murday, J. S.; Simon, A. C. J. Electrochem. Soc. 1973, 120, 1515.

6. Caulder, S. M.; Simon, A. C. J. Electrochem. Soc. 1974, 121, 1546.

7. Takehara, Z.; Kanamura, K. Bull. Chem. Soc. Jpn. 1987, 60, 1567.

8. Takehara, Z.; Kanamura, K. Electrochim. Acta 1984, 29, 1643.

9. Takehara, Z.; Kanamura, K.; Kawanami, M. J. Electrochem. Soc. 1989, 136, 620.

10. Levich, V. G. Physicochemical Hydrodynamics; Prentice Hall: Englewood Cliffs, New Jersey, 1962; p. 75.

11. Koutecky, J.; Levich, V. G. Zh. Fiz. Khim. 1965, 32, 1565.

12. Oyama, N.; Anson, F. C. Anal. Chem. 1980, 52, 1192.

13. Beck, F.; Schulz, H. J. Electroanal. Chem. 1987, 229, 339.

14. Mark, Jr., H. B.; Vosburgh, W. C. J. Electrochem. Soc. 1961, 108, 615.

15. LaCour[illegible], W. R.; Hsiao, Y.-L.; Feng, J.; Chang, H.; Johnson, D. C. unpublished results, Chemistry Dept., Iowa State University, Ames, Iowa, 1988.

16. Deakin, M.;Melroy, O. J. Electroanal. Chem. 1988, 239, 321.

17. (a) Takehara, Z.; Kanamura, K. J. Electrochem. Soc. 1987, 134, 13. (b) Ekdunge, P.; Simonsson, D. J. Electrochem. Soc. 1985, 132, 2521.

18. Bard, A. J. Encyclopedia of Electrochemistry of the Elements; Marcel Dekker Inc.: New York, 1973; Vol. I, Chap. I-5.

19. Asai, K.; Tsubota, M.; Yonezu, K.; Ando, K. J. Power Sources, 1981/1982, 7, 73.

20. Takehara, Z; Kanamura, K. Bull. Chem. Soc. Jpn. 1987, 60, 1567.

21. Bockris, J. O'M. J. Chem. Phys., 1956, 24, 817.

22. (a) Yeo, I.-H. Ph.D. dissertation, Iowa State University, Ames, Iowa, 1987. (b) Larew, L. A.; Gordon, J. S.; Hsiao, Y.-L.; Buttry, D. A.; Johnson, D. C. J. Electrochem. Soc. 1990, 137, 3701.

Table 1. Integrated intensities for the X-ray diffraction peaks corresponding to the designated crystal planes at the surface of PbO_2 films

Film	I_{101}[a]	I_{020}	I_{211}	I_{310}	I_{301}
1.6 V[b]	2065	2248	4022	1031	2183
1.7 V	2309	2964	4552	1185	1995
1.8 V	802	653	1243	0	5194

[a]Integrated peak intensities for the specified crystal planes.

[b]Deposition potentials for the PbO_2 films on Au.

Table II. Integrated intensities of X-ray diffraction peaks for the designated crystal planes for PbO_2, and $PbSO_4$ at specified number of cycles

Cycle	PbO_2			$PbSO_4$		
	I_{101}[a]	I_{020}	I_{211}	I_{210}	I_{021}	I_{002}
0	2309	2964	4552	0	0	0
50	2159	1974	2551	483	273	1891
150	1299	609	1890	1095	385	1767

[a]Integrated peak intensities for the specified crystal planes.

Table III. Heterogeneous rate constant for DMSO oxidation[a] at the PbO_2-film, deposited at 1.7 V, on Au RDE after specified number of cycles in 1 M H_2SO_4

Cycle number	10^3 x k (cm s^{-1})[b]
0	0.168
10	5.63
20	9.48
30	9.47
40	9.44
50	11.5
60	12.2
70	13.0
90	15.0
120	17.1
150	16.2

[a]Oxidation was carried out at 1.6 V in 1 M H_2SO_4.

[b]n = 2 was assumed for calculating the rate constant.

Table IV. Heterogeneous rate constant for benzyl alcohol oxidation at the PbO_2 on Au RDE after specified number of cycles in 1 M H_2SO_4

Cycle[a]	$10^3 \times n_{eff}k$(eq mol^{-1} cm s^{-1})[b]
0	1.35
10	22.41
20	36.01
30	45.01
41	50.41
50	49.43
101	45.01

[a]The PbO_2 film was electrodeposited at 1.7 V from 1 M $HClO_4$ containing 1.67 mM Pb^{2+}.

[b]Oxidation was carried out at 1.7 V in 1 M H_2SO_4.

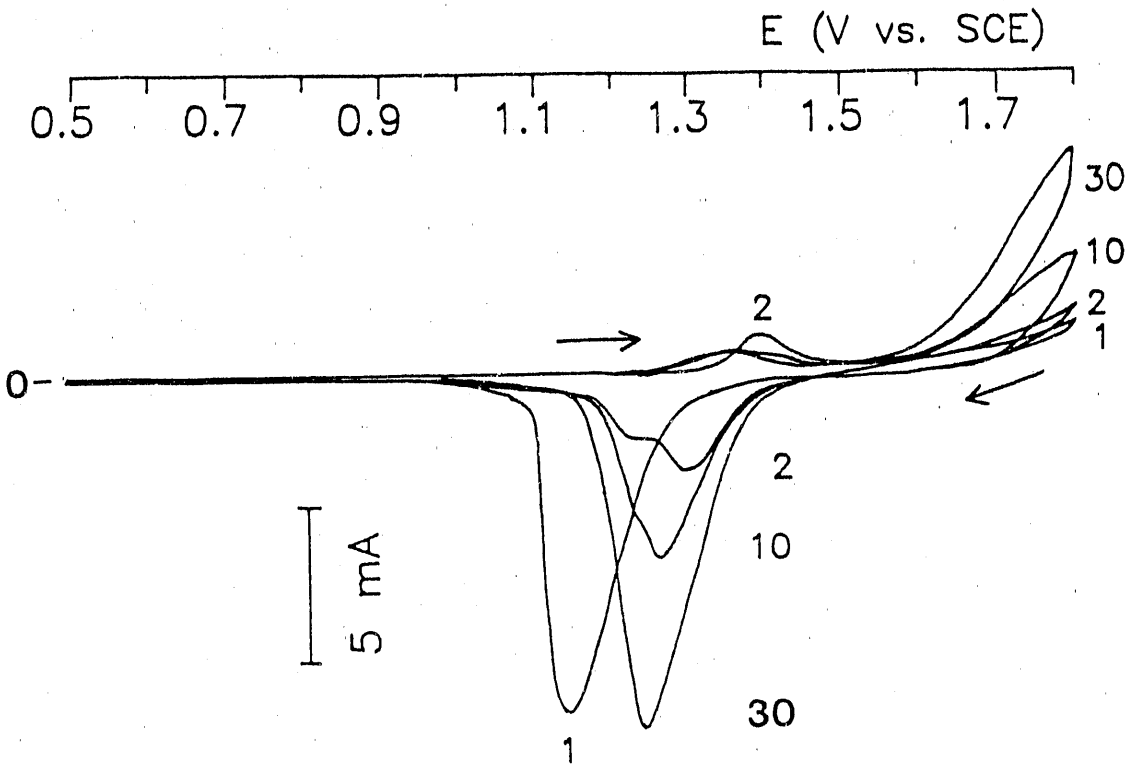

Figure 1A. Cyclic voltammograms at a pre-deposited PbO_2 film on Au RDE

Conditions: 1 M H_2SO_4,
50 mV s^{-1}, 1600 rev min^{-1}

Deposition potential for PbO_2: 1.7 V

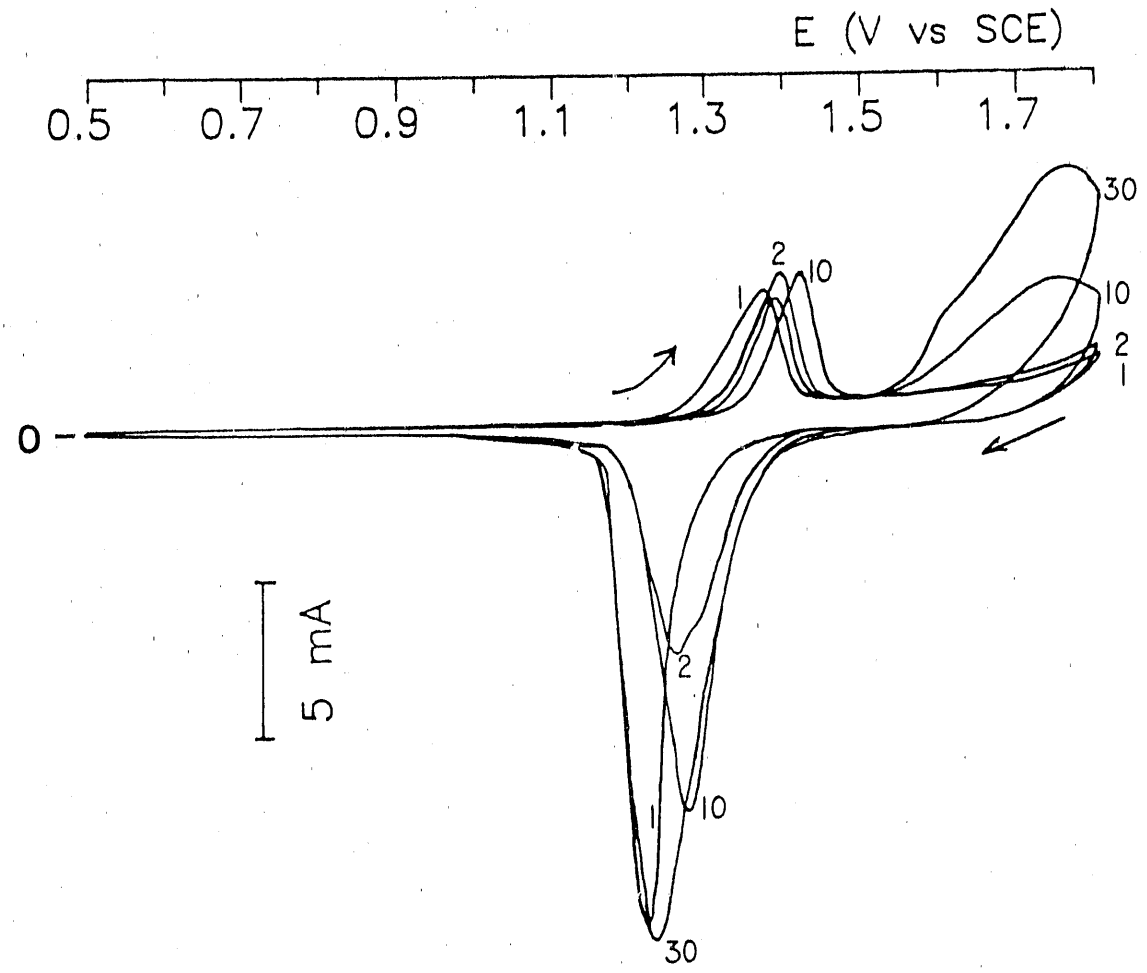

Figure 1B. Cyclic voltammograms at a pre-deposited PbO_2 film on Au RDE

Conditions: same as Fig. 1A

Deposition potential for PbO_2: 1.8 V

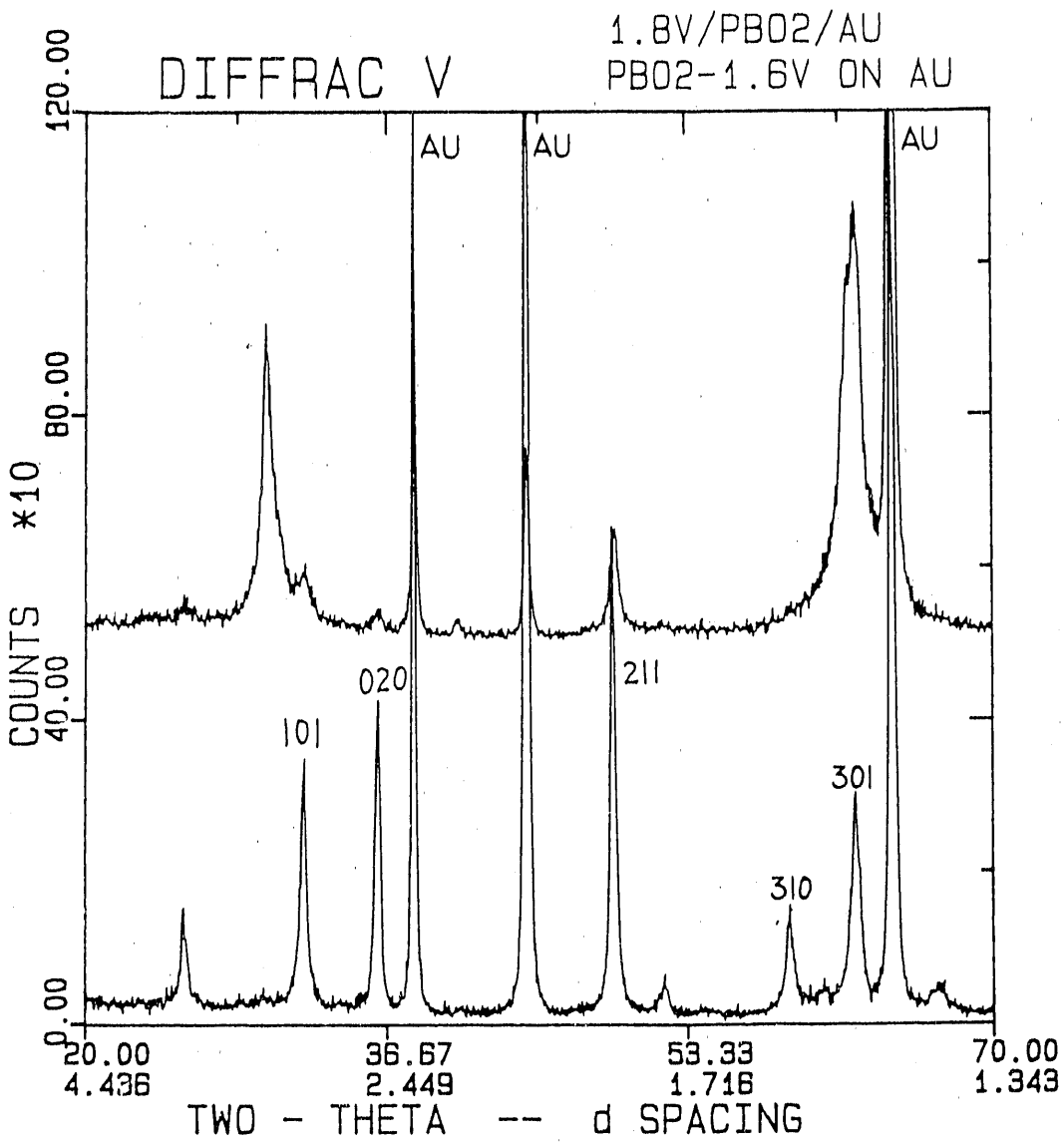

Figure 2A. X-ray diffraction patterns for PbO_2 film deposited at 1.6 V (a), and 1.8 V (b) on Au substrate

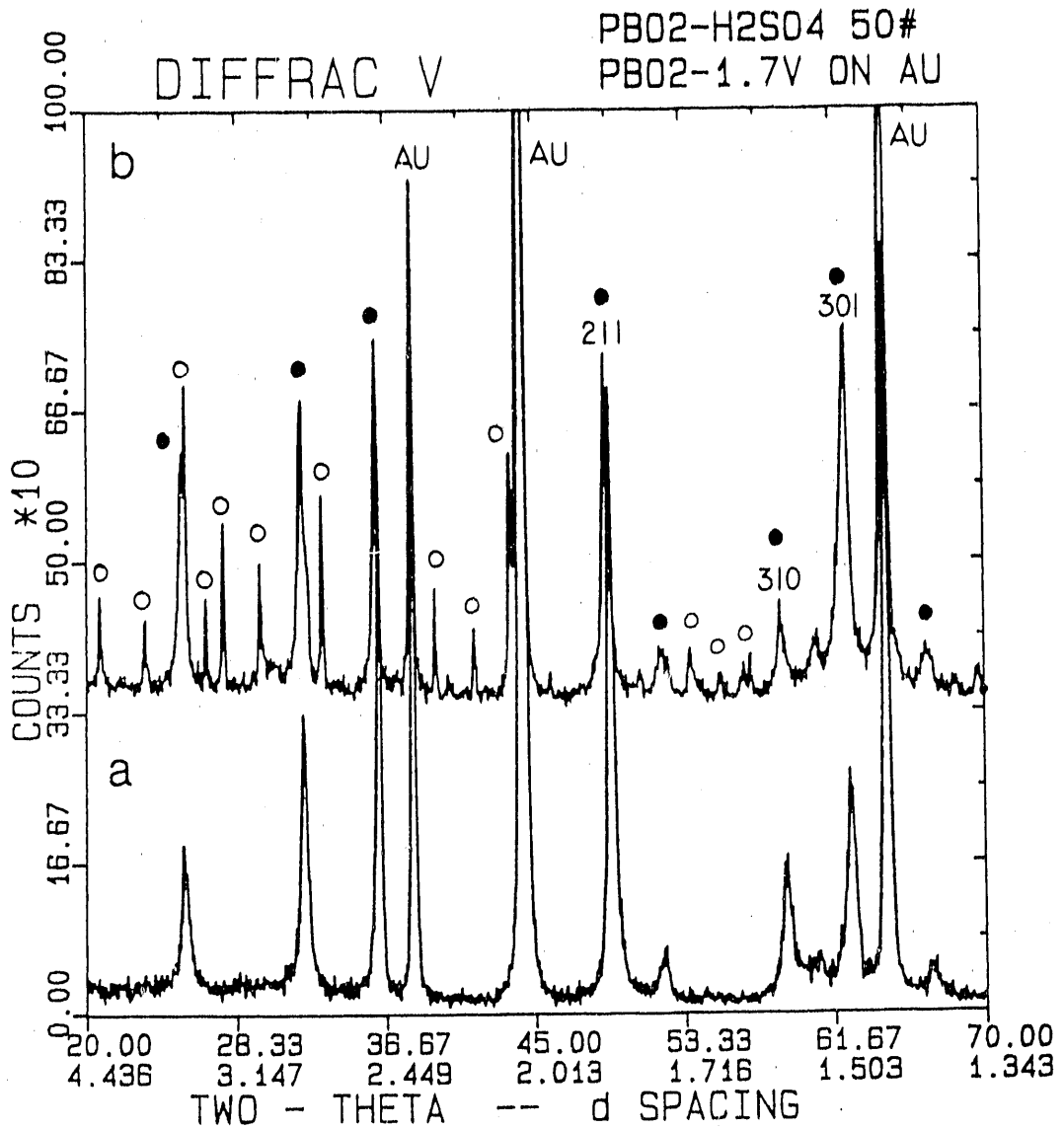

Figure 2B. X-ray diffraction patterns for PbO_2 film deposited on Au before (a), and after (b) 50 cyclic potential scans in 1 M H_2SO_4

Peaks: ○ $PbSO_4$
● PbO_2

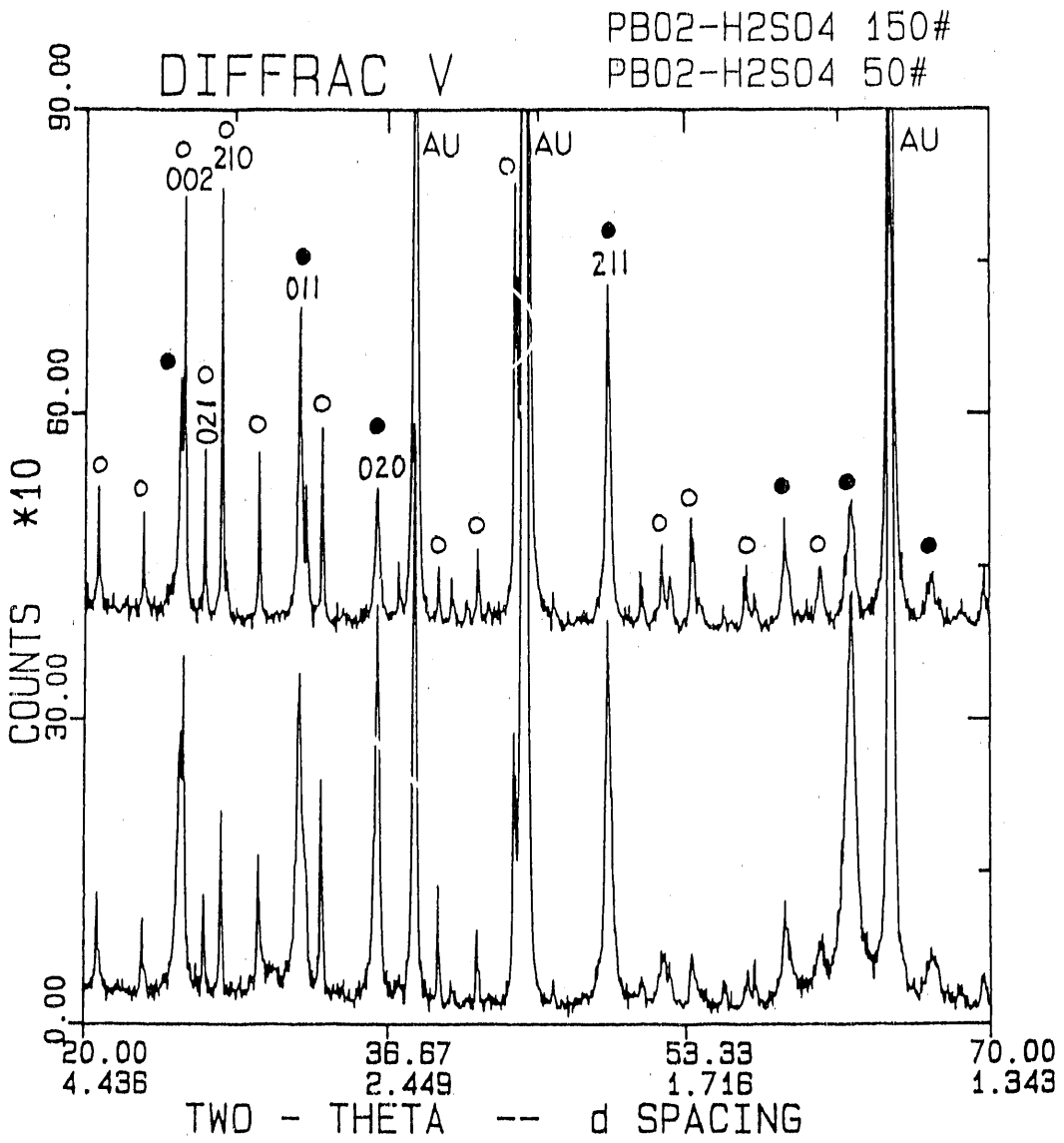

Figure 2C. X-ray diffraction patterns for PbO_2 film deposited on Au after 50 (a), and 150 (b) cyclic potentail scans in 1 M H_2SO_4

Peaks: O $PbSO_4$
● PbO_2

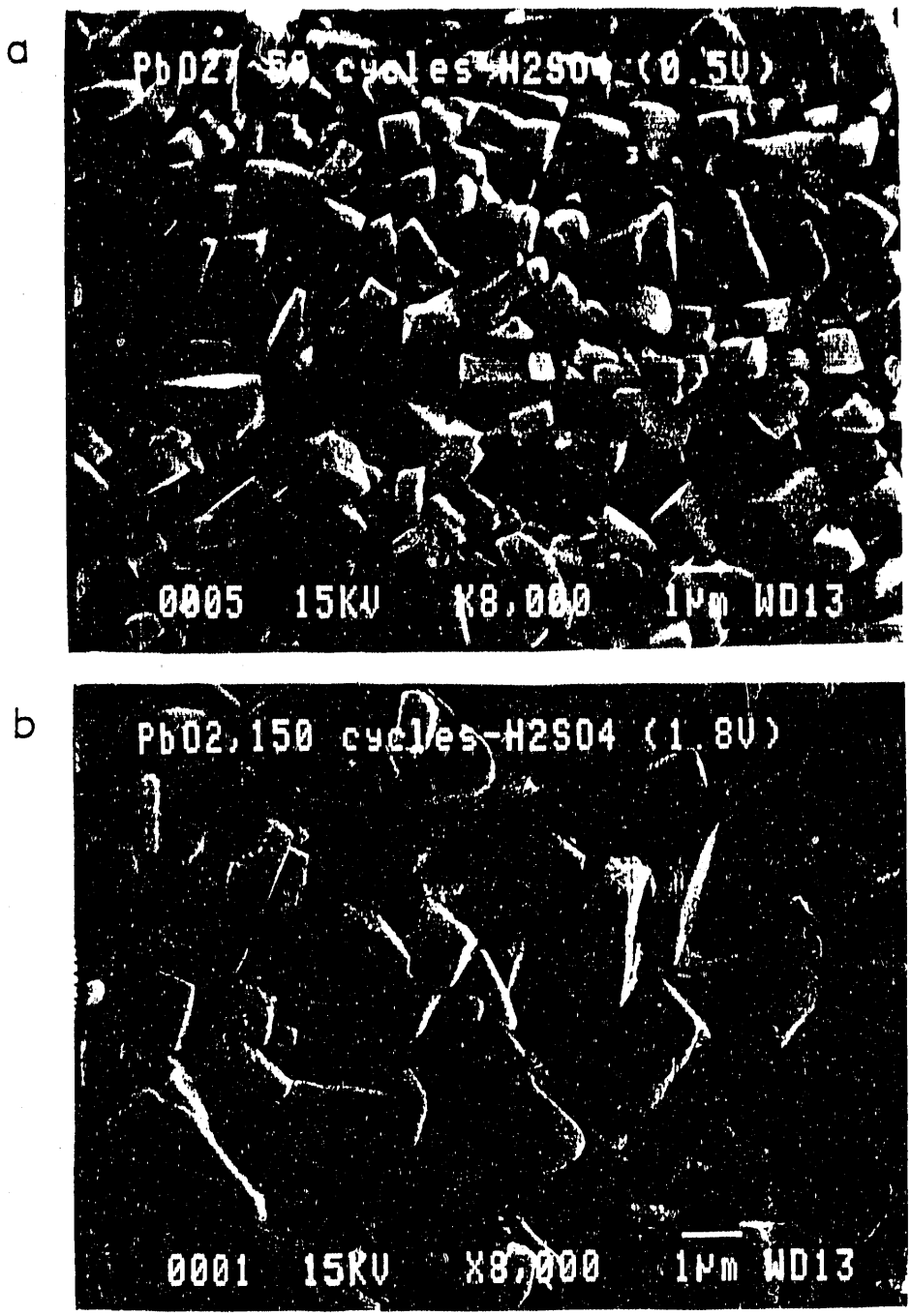

Figure 3. Scanning electron micrographs (X 8000) of the surface of PbO_2 film after 50 (a), and 150 (b) cyclic potential scans in 1 M H_2SO_4

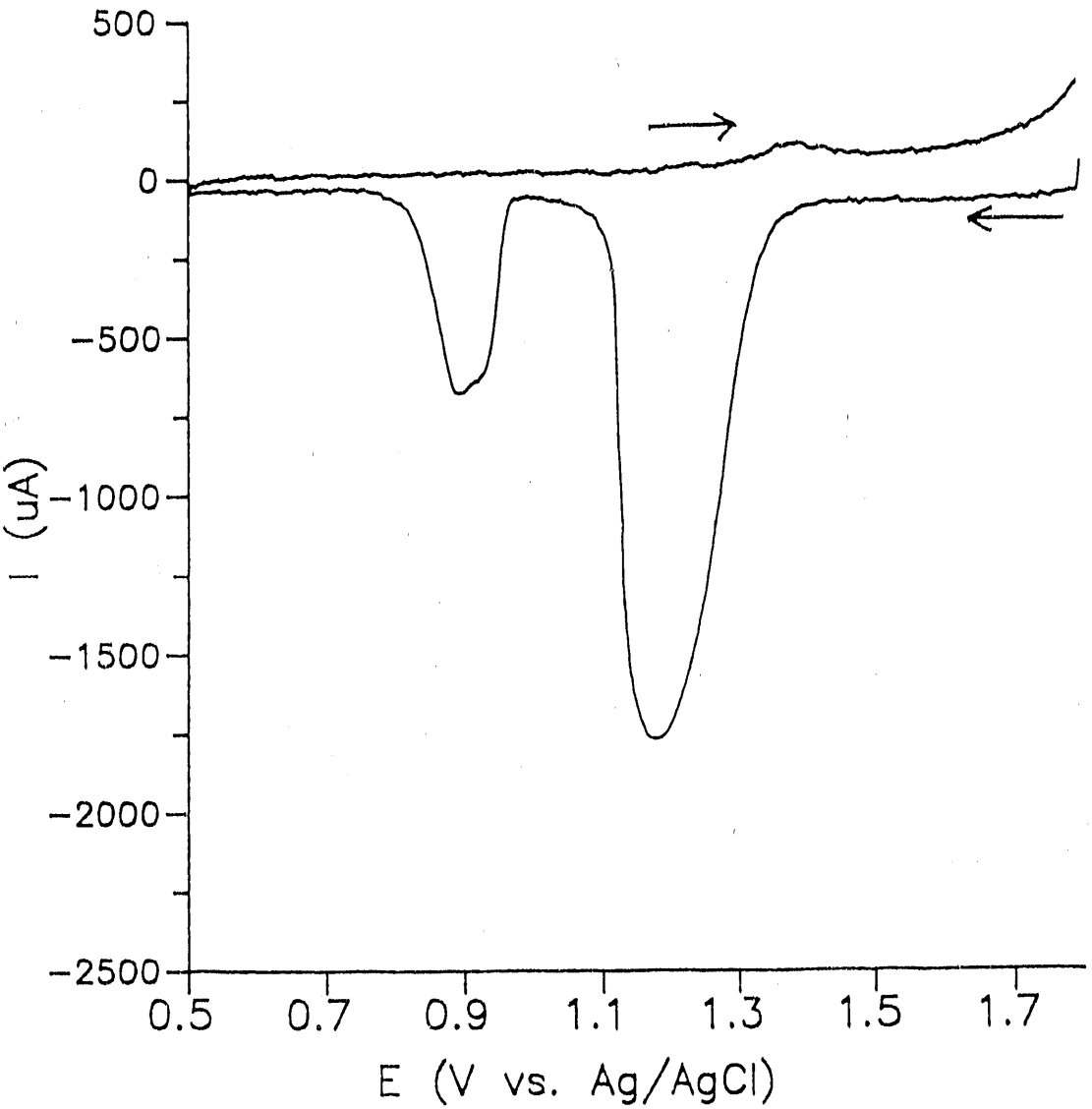

Figure 4A. Current response of EQCM during the cyclic potential scan at the PbO_2 film in 1 M H_2SO_4

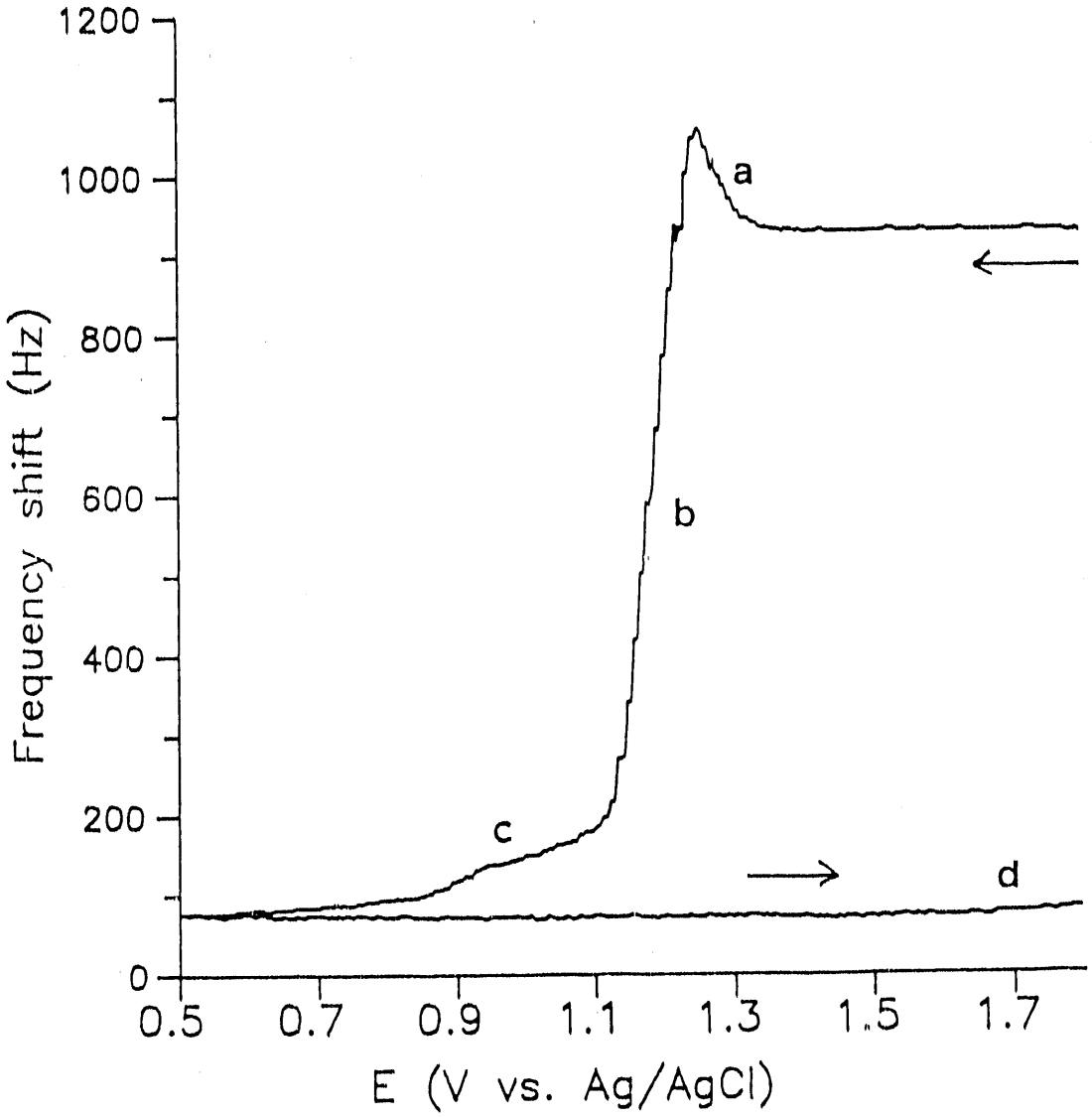

Figure 4B. Frequency response of EQCM during the cyclic potential scan at the PbO_2 film in 1 M H_2SO_4

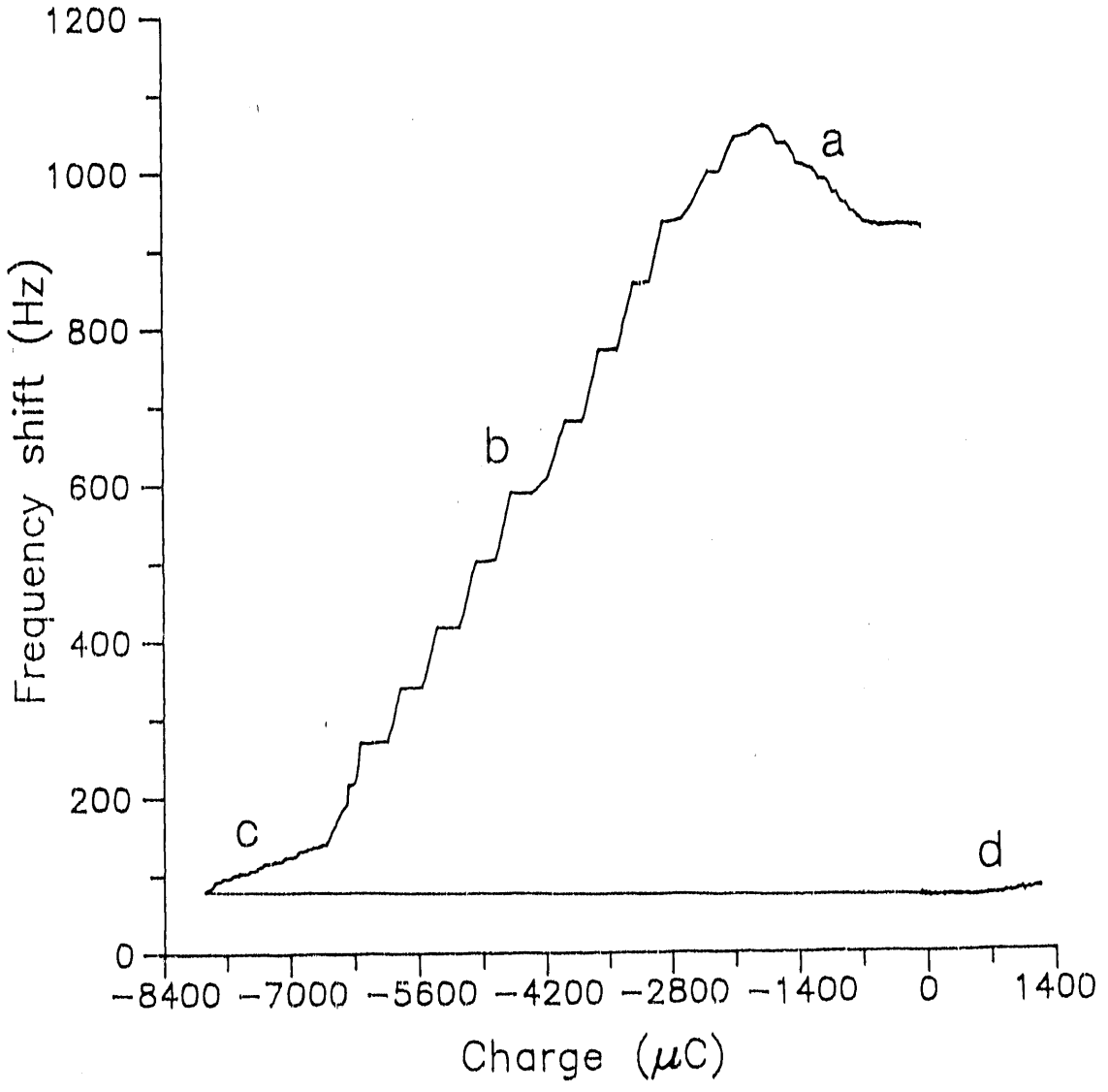

Figure 4C. Plot of frequency response *vs.* charge obtained during the cyclic potential scan atthe PbO_2 film in 1 M H_2SO_4

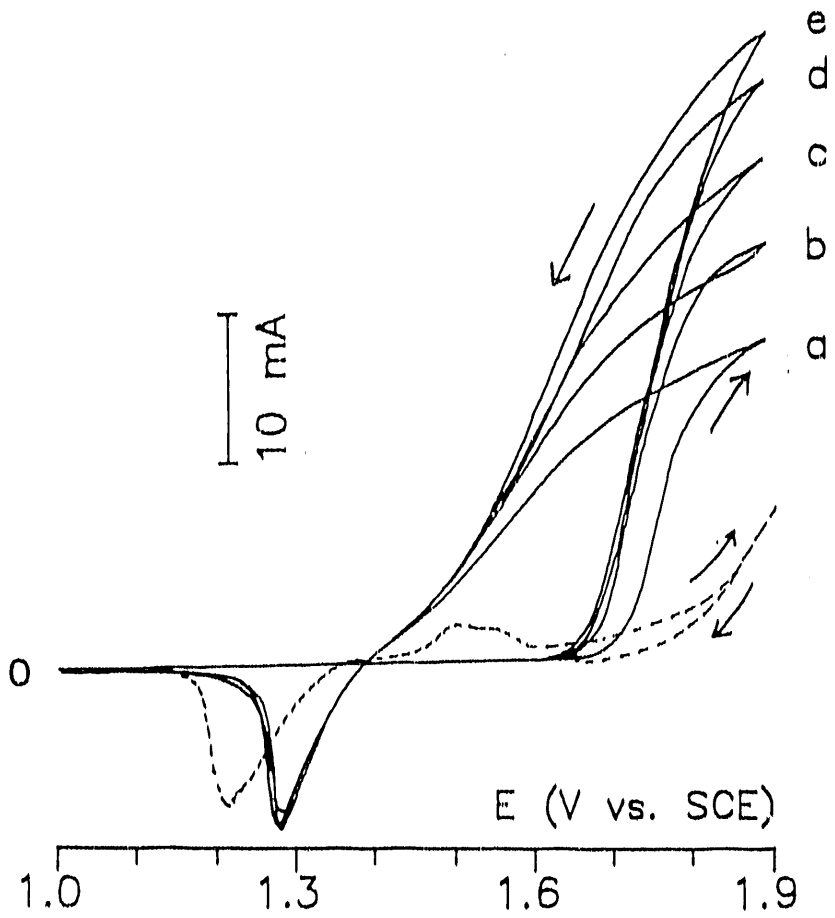

Figure 5A. Cyclic voltammograms of DMSO at the PbO_2 deposited on Au RDE

Conditions: 20 mV s^{-1}, 1 M H_2SO_4

Curves: (---) residual,
(——) 125 mM DMSO

Rotation speeds (rev min^{-1}): (a) 400, (b) 900, (c) 1600, (d) 2500, (d) 3600

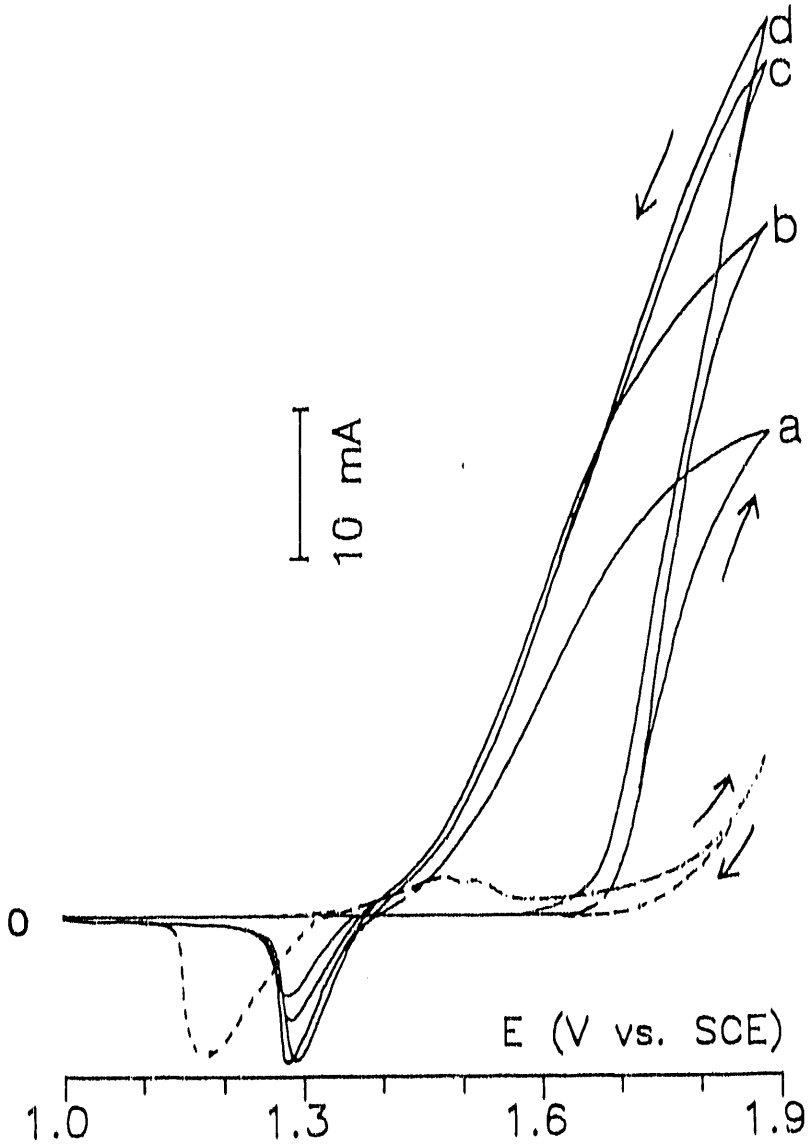

Figure 5B. Cyclic voltammograms of DMSO at the PbO_2 deposited on Au RDE

Conditions: 20 mV s^{-1}, 1600 rev min^{-1}, 1 M H_2SO_4

Concentrations of DMSO (mM): (---) 0, (a) 125, (b) 200, (c) 300, (d) 400

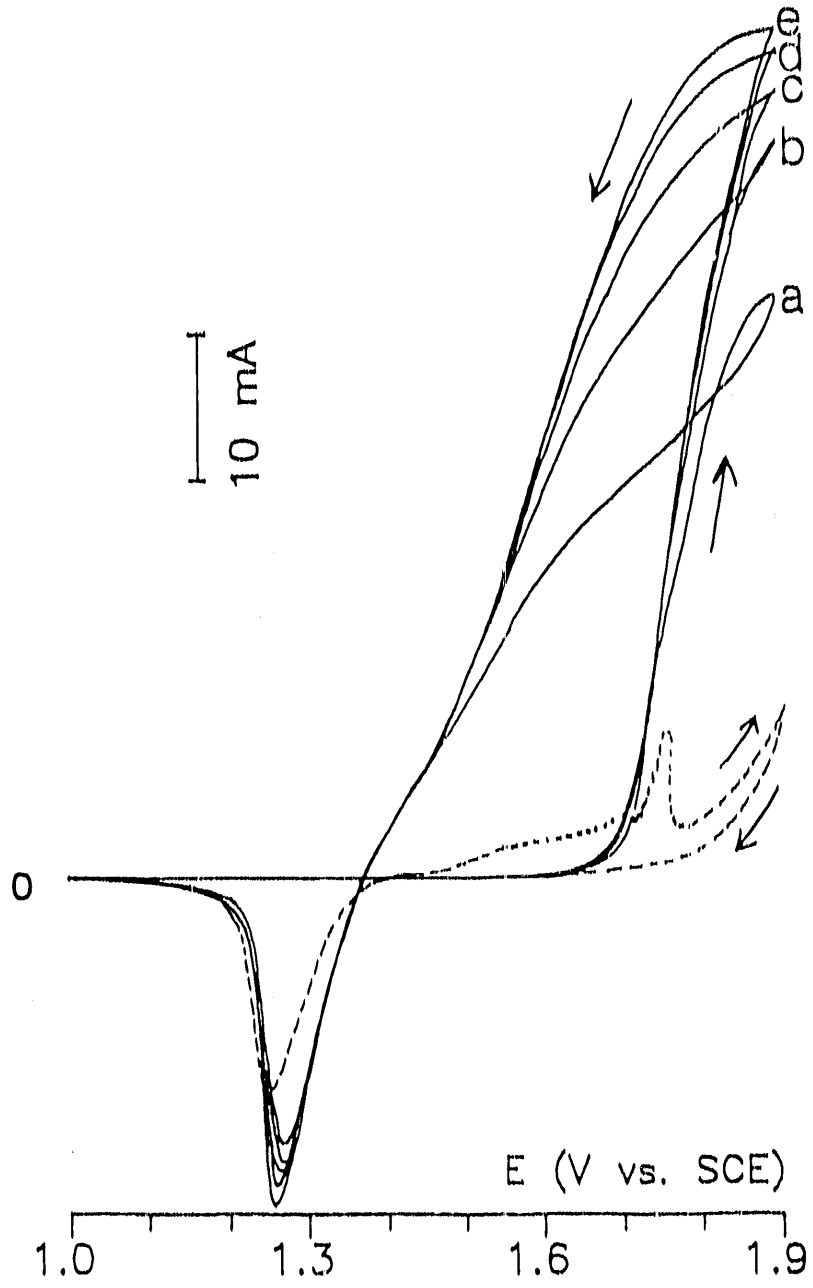

Figure 6A. Cyclic voltammograms of DMSO at the Cl-PbO_2 on Au

Conditions: 20 mV s^{-1},
200 mM DMSO, 1 M H_2SO_4

Curves: (---) residual

Rotation speeds (rev min^{-1}): (a) 400, (b) 900, (c) 1600, (d) 2500, (d) 3600

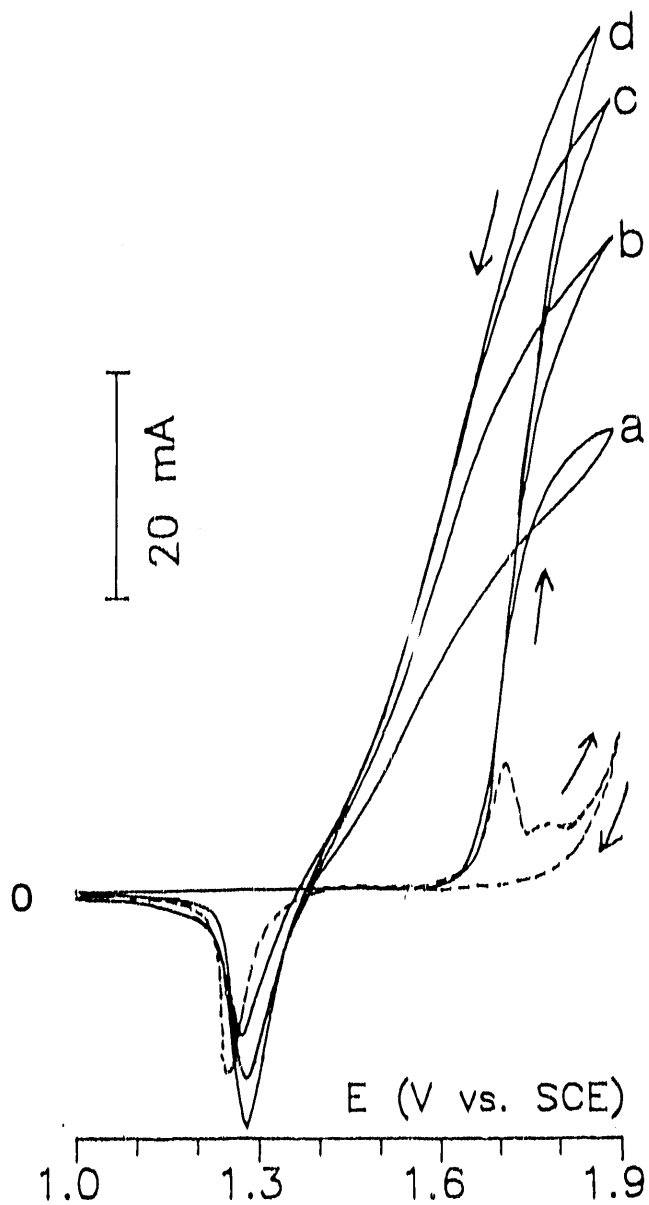

Figure 6B. Cyclic voltammograms of DMSO at the Cl-PbO_2 on a Au RDE

Conditions: 20 mV s^{-1}, 1600 rev min^{-1}, 1 M H_2SO_4

Concentrations of DMSO (mM): (---) 0, (a) 125, (b), 200, (c) 300, (d) 400

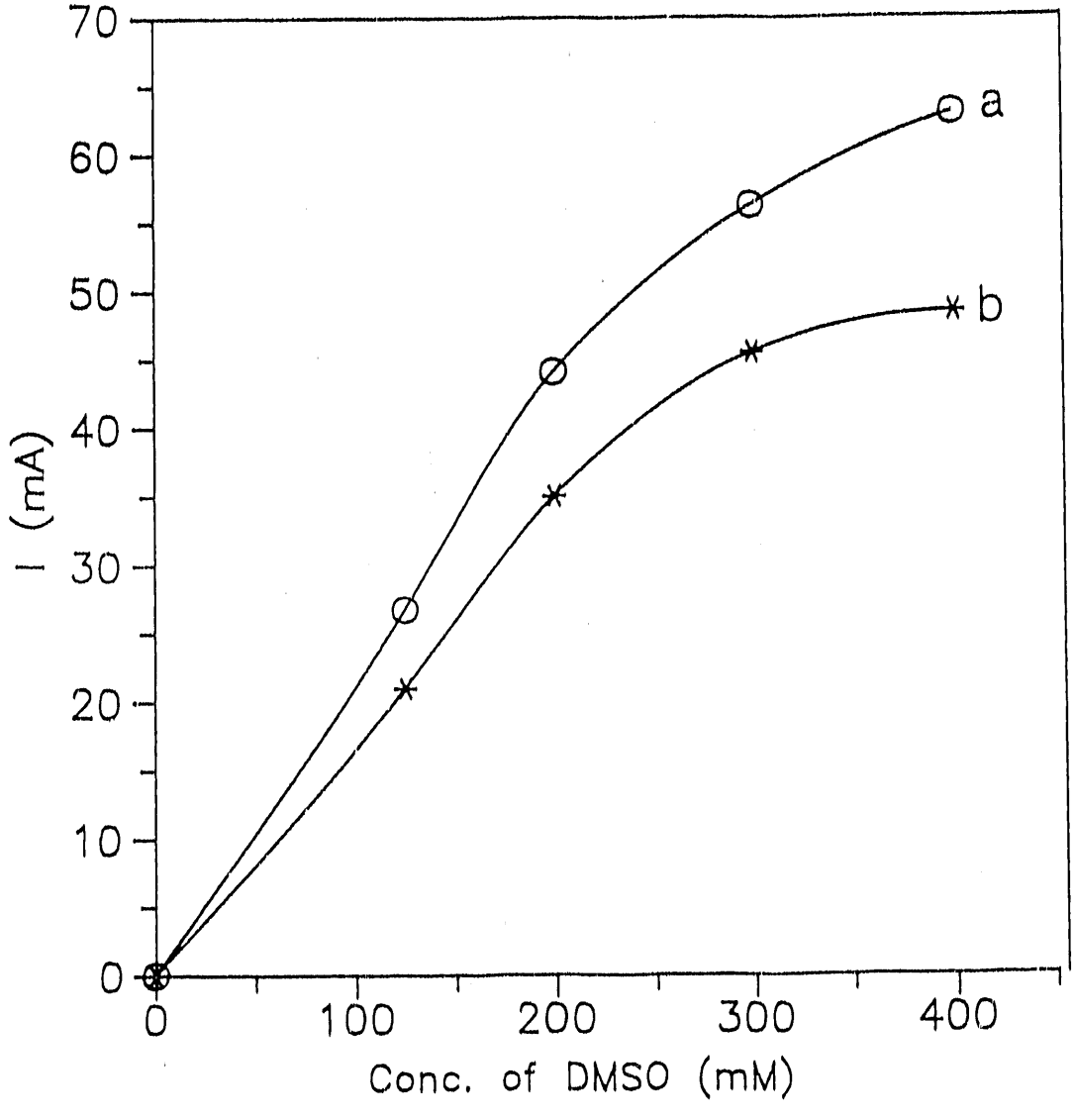

Figure 7. Plot of current (I) *vs*. DMSO concentrations at the Cl-PbO_2 (a), and the pure PbO_2 (b) films deposited on Au RDE

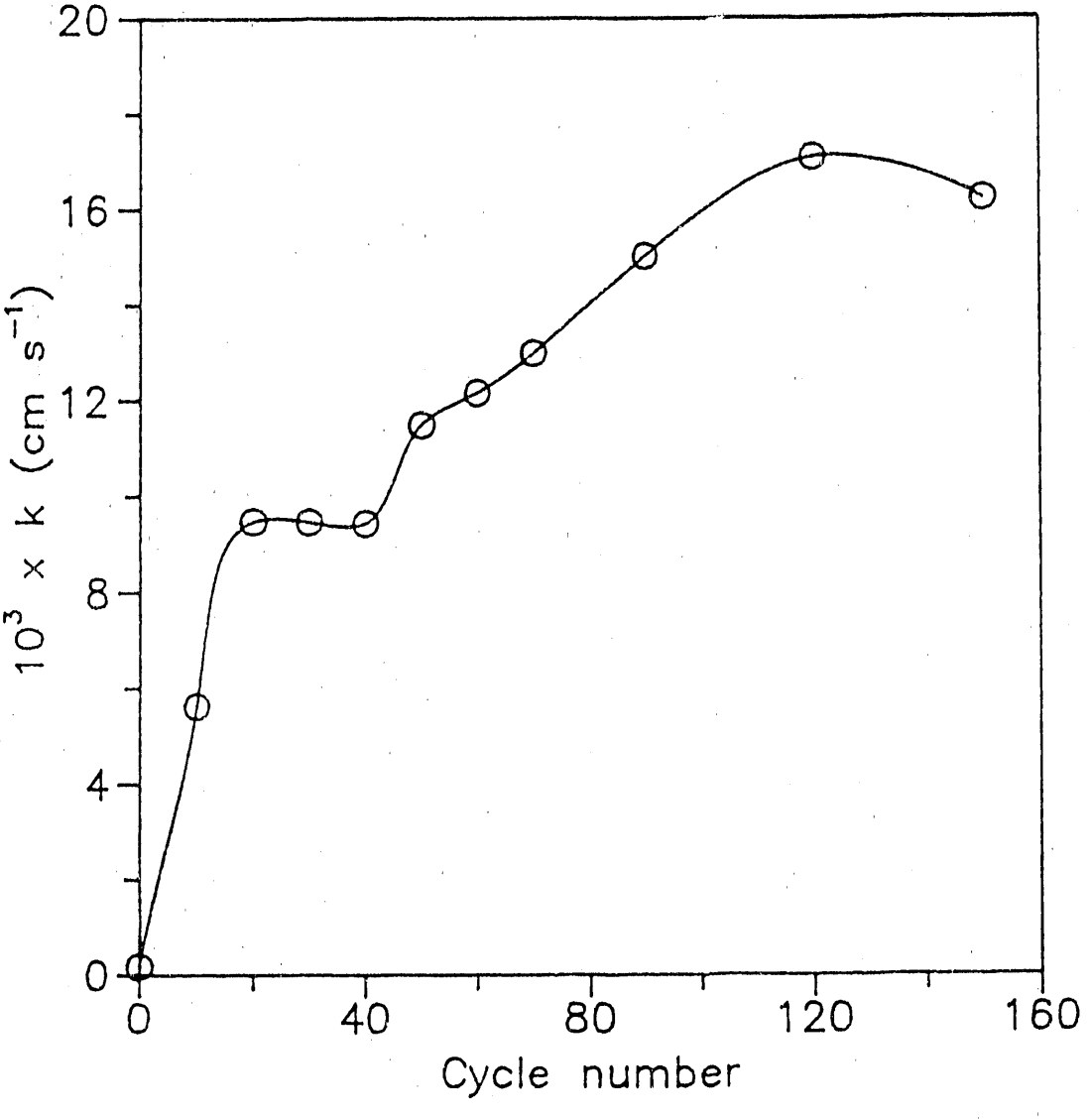

Figure 8. Plot of heterogeneous rate constant (k) for DMSO oxidation *vs.* cycle number at the cycled PbO_2-film electrode in 1 M H_2SO_4

Conditions: 5 mM DMSO, 1 M H_2SO_4, E = 1.6 V

Deposition potential for the PbO_2 film on Au RDE: 1.7 V

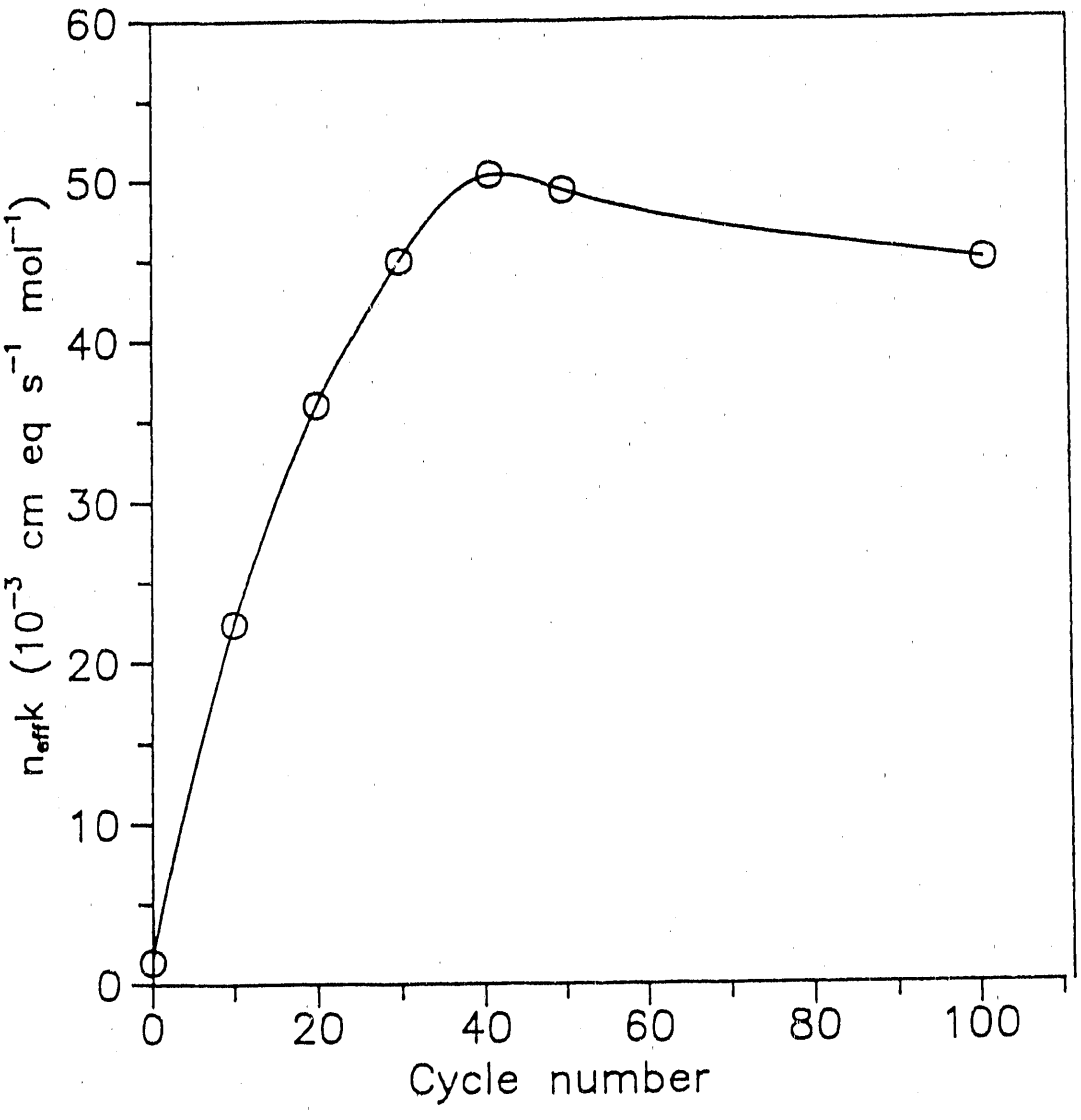

Figure 9. Plot of $n_{eff}k$ for the oxidation of benzyl alcohol *vs.* cycle number at the cycled PbO_2-film electrode in 1 M H_2SO_4

Conditions: 5 mM benzyl alcohol, 1 M H_2SO_4, E = 1.7 V

Deposition potential for the PbO_2 film on Au RDE: 1.7 V

CHAPTER VI.

ACTIVATION OF LEAD DIOXIDE-FILM ELECTRODES BY Bi(V) INCORPORATION AND Bi(V) ADSORPTION

Abstract

Two types of Bi(V)-modified PbO_2-film electrodes were demonstrated to be significantly more active for the oxidation of DMSO than the unmodified PbO_2. One involved the anodic codeposition of PbO_2 with Bi^{3+} to produce Bi^{5+}-doped PbO_2 film (Bi-PbO_2). The other involved exposure of pure PbO_2 films to a solution of trace Bi^{3+} to make the Bi^{5+}-adsorbed PbO_2 films (Bi^{5+}/PbO_2).

The lattice Bi^{5+} of Bi-PbO_2, and the adsorbed Bi^{5+} of Bi^{5+}/PbO_2 were concluded to catalyze the anodic discharge of H_2O to produce $\cdot OH_{ad}$, which is an intermediate required for both DMSO oxidation and O_2 evolution. The electrocatalytic activities of these Bi(V)-modified PbO_2-film electrodes was strongly dependent on both the doping level of Bi^{5+} in the Bi-PbO_2 films and the surface coverage by adsorbed Bi^{5+} of the Bi^{5+}/PbO_2 films.

The HSO_4^--modified chloride-doped PbO_2 (Cl-PbO_2) and acetate-doped PbO_2 (OAc-PbO_2) films also showed improved catalytic properties for DMSO oxidation following adsorption of Bi^{5+}.

Introduction

Modification of supported PbO_2 electrodes by co-deposition of Group V cations, e.g., Bi(III) (1-2), As(V) (1), has proven to be significantly successful in the enhancement of various anodic O-transfer reactions in acidic media. The anodic discharge of H_2O to produce adsorbed OH radicals ($^{\cdot}OH_{ad}$) has been proposed as the rate limiting step for the anodic O-transfer reactions which require transfer oxygen from H_2O to the oxidation products (1-3). Application of such electrocatalytic electrodes are anticipated for electrosynthesis as electroanalytical sensors, and in anodic degradation of toxic chemical waste (electrochemical incineration) (3b).

The Bi(V)-modified PbO_2 films are very active anode materials for numerous O-transfer reactions in acidic media (1-3). Many efforts have been made to study the kinetic secret of this electrocatalytic anode in this research group since its early discovery in 1986 by Yeo and Johnson (1-3). Because the ionic sizes for Bi^{5+} (0.74 Å) and Pb^{4+} (0.84 Å) are relatively close, it is concluded that Bi^{5+} was incorporated in the PbO_2 film without substantial distortion of the oxide matrix (1). The incorported Bi(V) functioned as the O-transfer mediator, which differed from an electron-transfer mediator by not undergoing redox change during the catalytic reaction (3a). The lattice Bi(V) was proposed to be the active center which catalyzed anodic discharge of water to produce $^{\cdot}OH_{ad}$ (3). It has been concluded, based on the studies of X-ray photoelectron spectrometry (XPS) and X-ray energy dispersive

spectrometry (EDS) (2), that Bi^{5+} content in the mixed oxide ($Bi\text{-}PbO_2$) increased with increasing concentration ratio of $[Bi^{3+}]/[Pb^{2+}]$ in the deposition solution.

Experimental results described for this chapter are portions of work focused on the correlation of the reaction rate of DMSO oxidation and O_2 evolution at $Bi\text{-}PbO_2$ and at Bi^{5+}/PbO_2 anodes. Kinetic studies were also performed at the HSO_4^--modified Cl^--doped and OAc^--doped PbO_2 films ($Cl\text{-}PbO_2$ and $OAc\text{-}PbO_2$) to investigate the catalytic proterities of these anodes following the adsorption of Bi^{5+}.

Experimental

Reagents

All chemicals were analytical reagent grade. Solutions were prepared with deionized H_2O purified in a Barnstead NANOpure-II system (Boston, MA).

Instrumentation

The Au disk electrode (RDE; 0.1642 cm^2; Pine Instrument Company, Grove City, PA) was operated in A Model MSR rotator (Pine Instrument). Chronoamperometry was obtained with a Model RDE3 potentiostat (Pine Instrument) and a Model 2000 X-Y recorder (Houston Instrument, Houston, TX). A three-compartment electrolysis cell was used with a Pt wire counter electrode separated from the working solution by a fritted glass junction. The saturated calomel electrode (SCE, 0.241 V vs. NHE)

reference contacted the working solution through a Harber-Luggin capillary.

Potentiostatic control for cyclic voltammetry, data acquisition and analysis were achieved by interfacing the RDE3 potentiostat to a Zenith PC using a DT 2800 board (DATA Translation, Marlboro, MA).

Procedures

Prior to electrodeposition, the Au RDE was cleaned according to the procedure described before (4). The Bi-PbO_2 film was electrochemically deposited on the clean Au disk from 1 M $HClO_4$ solutions containing 1.67 mM $Pb(NO_3)_2$ and $Bi(NO_3)_3$ with various ratios $[Bi^{3+}]/[Pb^{2+}]$ from 0.1 to 1.0. A uniformly black oxide film was apparent after 20 min of deposition at a constant potential of 1.6 V. Deposition of each film was done in a new plating solution to avoid any influence from the previous plating solution. The depositions of Cl-PbO_2 and OAc-PbO_2 films were carried out according to the exact conditions described previously (4).

Reactions under mixed transport-kinetic control at the rotated electrodes were assumed to be consistent with the Koutecky-Levich equation given as follows (5-8).

$$\frac{1}{I} = \frac{1}{n_{eff}FAk_{app}C^b} + \frac{1}{0.62n_{eff}FAD^{2/3}\nu^{-1/6}C^b}\left[\frac{1}{w^{1/2}}\right] \qquad [1]$$

The significance of this equation has been discussed (4). Values of the heterogeneous rate constant k were calculated from intercepts of the plots of $1/I$ *vs.* $1/w^{1/2}$ according to Eq. [1]. Values of I were corrected for the background signals measured in the absence of solution reactants.

Results and Discussions

Electrocatalysis at Bi-doped PbO_2

Cyclic voltammetry The electrocatalytic reactivities of the pure and Bi-doped PbO_2-film electrodes were compared. Cyclic voltammograms at these two electrodes are shown in Fig. 1A before (——) and after (---) the addition of 5 mM DMSO to 1 M $HClO_4$. The current of O_2 evolution at E > 1.8 V was apparently larger at the Bi-PbO_2 film (curve c) than that at the pure PbO_2 film (curve a) indicating a catalyzed process for O_2 evolution at Bi-PbO_2.

The currents of DMSO oxidation at the pure PbO_2 film were small and showed very little rotation speed dependence (Fig. 1A, curve b), and the oxidation only became apparent at E > 1.75 V. On the other hand, oxidation of DMSO at the Bi-PbO_2 electrode became apparent at 200 mV less positive than that at pure PbO_2 film (1.55 V), and, well-defined current plateaus were observed with a half wave potential ($E_{1/2}$) = 1.664 V (Fig. 1A, curves c-i).

The currents of DMSO oxidation were plotted in Fig. 1B as a function of rotation speed of the disk electrode. The currents were

measured at 1.8 V from the voltammograms shown in Fig. 1A on the positive scan. A straight line with zero intercept was obtained, which indicated a mass-transport limited mechanism for DMSO oxidation at the Bi-PbO_2 electrode.

It has been concluded that the rate limiting step for both O_2 evolution and O-transfer reactions is the anodic discharge of H_2O to produce $'OH_{ad}$ (1-3, 9-10). Since these two processes were greatly enhanced at the Bi-PbO_2 films, the Bi-PbO_2 films were concluded to promote the production of $'OH_{ad}$.

Kinetic results of DMSO oxidation The kinetic results of DMSO oxidation at the Bi-PbO_2 film electrodes were studied. Experimentations were performed at eleven Bi-PbO_2 films which were electrodeposited on Au RDE from 1 M $HClO_4$ containing concentration ratio of $[Bi^{3+}]/[Pb^{2+}]$ from 0.0 to 1.0. Values of heterogeneous rate constants of DMSO oxidation at these electrodes in 1 M $HClO_4$ were plotted as a function of $[Bi^{3+}]/[Pb^{2+}]$, and the results are shown in Fig. 2A and Table I. Apparently, high electrocatalytic properties of Bi-PbO_2 were obtained at intermediate values of $[Bi^{3+}]/[Pb^{2+}] \approx 0.4 - 0.7$. Loss of electrocatalytic activities of Bi-PbO_2 was observed for $[Bi^{3+}]/[Pb^{2+}] \geq 0.9$.

It is anticipated that DMSO needs to be adsorbed to undergo O-transfer reaction. Therefore, when the numbers of $DMSO_{ad}$ and $'OH_{ad}$ approach the same value, maximum catalytic currents will be obtained. The doping level of Bi^{5+} in the Bi-PbO_2 film increased with increasing

concentration ratio of $[Bi^{3+}]/[Pb^{2+}]$ in the deposition solution (1-2), and the incorporated Bi(V) which substituted for surface Pb(IV) catalyzed the production of $^{\cdot}OH_{ad}$ (1-3); therefore, it was speculated that the electrode surface was highly covered by $^{\cdot}OH_{ad}$ for large values of $[Bi^{3+}]/[Pb^{2+}]$. When the electrode surface was highly populated with $^{\cdot}OH_{ad}$, there was a lack of active sites for pre-adsorbed DMSO, thereby resulting in the decreased rate for DMSO oxidation.

A correlation was expected between the rate of anodic evolution of O_2, and the rate of DMSO oxidation at the Bi-PbO_2 surface. Figure 2B shows the plot of heterogeneous rate constant (k) of DMSO oxidation, measured at 1.7 V, and the current of O_2 evolution (I_{O2}), measured at 1.8 V. An approximately linear positive relation is apparent for $[Bi^{3+}]/[Pb^{2+}] \leq 0.8$ (Fig. 2B, points a-i).

Degradation of electrode property occurred for $[Bi^{3+}]/[Pb^{2+}] > 0.9$ (Fig. 2B, points j-k), while I_{O2} remained nearly constant. For a large concentration ratio of $[Bi^{3+}]/[Pb^{2+}]$, the surface of Bi-PbO_2 was highly covered by $^{\cdot}OH_{ad}$; therefore, the current of O_2 evolution was large while the rate of DMSO oxidation decreased.

Electrocatalysis at pure PbO_2-film electrode by adsorbed Bi^{5+}

Cyclic voltammetry The electrocatalytic activities of the pure PbO_2-films for Mn^{2+} oxidation were observed to be significantly increased by exposure to 1 M $HClO_4$ of trace Bi^{3+} (1-2, 11-13). The Bi species were proven to be electrosorbed at the PbO_2 surface as Bi^{5+} ions (3).

Results shown in Fig. 3 were the voltammetric responses for DMSO oxidation at the pure PbO_2 film before (curve a) and after (curves b-h) the addition of Bi^{3+}. The dashed curve corresponds to the residual current obtained in the absence of DMSO and Bi^{3+}. Other currents shown (curves a-h) have been corrected for this residual signal. A catalytic effect was observed with the addition of Bi^{3+} at a concentration as low as 2 μM (curve b). Well-defined current plateaus of DMSO oxidation were observed at both positive and negative scans for 11 μM Bi^{3+} (curve c), and at positive scans for 23 - 43 μM Bi^{3+} (curves d-e).

Because Bi^{3+} was oxidatively adsorbed (3), the surface coverage of Bi^{5+} was expected to increase with increasing value of applied potential. Results indicated that there was relatively no Bi^{5+} adsorbed at 1.4 V (3, 13). At a fixed potential value, the equilibrium surface-coverage of Bi^{5+}_{ad} should also increase with increasing concentrations of Bi^{3+} in the solution. The decreased currents of DMSO oxidation for $[Bi^{3+}] \geq 23$ μM (Fig. 3, curves d-h) were anticipated to result from the blocked surface active sites for DMSO adsorption by electrosorbed Bi^{5+} (13).

Cyclic voltammograms of Bi^{3+} are shown in Fig. 4A to reveal the oxidative adsorption of Bi^{3+} at the PbO_2 surface in 1 M $HClO_4$. Curves a-d have been corrected for the background current measured in the absence of Bi^{3+}. Anodic peaks at 1.6 V on the positive scans correspond to the oxidative adsorption of Bi^{3+} to Bi^{5+}. The cathodic peaks obtained on the succeeding negative scans were expected to be the result

from the reductive stripping of adsorbed Bi^{5+}. Peak heights increased with increasing concentrations of Bi^{3+} from 3 to 52 μM, because the surface coverage of Bi^{5+} was a positive function of Bi^{3+} concentrations. Since the concentration of bulk Bi^{3+} (5.2×10^{-5} M) was only one millionth of that of H_2O (55.6 M), the current of bulk-Bi^{3+} oxidation was expected to be negligible in comparison with that of H_2O oxidation. Therefore, the currents measured at $E > 1.7$ V on the positive scan were concluded to be virtually due to the catalyzed O_2 evolution.

The anodic peak currents measured at 1.61 V are plotted in Fig. 4B as a function of Bi^{3+} concentrations in the solution. A negative deviation of the curve from the linearity was obtained at high concentrations of Bi^{3+}, which is an indication of the adsorption isotherm of Bi^{3+} at the PbO_2 surface.

Chronoamperometric response The current-time response measured for DMSO oxidation at the PbO_2-film electrode is shown in Fig. 5 as a function of Bi^{3+} concentration. The I-t curves were obtained following a potential step from 1.4 V to 1.7 V at newly prepared film electrodes to avoid any influence from preceding experiments. It was determined, however, that the I-t response was reproducible at a single electrode provided the potential was kept at 1.4 V for 3 min, during which the total desorption of previously adsorbed Bi^{5+} was achieved.

The current for DMSO oxidation increased slowly following the potential step following the addition of 3.2 μM Bi^{3+} (curve a). For

intermediate values of [Bi^{3+}] (i.e., 32 - 96 μM, curves b - e), anodic currents reached steady state values within 1 min following the potential step. At high concentrations of [Bi^{3+}] (i.e., > 183 μM, curves d - f), limiting currents were reached very quickly following the potential step; however, currents began to decrease from their limiting values within 0.5 min.

It is apparent from the I-t curves in Fig. 5 that the rate of current increase increased with increasing Bi^{3+} concentrations. It was anticipated that the time required to achieve an equilibrium coverage of Bi^{5+}_{ad} at the PbO_2 electrode decreased with increasing Bi^{3+} concentrations in the solution. The decay in the current for DMSO oxidation at Bi^{3+} > 183 μM was consistent with the interpretation described previously for Fig. 3 that small amount of adsorbed Bi^{3+} will function catalytically; however, a high surface coverage resulting from high Bi^{3+} concentrations is disadvantageous to the catalytic mechanism.

The rate of increase in the catalytic activity was also dependent on the flux of Bi^{3+} arriving at the rotation disc electrode. Figure 6 shows the I-t responses for DMSO oxidation at the PbO_2-film electrodes in 1 M $HClO_4$ following the potential step from 1.4 V to 1.7 V before (curve a) and after (curves b - f) the addition of 3 μM Bi^{3+}. It is apparent that the currents measured increased with increasing rotation speeds of the RDE. It was expected that the time required to achieve the equilibrium value of surface coverage by adsorbed Bi^{5+} decreased with increasing flux of Bi^{3+} coming to the electrode surface.

The correlation between the heterogeneous rate constant (k) for DMSO oxidation, measured at 1.7 V, and the current of O_2 evolution (I_{O2}), measured in the absence of DMSO is shown in Fig. 7A as a function of Bi^{3+} concentration. Current values for O_2 evolution were taken at 1.9 V from voltammetric curves recorded during the positive scan (20 mV s^{-1}; 900 rev min^{-1}) starting at 1.4 V. It is apparent from this figure that a positive correlation was obtained between k and I_{O2} for $[Bi^{3+}] \leq 131.2$ μM (points a-g). However, a loss of electrode activity was observed for $[Bi^{3+}] \geq 291.2$ μM (points h-j).

Experimentation was also done according to the exact conditions described for Fig. 7A except for using a higher rotation speed of 1600 rev min^{-1} to investigate the effect of Bi^{3+} flux on the catalytic mechanism of DMSO oxidation. Kinetic data are shown in Fig. 7B for the rate constant of DMSO oxidation (k) against the current of O_2 evolution (I_{O2}). Data were obtained in the same way as described for Fig. 7A. A positive correlation was observed between k and I_{O2} for $[Bi^{3+}] < 51.2$ μM (points a-e). However, for Bi^{3+} concentrations ≥ 51.2 μM (points f-j), a rapid decrease of the rate constant for DMSO oxidation was obtained without a substantial decrease in the current for O_2 evolution.

In comparison with Fig. 7A, the retardation of DMSO oxidation by high coverage of Bi^{5+}_{ad} at 1600 rev min^{-1} occurred at lower $[Bi^{3+}]$ (51.2 μM) than that at 900 rev min^{-1} (291.2 μM). In conjuction with the results shown in Fig. 6, it was speculated that the equilibrium coverage at PbO_2 surface by Bi^{5+}_{ad} was achieved within a shorter time period at

higher rotation speeds than at lower rotation speeds of the RDE. An optimal coverage of Bi^{5+}_{ad} was required to achieve a maximum catalytic activity of the PbO_2-film electrode. Therefore, a high surface coverage of Bi^{5+}_{ad} can catalyze the production of $'OH_{ad}$; however, which in return diminished the number of catalytic sites for pre-adsorbed DMSO.

Electrocatalysis by Bi(V) adsorption at the anion doped PbO_2-film electrodes

The application of Cl-PbO_2 film electrode has proven successful for numerous catalytic anodic O-transfer reactions in sulfuric acid media (Chap. II). It was concluded that an ion-exchange reaction occurred between the exchangeable surface anion (Cl^-) and the solution anion (HSO_4^-). This reaction occurred as a result of exposure of Cl-PbO_2 to 1 M H_2SO_4 (14). The resulting HSO_4^--modified PbO_2 films showed significant enhancement in the rate for various oxidation reactions (14-15).

Experimentation was done to compare the catalytic results at the pure and Cl-doped PbO_2-film electrodes by Bi^{5+} adsorption. The unfolded cyclic voltammograms of DMSO are shown in Fig. 8 at the Bi^{5+} adsorbed Cl-PbO_2-film electrodes in 1 M H_2SO_4. Dashed curve corresponds to the background current measured in the absence of DMSO and Bi^{3+}. Other currents shown have been corrected for this background signal to clearly reveal the change in the net current produced from DMSO oxidation. It should be noted that the current of Bi^{3+} oxidation was relatively

negligible in comparison with that of DMSO oxidation (0.4 mA at $[Bi^{3+}]$ = 273 μM). Curve a corresponds to the oxidation of DMSO in the absence of Bi^{3+}, this current is evidently larger than that at the pure PbO_2 (Fig. 3, curve a).

The anodic currents of DMSO were observed to increase with increasing concentration of Bi^{3+} in the solution (i.e., $[Bi^{3+}] \leq 153$ μM, curves b-f). The electrode activity was lost only for $[Bi^{3+}] \geq 273$ μM (curve g).

It is apparent from Fig. 8 that the rate of increase in the catalytic reactivity of Cl-PbO_2 by the adsorbed Bi^{5+} is slower than that at the pure PbO_2 (Fig. 3). However, loss of the electrode activity for the HSO_4^--modified Cl-PbO_2 electrode occurred at a much higher concentration of Bi^{3+} (273 μM) than that for the pure PbO_2 (43 μM).

Activation of the OAc-PbO_2-film electrode by HSO_4^- has been discussed previously (16). The unfolded cyclic voltammograms of DMSO are shown in Fig. 9 at the Bi^{5+} adsorbed OAc-PbO_2 film 1 M H_2SO_4. The dashed curve corresponds to the residual current measured in the absence of Bi^{3+} and DMSO.

Additions of Bi^{3+} up to 95 μM were determined to catalyze the oxidation of DMSO (curves b-e). Degradation of the electrode property only occurred for $[Bi^{3+}] \geq 608$ μM on the negative scan (curve f). Currents were observed to decrease from limiting values at E > 1.75 V to form the peak-shaped curves. These results were tentatively assigned to the loss of active sites for the pre-adsorbed reactants at very positive potential as a result of severe O_2 evolution (16).

Chronoamperometric studies of Cl-PbO_2 The typical current-time responses are shown in Fig. 10 for DMSO oxidation at the Bi^{5+} (320 μM) adsorbed surfaces following the potential step from 1.4 V to 1.7 V. Curve a corresponds to a Cl-PbO_2 in 1 M $HClO_4$, and b to a Cl-PbO_2 in 1 M H_2SO_4. The currents measured at both electrodes reached the limiting value within 0.5 min; however, a slow decay in the anodic current was observed for that in 1 M $HClO_4$ (curve a).

Curve c corresponds to a HSO_4^--pretreated Cl-PbO_2 film in 1 M $HClO_4$. The pretreatment involved 3 cyclic potential scans between the scan limits of 1.4 V and 1.9 V with Cl-PbO_2 immersed in 1 M H_2SO_4. Steady state current was obtained throughout the entire electrolysis of 10-min duration. Solution HSO_4^- was expected to substitute for the surface Cl^- during the pretreatment period. This substitution was concluded to be an irreversible process, during which HSO_4^- remained at the electrode surface even in 1 M $HClO_4$ containing no HSO_4^-.

Cyclic voltammetry at Bi-doped PbO_2 electrodes

Co-deposition of PbO_2 with Bi^{3+} resulted in the Bi^{5+}-doped PbO_2 (Bi-PbO_2) films. The incorporated Bi(V) was concluded to substitute for lattice Pb(IV) (1-3, 11-12), and functioned as catalytic centers for the anodic discharge of H_2O to produce the $\cdot OH_{ad}$ (3, 13).

Cyclic voltammograms of DMSO are shown in Fig. 11A at Bi^{5+} adsorbed Bi-PbO_2 film electrodes in 1 M $HClO_4$. Curve a corresponds to the oxidation of 5 mM DMSO in 1 M $HClO_4$. Addition of 29 uM Bi^{3+} resulted in a loss of electrode reactivity during the negative potential scan

(curve b). Rapid degradation of the electrocatalytic properties of Bi-PbO_2 were observed for $[Bi^{3+}] \geq 89$ μM (curves c-e). The degradation was concluded to occur as a result of catalytic mechanism being blocked by the adsorbed Bi^{5+}.

Slowing down the potential scan rate of the electrode allowed enough time to reveal two anodic peaks during the oxidation of DMSO at the Bi^{5+} adsorbed Bi-PbO_2 electrode. Cyclic voltammograms are shown in Fig. 11B for potential scan rates of 20 mV s^{-1} (curve a), 5 mV s^{-1} (curve b), and 1 mV s^{-1} (curve c). Shifting of the peak potential toward less positive values was observed as the potential scan rate decreased. The negative shift of the anodic peak potential was the result of increase in the reversibility of the electrode reaction.

It is speculated from the results shown in Fig. 11B that two kinds of active sites existed at the surface of Bi-PbO_2 where electrosorption of Bi^{3+} can occur. These active sites were tentatively assigned to the surface Bi(V) and Pb(IV) of Bi-PbO_2. The anodic peaks at less positive potentials were concluded to correspond to the catalytic oxidation of DMSO by the Bi^{5+}_{ad} at the more active Bi(V) sites, and that at more positive potential corresponded to the less active sites of Pb(IV).

It was concluded that number of Bi(V) sites at the Bi-PbO_2 surface was related to the ratio $[Bi^{3}]/[Pb^{2+}]$ in the deposition solution (3, 13). If the interpretation drawn in the preceding paragraph is true, then, increasing the ratio $[Bi^{3+}]/[Pb^{2+}]$ for the deposition of Bi-PbO_2 is expected to result in an increased height of the anodic peak measured at less positive potential shown in Fig. 11B. This enhancement in the

peak current was due to a increased number of Bi(V) sites been created.

Figure 11C shows the cyclic voltammograms of DMSO at the Bi^{5+} adsorbed Bi-PbO_2 films in 1 M $HClO_4$. These Bi-PbO_2 films were deposited from 1 M $HClO_4$ containing various concentration ratios of $[Bi^{3+}]/[Pb^{2+}]$ from 0.0 to 1.0. Single peak was obtained at the pure PbO_2-film electrode (curve a); whereas two peaks were measured at the Bi-PbO_2 film electrode (curves b-e). The anodic peak at E = 1.6 V, which was assigned to the oxidation of DMSO by the catalytically adsorbed Bi^{5+} at the Bi^{5+} sites of Bi-PbO_2, grew as the doping level of Bi^{5+} in Bi-PbO_2 increased.

Opposite phenomena were observed for the peaks measured at 1.7 V. These anodic peaks were concluded to correspond to the catalytic oxidation of DMSO by adsorbed Bi^{5+} at the Pb^{4+} sites of Bi-PbO_2. The height of these anodic peaks decreased with increasing doping level of Bi^{5+} in Bi-PbO_2. It was concluded that the substitution of Bi^{5+} for Pb^{4+} did not result in substantial distortion of the crystal lattice (1, 11-12). Therefore, total number of the cation sites at the surface of Bi-PbO_2 can be assumed constant at various doping levels of Bi^{5+} in the mixed oxide:

$$N_{cation} = N_{Bi(V)} + N_{Pb(IV)} \qquad [2]$$

where N_{cation}, $N_{Bi(V)}$, and $N_{Pb(IV)}$ represent the number of cation sites, Bi^{5+} sites, and Pb^{4+} sites, respectively. An increase in $N_{Bi(V)}$ as a result of higher doping level of Bi^{5+} in Bi-PbO_2 causes a decrease of $N_{Pb(IV)}$.

Information extracted from Fig. 11C concluded that Bi^{3+} oxidatively adsorbed at the cationic sites of Bi-PbO_2 and functioned catalytically as the O-transfer mediator during the oxidation of DMSO.

Conclusion

The anodic discharge of H_2O has been determined to be the rate limiting step of both the O_2 evolution (17) and anodic O-transfer reactions (2-3). The production of $^{\cdot}OH_{ad}$ occurred at the active cationic sites of the PbO_2 surface. The rate of this limiting step is significantly increased by the surface-Bi^{5+} species which are either electrosorbed at PbO_2 (Bi^{5+} adsorbed PbO_2) or incorporated in the PbO_2 matrix (Bi^{5+}-doped PbO_2).

The current of O_2 evolution increased with increasing content of Bi(V) in the doped oxide (Bi-PbO_2), and also increased with increasing surface coverage of Bi^{5+}_{ad} at PbO_2. Surface coverage of Bi^{5+}_{ad} is strongly dependent on the applied potential as well as concentrations of Bi^{3+} in the solution. An optimal coverage of Bi^{5+}_{ad}, or Bi^{5+} level in Bi-PbO_2 was necessary for a maximum catalytic efficiency of DMSO oxidation. However, a PbO_2 film which was highly covered by Bi^{5+}_{ad}, or heavily doped with Bi^{5+} is detrimental to the catalytic mechanism for DMSO oxidation. The decreased catalytic reactivity of the oxide electrode is a result of the diminished number of active sites for the pre-adsorbed DMSO.

Two kinds of active sites for the catalytic adsorption of Bi^{5+} are determined to exist at the surface of Bi-PbO_2. These sites are concluded to be the surface Bi^{5+} and Pb^{4+} with Bi^{5+} being the more active one. The half wave potential ($E_{1/2}$) obtained for DMSO oxidation at Bi-doped PbO_2 (1.664 V, Fig. 1A) is consistent with that for the Bi^{5+} adsorbed PbO_2 (1.663 V, Fig. 3). For both cases, the anodic discharge of H_2O to produce $^{\cdot}OH_{ad}$ is highly enhanced at Bi(V) sites regardless of the chemical environments around Bi^{5+}.

Increases of the rate of DMSO oxidation by adsorbed $Bi^{5+}{}_{ad}$ are much significant at the HSO_4^--modified Cl-PbO_2 and OAc-PbO_2 film electrodes than that for the pure PbO_2. Loss of electrode reactivities due to blocked catalytic mechanism by $Bi^{5+}{}_{ad}$ was obtained at much higher concentrations of Bi^{3+} at the anion-doped PbO_2 ($[Bi^{3+}] \geq 608$ μM for OAc-PbO_2, and $[Bi^{3+}] \geq 273$ μM for Cl-PbO_2) than that for the pure PbO_2 ($[Bi^{3+}] \geq 43$ μM). The modification of anion-doped PbO_2 by HSO_4^- is tentatively concluded to result in changes of the electron density around lattice Pb^{4+} by the neighboring HSO_4^-. This change increases the tendency for catalytic adsorption of $^{\cdot}OH$, which in return speeds up the rate limiting step for both O_2 evolution and O-transfer reactions.

References

1. (a) Yeo, I.-H.; Johnson, D. C. J. Electrochem. Soc., 1987, 134, 1973.
(b) Yeo, I-H. Ph.D. Dissertation, Iowa State University, Ames, Iowa, 1987.

2. Chang, H. Ph.D. Dissertation, Iowa State University, Ames, Iowa, 1989.

3. (a) Larew, L. A.; Gordon, J. S.; Hsiao, Y.-L.; Buttry, D. A.; Johnson, D. C. J. Electrochem. Soc. 1990, 137, 3701.
(b) Feng, J.; Johnson, D. C. J. Electrochem. Soc., 1990, 137, 507.

4. This dissertation, Chap. II.

5. Levich, V. G. "Physicochemical Hydrodynamics"; Prentice Hall: Englewood Cliffs, NJ, 1962, p. 75.

6. Koutecky, J.; Levich, V. G. Zh. Fiz. Khim. 1956, 32, 1565.

7. Oyama, N.; Anson, F. C. Anal. Chem. 1980, 52, 1192.

8. Beck, F.; Schulz, H. J. Electroanal. Chem. 1987, 229, 339.

9. Trasatti, S.; Lodi, G. "Electrodes of Conductive Metallic Oxides"; Elsevier Pub. Co.: New York, 1981, Part B, p. 521.

10. (a) Anderson, A. B. J. Electrochem. Soc. 1989, 136, 158.
(b) Bockris, J. O'M. J. Chem. Phys., 1956, 24, 817.

11. Yeo, I-H.; Johnson, D. C. J. Electrochem. Soc. 1987, 134, 1973.

12. Yeo, I-H.; Kim, S.; Jacobson, R.; Johnson, D. C. J. Electrochem. Soc. 1989, 136, 1395.

13. Chang, H.; Johnson, D. C. J. Electrochem. Soc. submitted for publication.

14. This dissertation, Chap. III.

15. Hsiao, Y.-L.; Johnson, D. C. J. Electrochem. Soc. 1989, 136, 3704.

16. This dissertation, Chap. V.

Table I. Kinetic data for DMSO oxidation at the Bi-PbO_2 films on Au RDE

Ratio[a] $[Bi^{3+}]/[Pb^{2+}]$	10^3 x k (cm s^{-1})[b]
0.0	< 0.1
0.1	5.95 ± 0.02
0.2	8.71 ± 0.04
0.3	33.5 ± 0.5
0.4	35.0 ± 0.2
0.5	37.8 ± 0.1
0.6	44.5 ± 0.4
0.7	31.5 ± 0.5
0.8	47.3 ± 0.7
0.9	28.0 ± 0.4
1.0	21.2 ± 0.3

[a]Concentration ratio for the deposition of Bi-PbO_2 in 1 M $HClO_4$.

[b]E = 1.7 V was applied for the oxidation of DMSO, and heterogeneous rate constant was calculated assuming n_{eff} = 2 eq mol^{-1}.

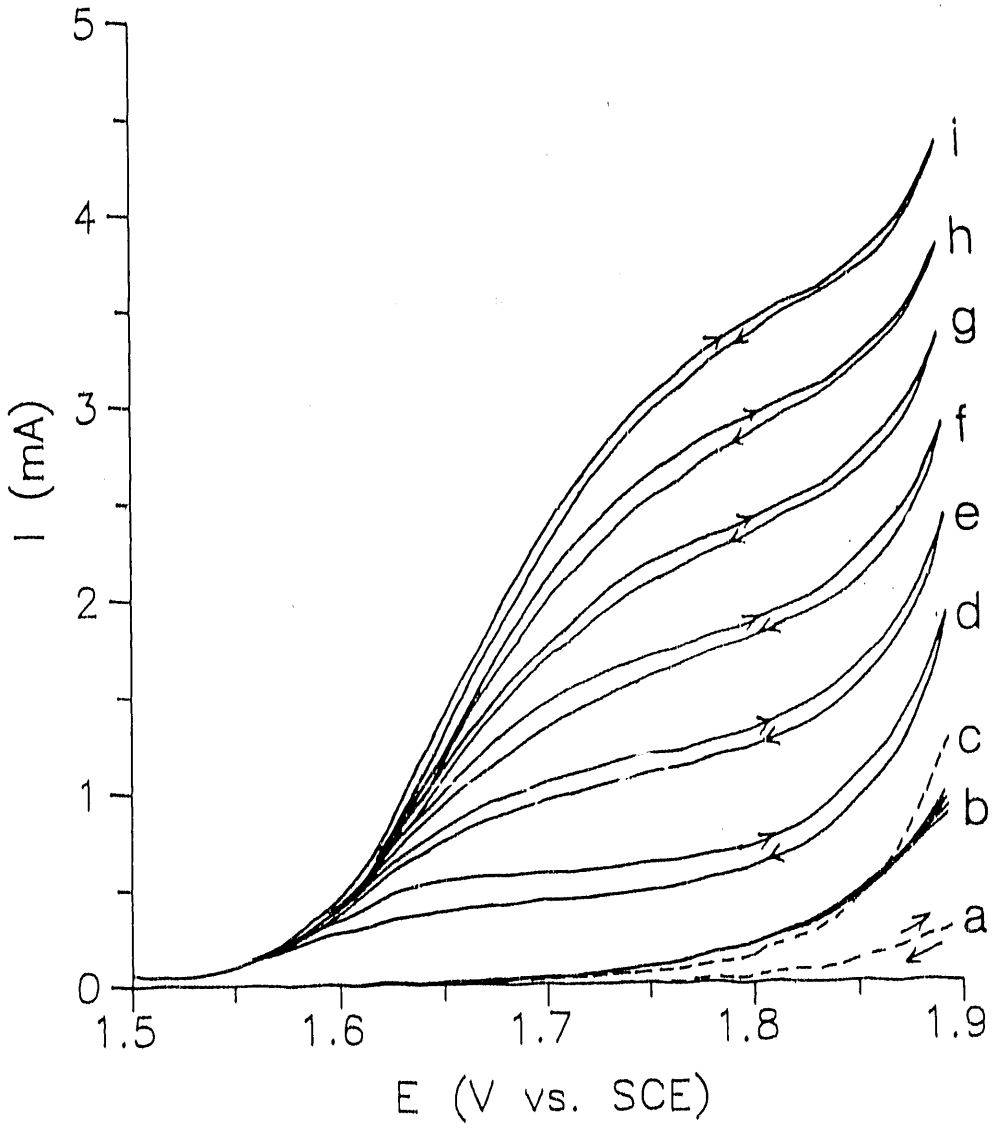

Figure 1A. Cyclic voltammograms for DMSO oxidation in 1 M $HClO_4$

Conditions: 20mV s^{-1}, 5 mM DMSO, 1 M $HClO_4$

Electrodes: (a-b) pure PbO_2 film on Au,
(c-i) Bi-PbO_2 film on Au

[DMSO] (mM): (a, c) 0, (b, d-i) 5

Rotation speed (rev min^{-1}): (a, c) 900, (b) 100 - 3600,
(d) 100, (e) 400, (f) 900,
(g) 1600, (h) 2500, (i) 3600

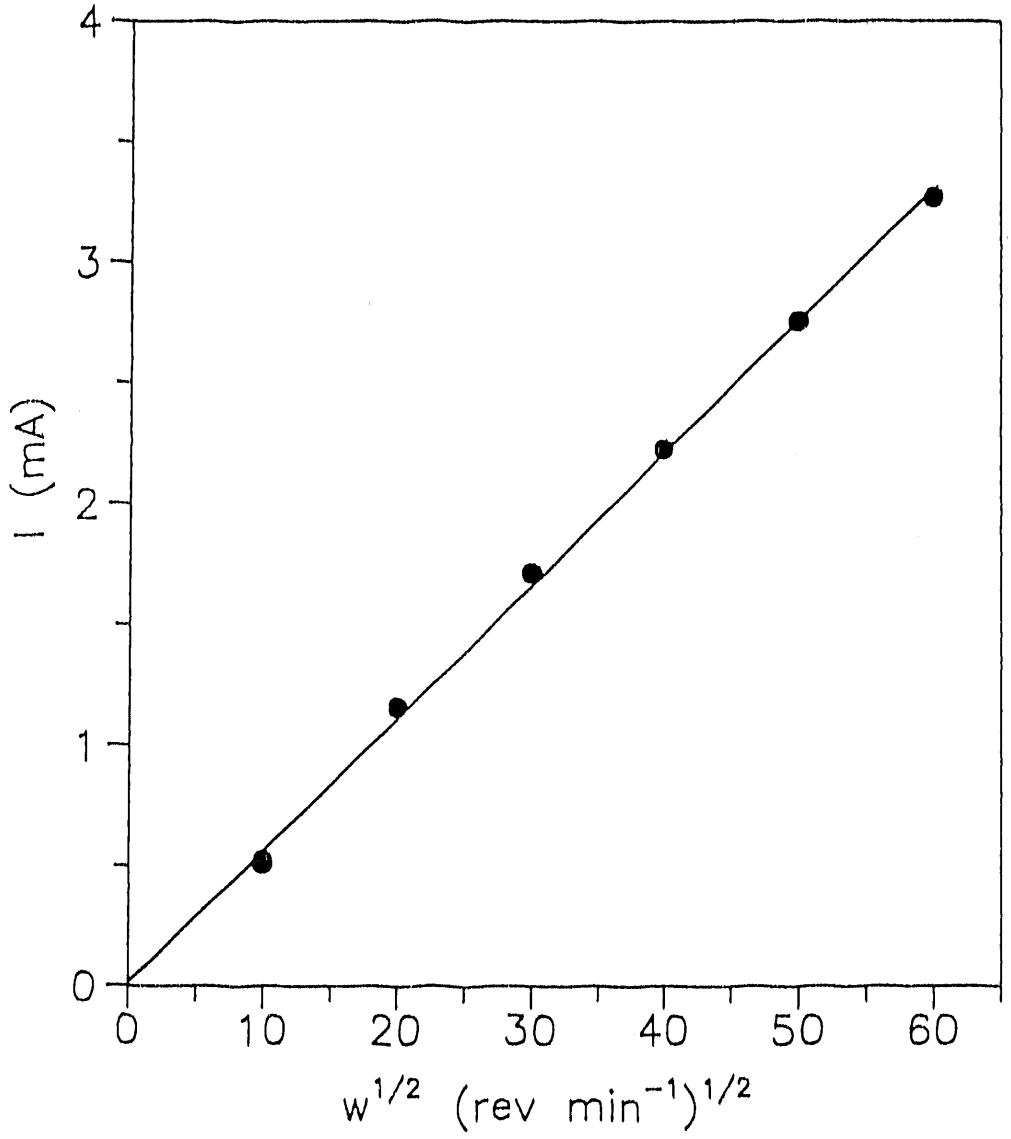

Figure 1B. Plot of I *vs.* $w^{1/2}$ for DMSO oxidation at a Bi-PbO_2 in 1 M $HClO_4$ at E = 1.8 V

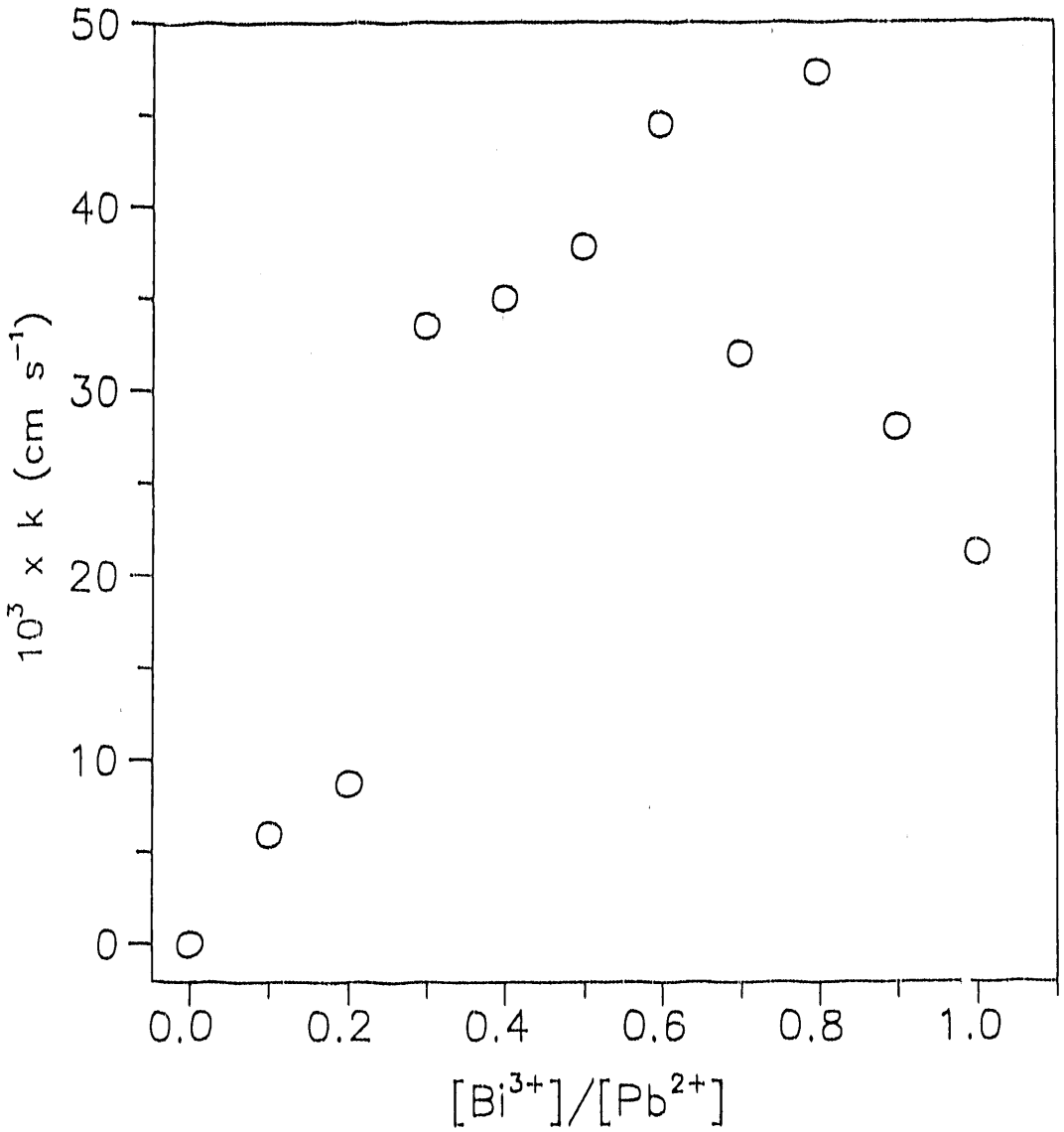

Figure 2A. Plot of k_{app} for DMSO oxidation at Bi-PbO_2 *vs.* concentration ratio of $[Bi^{3+}]/[Pb^{2+}]$ in the deposition solution

Conditions: 5 mM DMSO, 1 M $HClO_4$,
E = 1.7 V

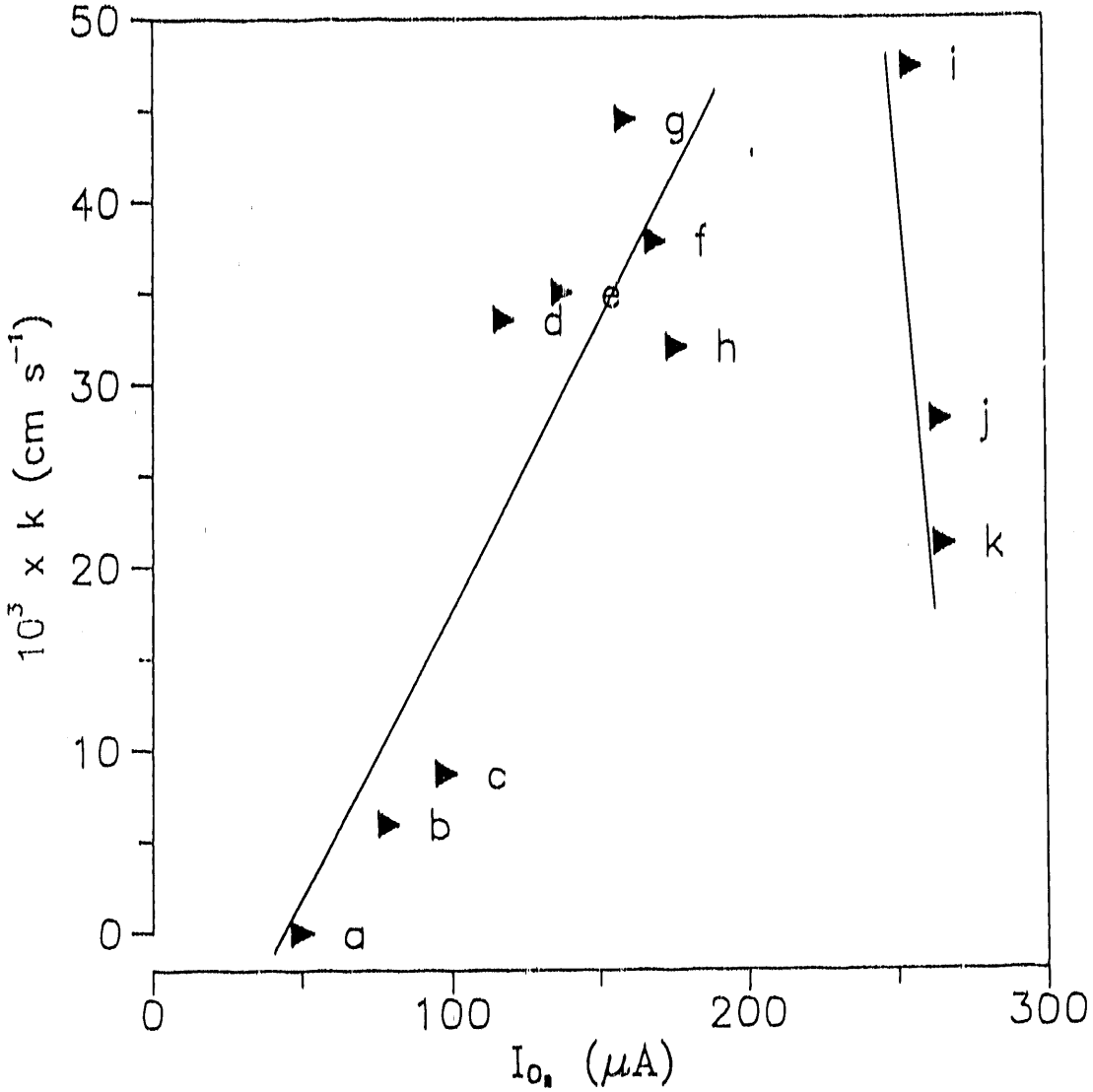

Figure 2B. Plot of k_{app} for DMSO oxidation *vs.* current of O_2 evolution at the Bi-PbO_2 film on a Au RDE

Conditions: 5 mM DMSO, 1 M $HClO_4$,
E = 1.7 V for DMSO oxidation,
E = 1.8 V for O_2 evolution

$[Bi^{3+}]/[Pb^{2+}]$: (a) 0.0, (b) 0.1, (c) 0.2, (d), 0.3
(e) 0.4, (f) 0.5, (g) 0.6, (h) 0.7,
(i) 0.8, (j) 0.9, (k) 1.0

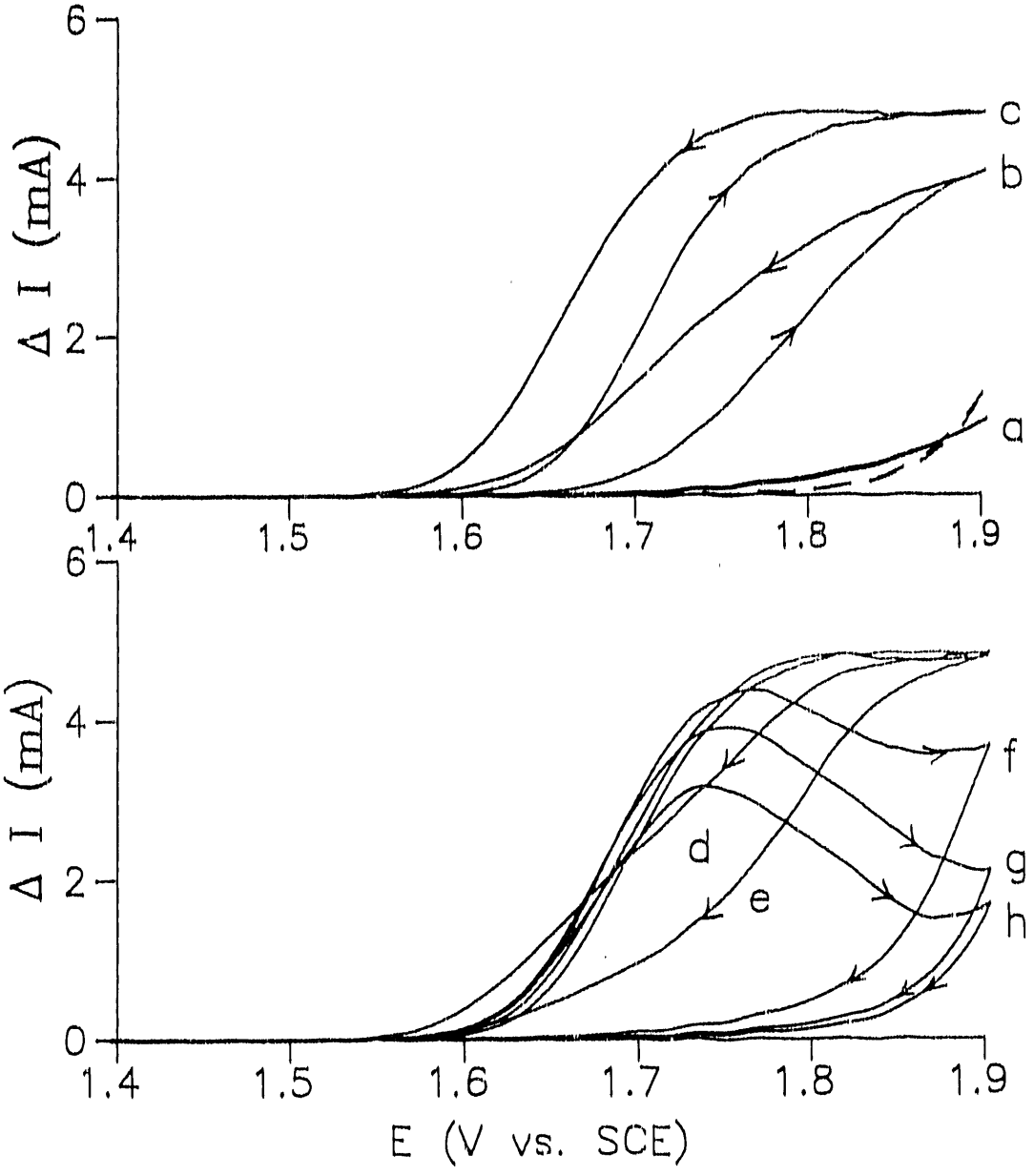

Figure 3. Cyclic voltammograms for DMSO oxidation at the Bi^{5+}-adsorbed pure PbO_2 film on Au RDE

Conditions: 2500 rev min^{-1}, 1 V min^{-1},
10 mM DMSO, 1 M $HClO_4$

$[Bi^{3+}]$ (μM): (a) 0, (b) 2, (c) 11, (d), 23, (e), 43,
(f) 93, (g) 153, (h) 273

Curves: (---) residual,
(a-h) net currents produced for DMSO oxidation

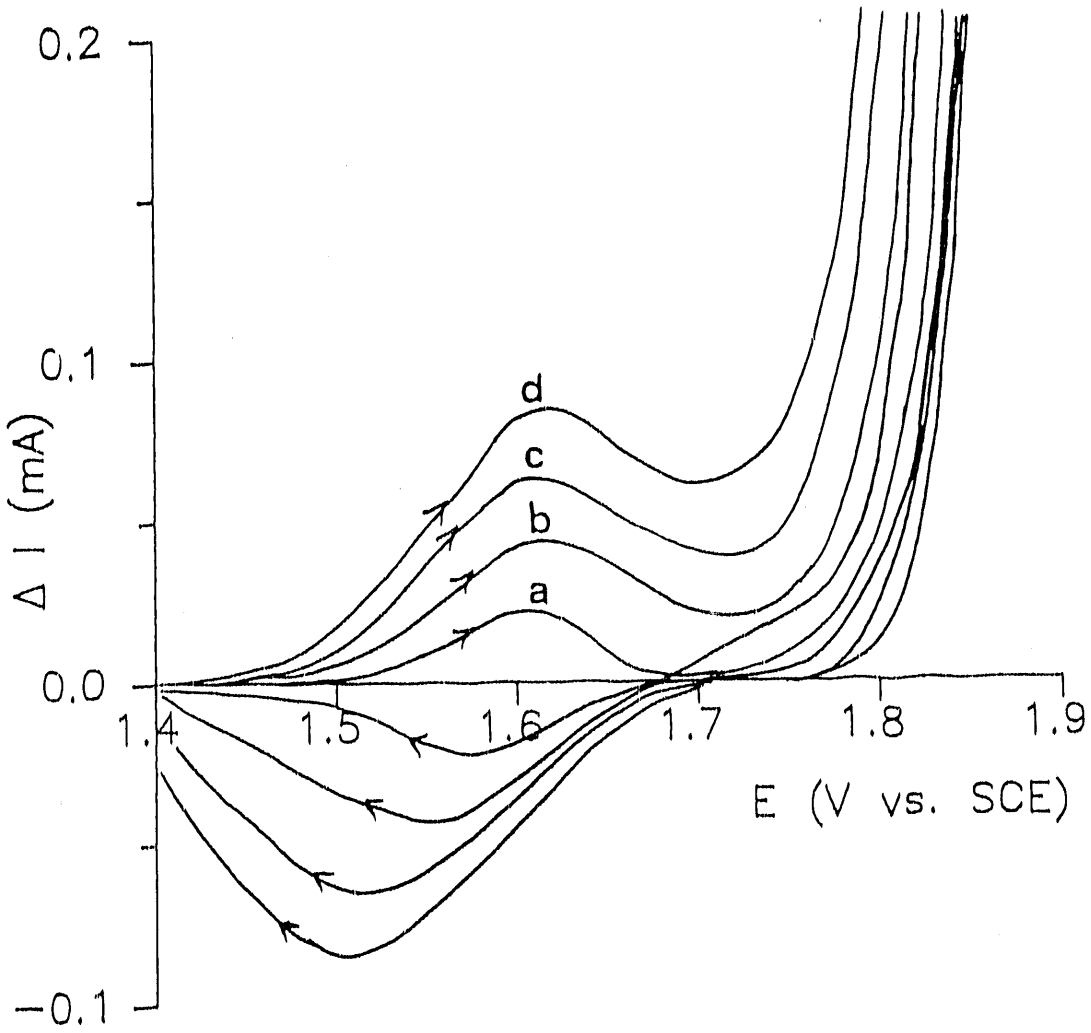

Figure 4A. Cyclic voltammograms of Bi^{3+} at a pure PbO_2 film on a Au RDE (Currents shown have been corrected for background signal measured in the absence of DMSO)

Conditions: 1600 rev min^{-1}, 1 V min^{-1}, 1 M $HClO_4$

$[Bi^{3+}]$ (μM): (a) 3, (b) 12, (c) 32, (d) 52

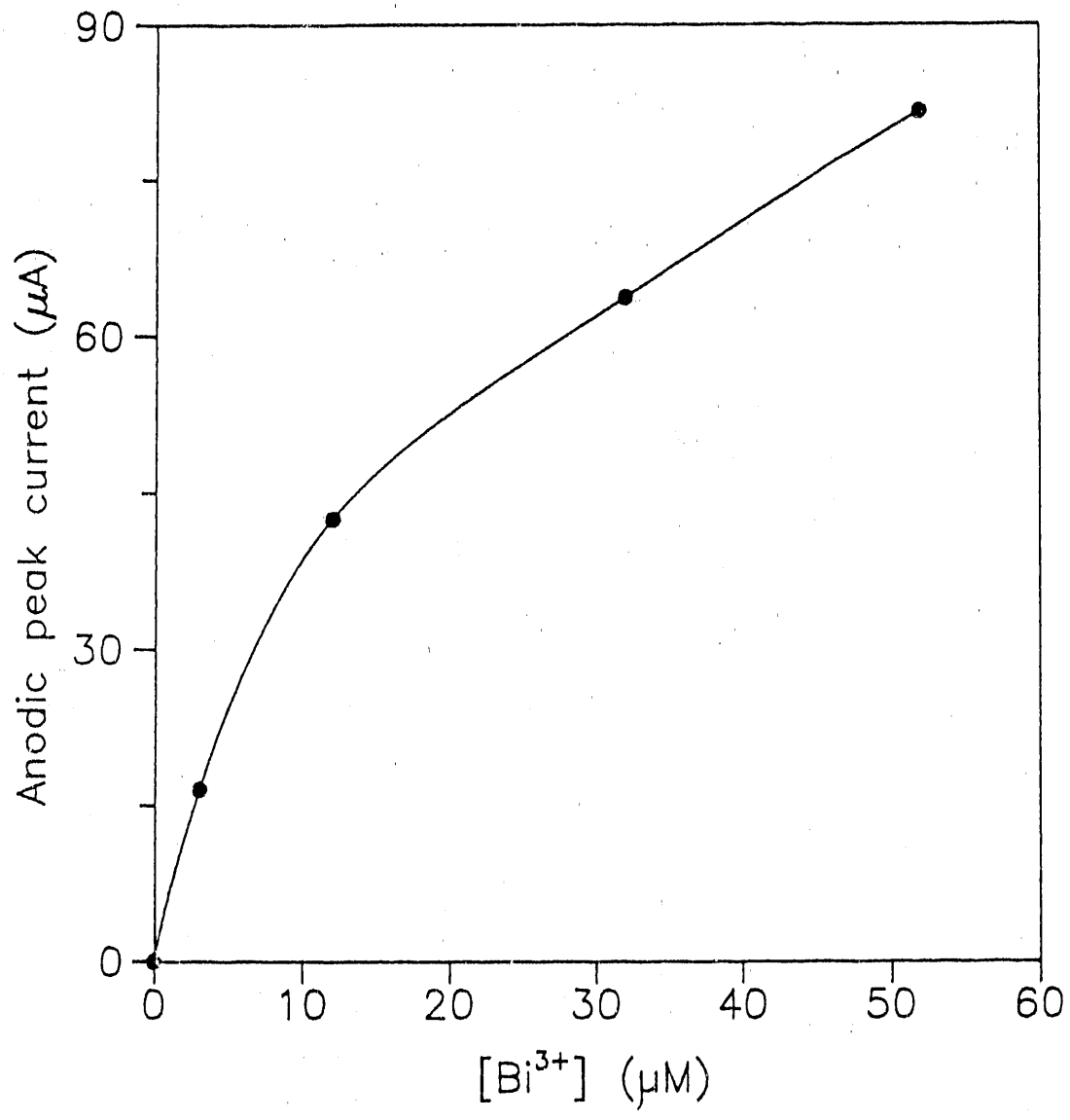

Figure 4B. Plot of anodic peak current *vs.* Bi^{3+} concentration

Conditions: same as Fig. 4A

Peak potential: 1.61 V

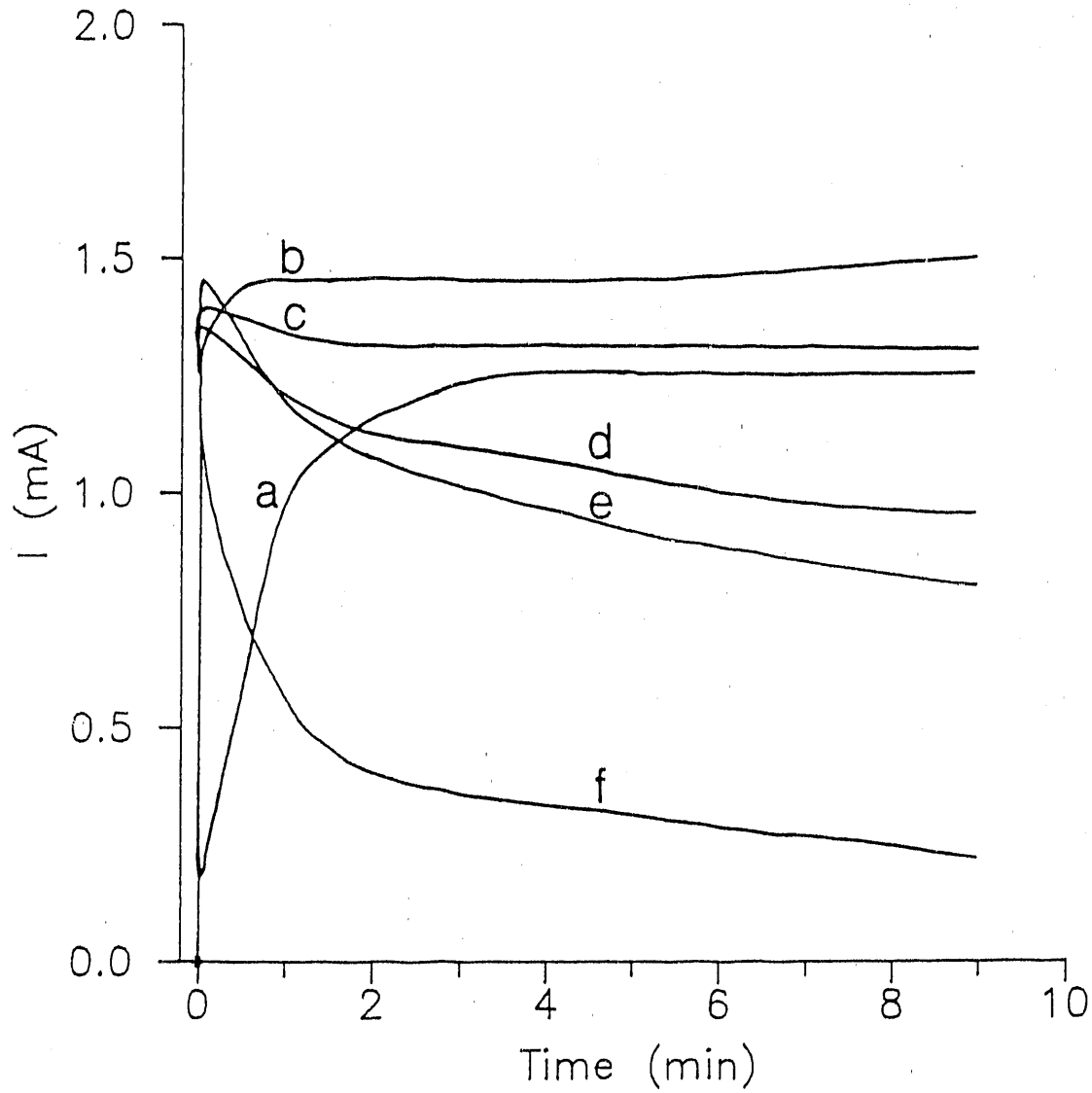

Figure 5. Current-time response for DMSO oxidation at the pure PbO_2 film on Au RDE obtained following a potential step from 1.4 V to 1.7 V

Conditions: 10 mM DMSO, 1 M $HClO_4$, 400 rev min^{-1}

$[Bi^{3+}]$ (μM): (a) 3.2, (b) 32, (c) 96, (d) 183.5, (e) 320, (f) 640

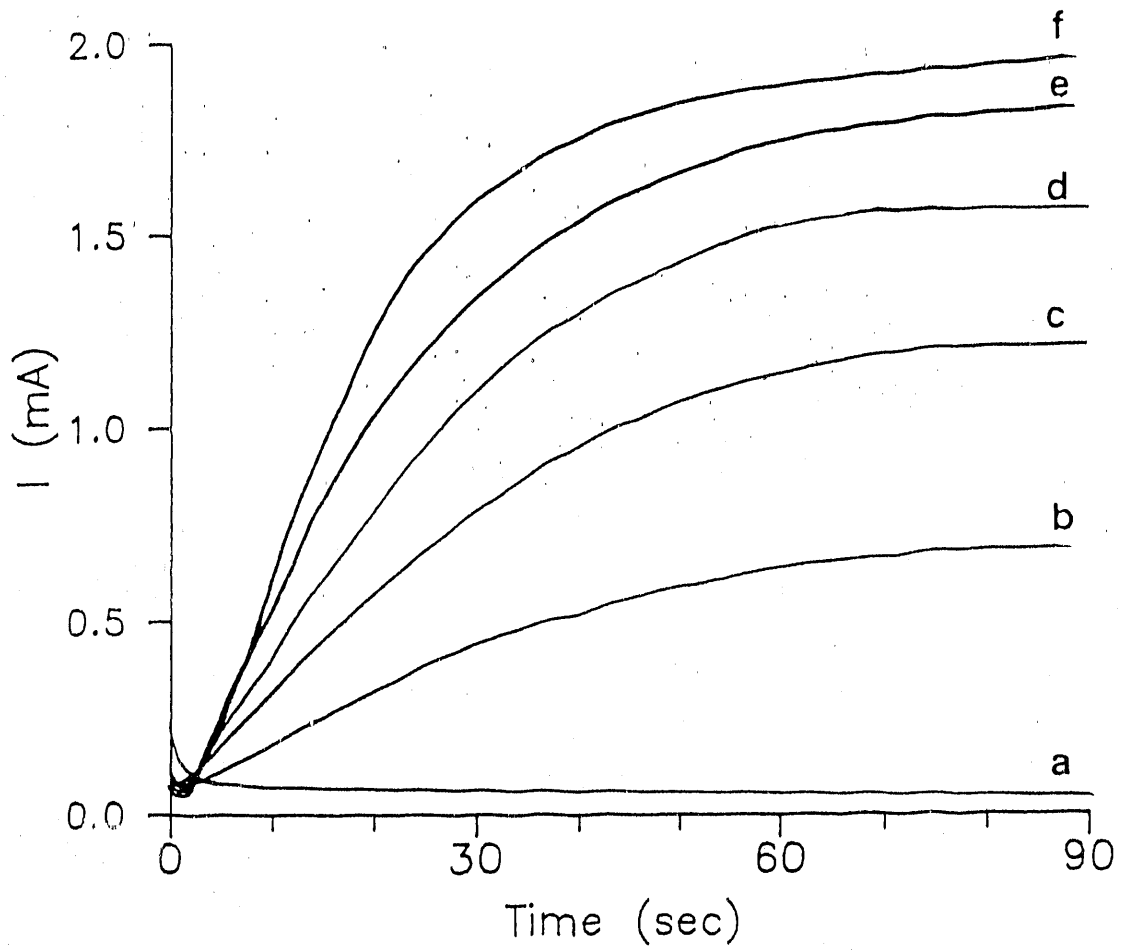

Figure 6. Current-time response for DMSO oxidation at the pure PbO_2 film on Au RDE obtained following the potential step from 1.4 V to 1.7 V

[DMSO] (mM): (a-f) 5

[Bi^{3+}] (μM): (a) 0, (b-f) 3

Rotation speed (rev min^{-1}): (a) 900 - 3600, (b) 400, (c) 900, (d) 1600, (e) 2500, (f) 3600

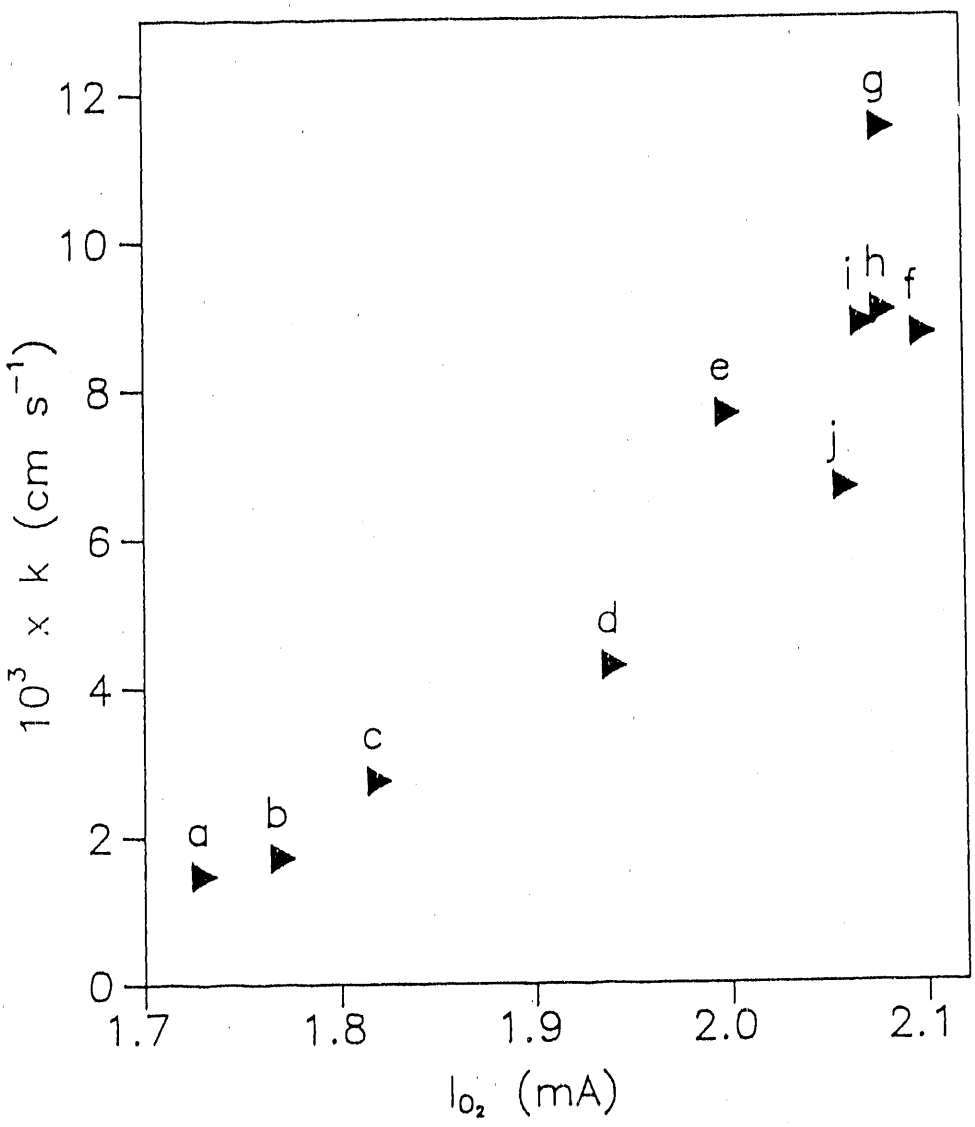

Figure 7A. Plot of k_{app} for DMSO oxidation *vs.* current of O_2 evolution at the pure PbO_2 film on a Au RDE

Conditions: 5 mM DMSO, 1 M $HClO_4$, E = 1.7 V

Rotation speed: 900 rev min^{-1}

$[Bi^{3+}]$ (μM): (a) 0, (b) 1.6, (c) 3.2, (d) 9.6, (e) 19.2, (f) 51.2, (g) 131.2, (h) 291.2, (i) 611.2, (j) 931.2

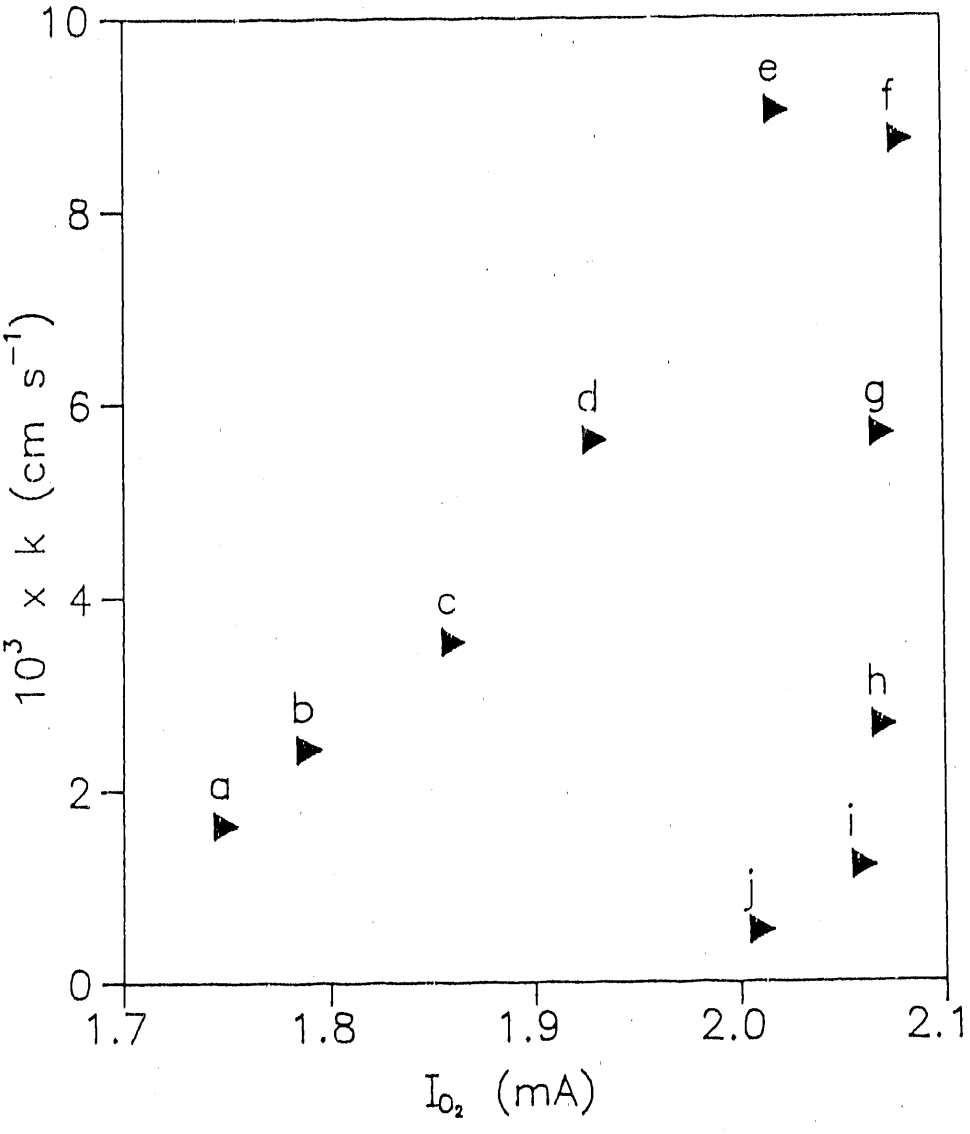

Figure 7B. Plot of k_{app} for DMSO oxidation *vs.* current of O_2 evolution at the pure PbO_2 film on a Au RDE

Conditions: same as Fig. 7A

Rotation speed: 1600 rev min^{-1}

$[Bi^{3+}]$ concentrations (μM): same as Fig. 7A

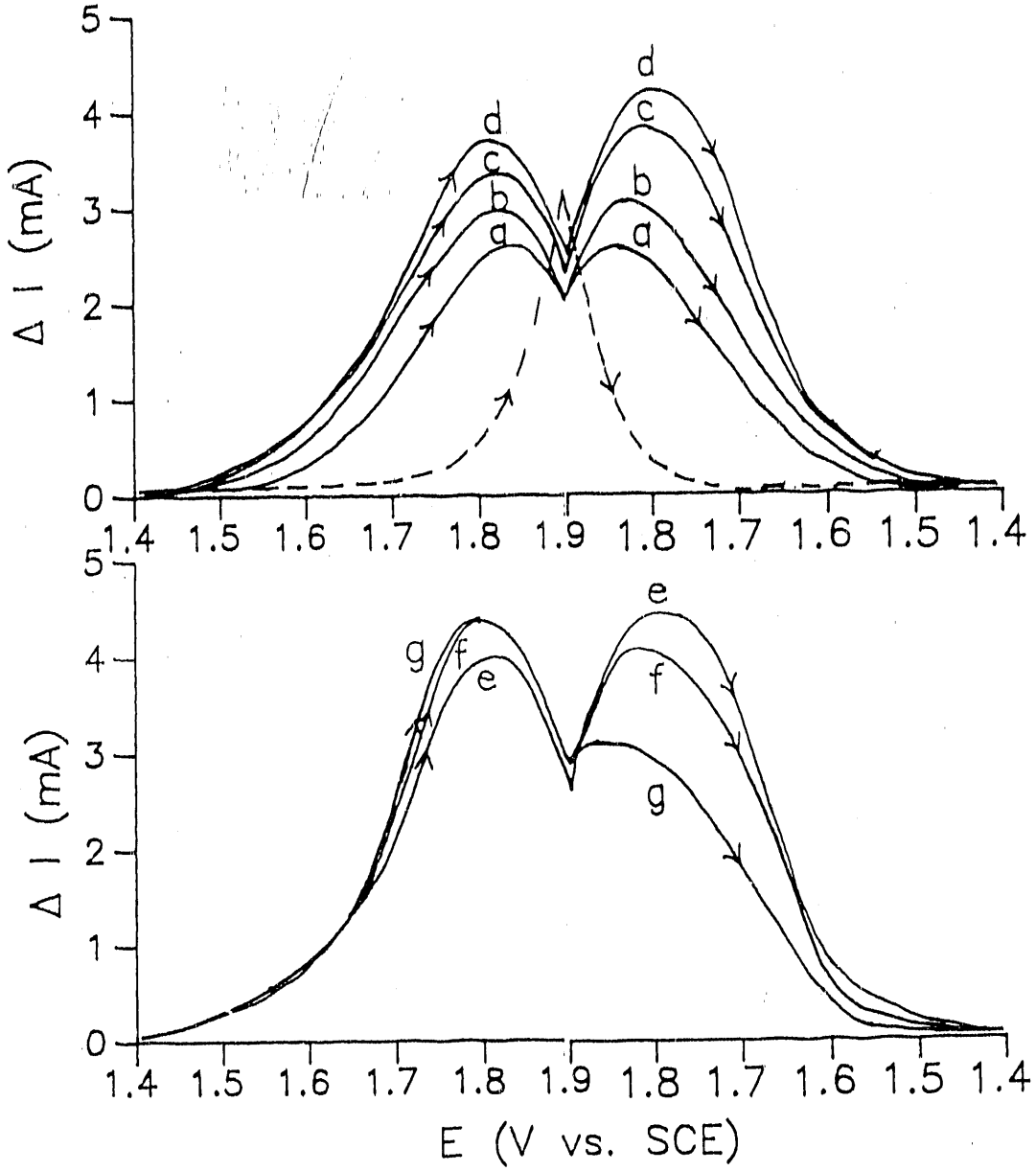

Figure 8. Unfolded cyclic voltammograms for DMSO oxidation at the Cl-PbO_2 film on a Au RDE

Conditions: 2500 rev min^{-1}, 1 V min^{-1}, 10 mM DMSO, 1 M H_2SO_4

$[Bi^{3+}]$ (μM): (a) 0, (b) 2, (c) 11, (d) 23, (e) 43, (f) 153, (g) 273

Curves: (---) residual, (a-g) net current of DMSO oxidation

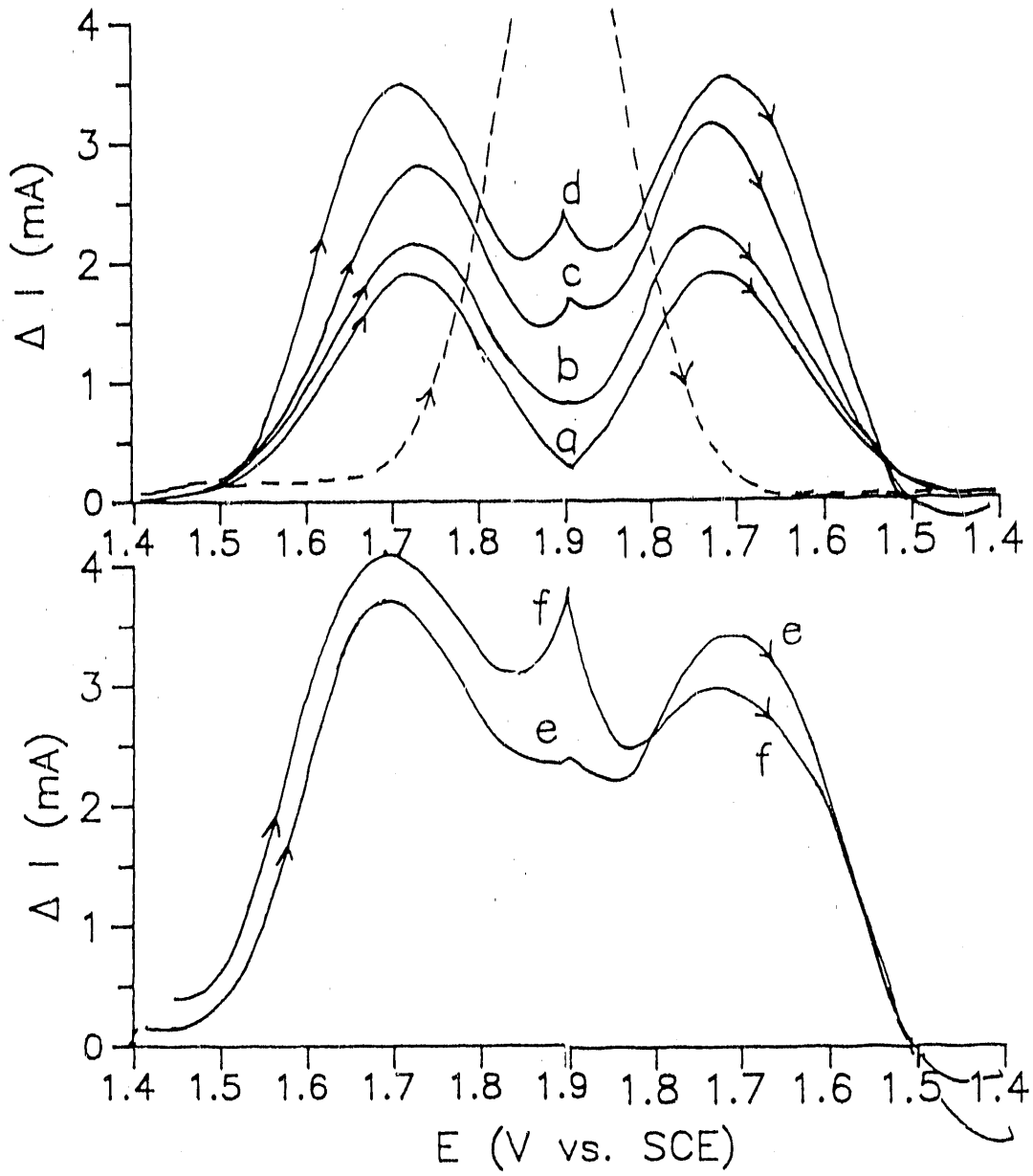

Figure 9. Unfolded cyclic voltammograms for DMSO oxidation at the OAc-PbO_2 film on a Au RDE

Conditions: same as Fig. 8

$[Bi^{3+}]$ (μM): (a) 0, (b) 2, (c) 11, (d), 47, (e) 95, (f) 608

Curves: (---) residual, (a-f) net current of DMSO oxidation

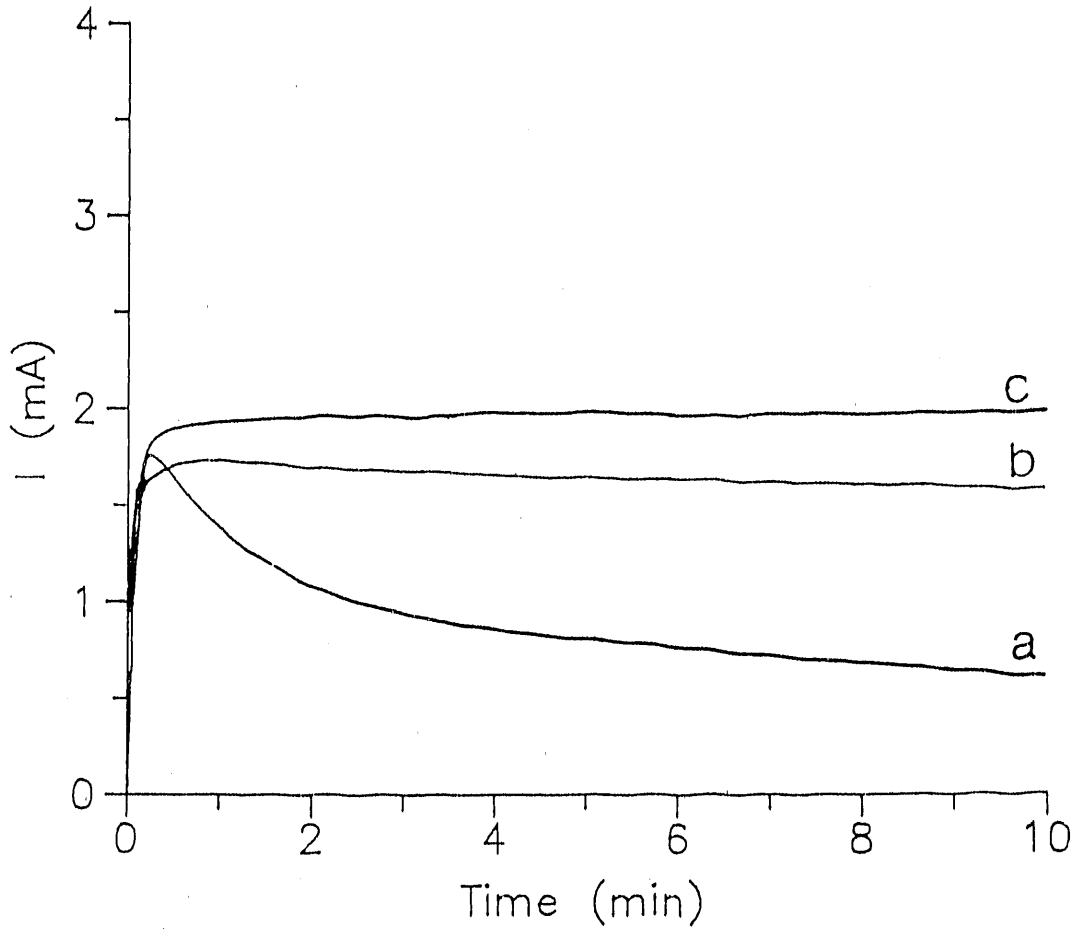

Figure 10. Current-time response for DMSO oxidation obtained following a potential step from 1.4 V to 1.7 V

Conditions: 10 mM DMSO, 320 μM Bi^{3+}, 400 rev min^{-1}

Curves: (a) Cl-PbO_2 in 1 M $HClO_4$,
(b) Cl-PbO_2 in 1 M H_2SO_4,
(c) HSO_4^- pretreated Cl-PbO_2 in 1 M $HClO_4$

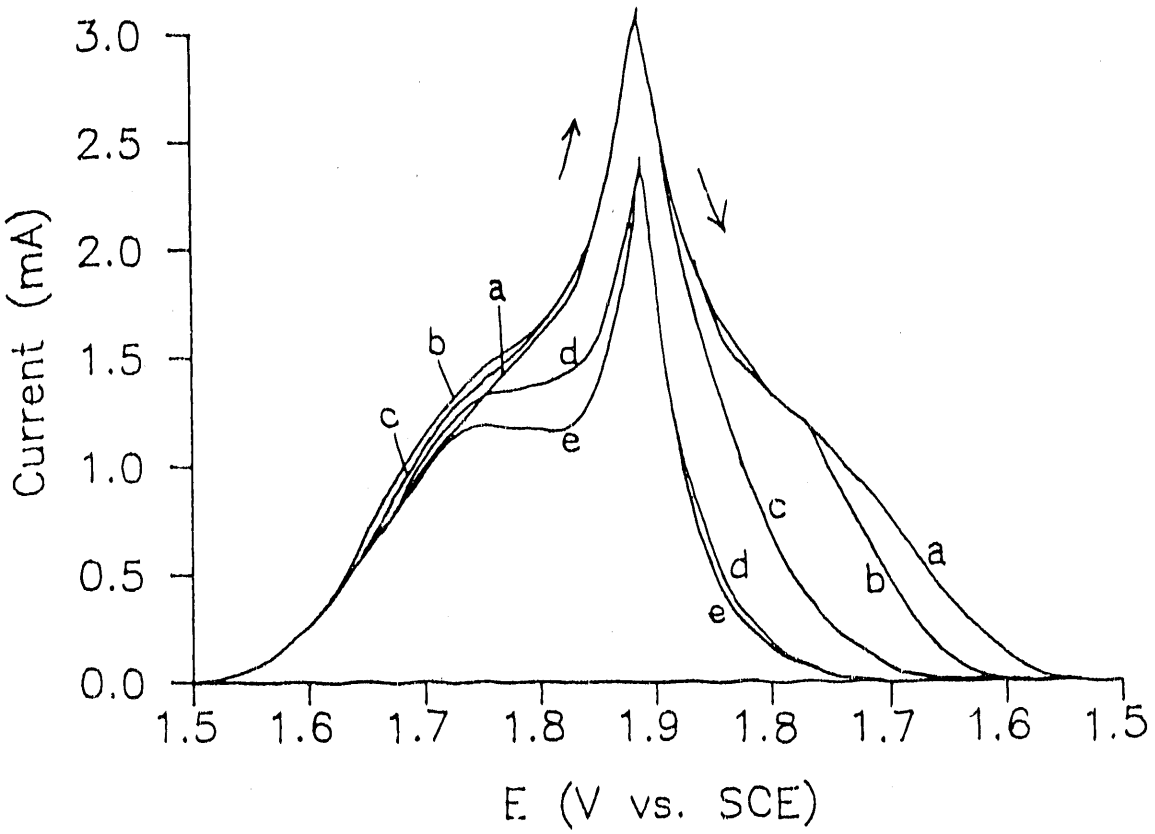

Figure 11A. Unfolded cyclic voltammograms of DMSO at the Bi-PbO_2 film on a Au RDE

Conditions: 900 rev min^{-1}, 20 mV s^{-1}, 5 mM DMSO, 1 M $HClO_4$

$[Bi^{3+}]$ (μM): (a) 0, (b) 29, (c) 89, (d) 239, (e) 439

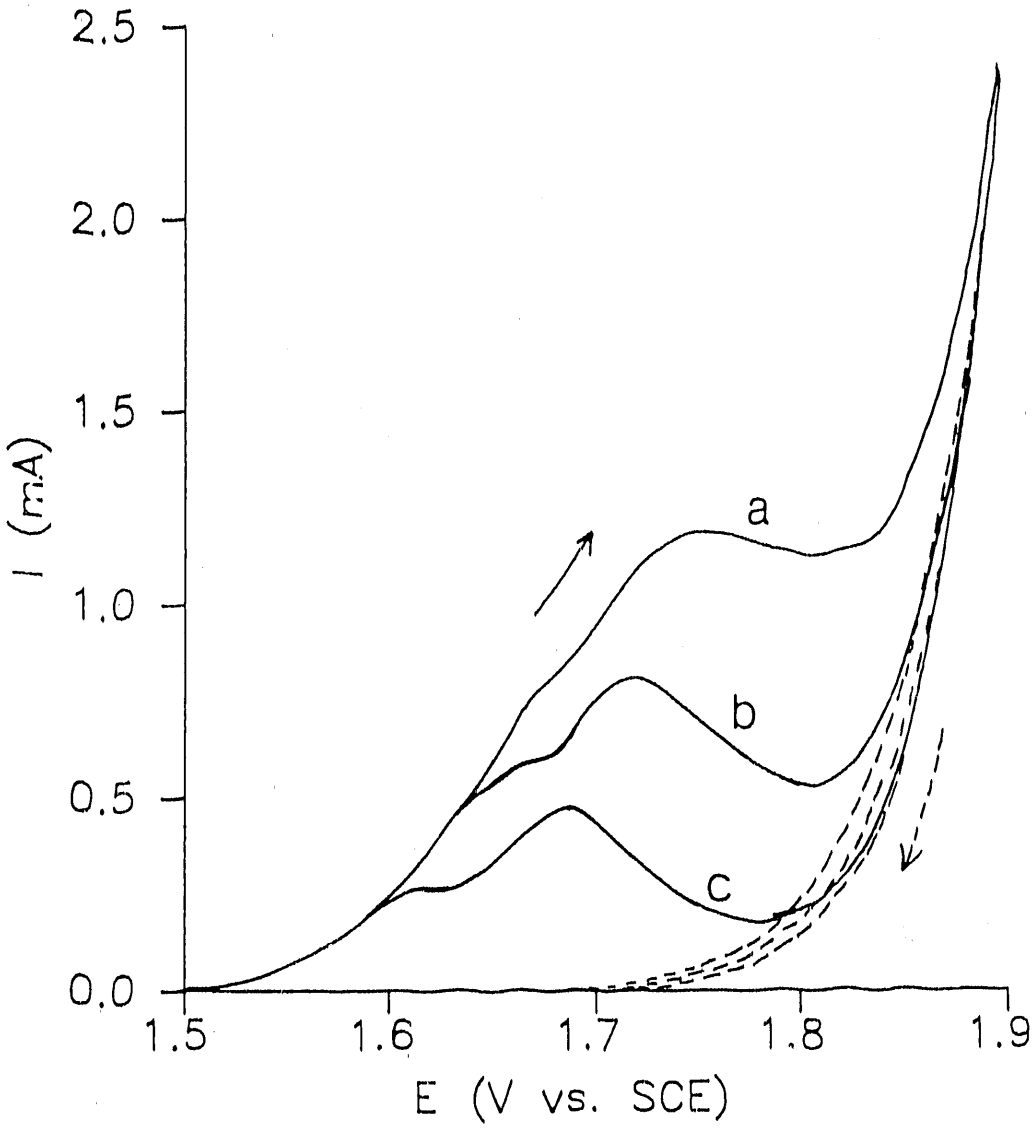

Figure 11B. Cyclic voltammograms of DMSO at the Bi-PbO_2 film on a Au RDE

Conditions: 5 mM DMSO + 439 μM Bi^{3+}, 1 M $HClO_4$, 900 rev min^{-1}

Scan rate (mV s^{-1}): (a) 20, (b) 5, (c) 1

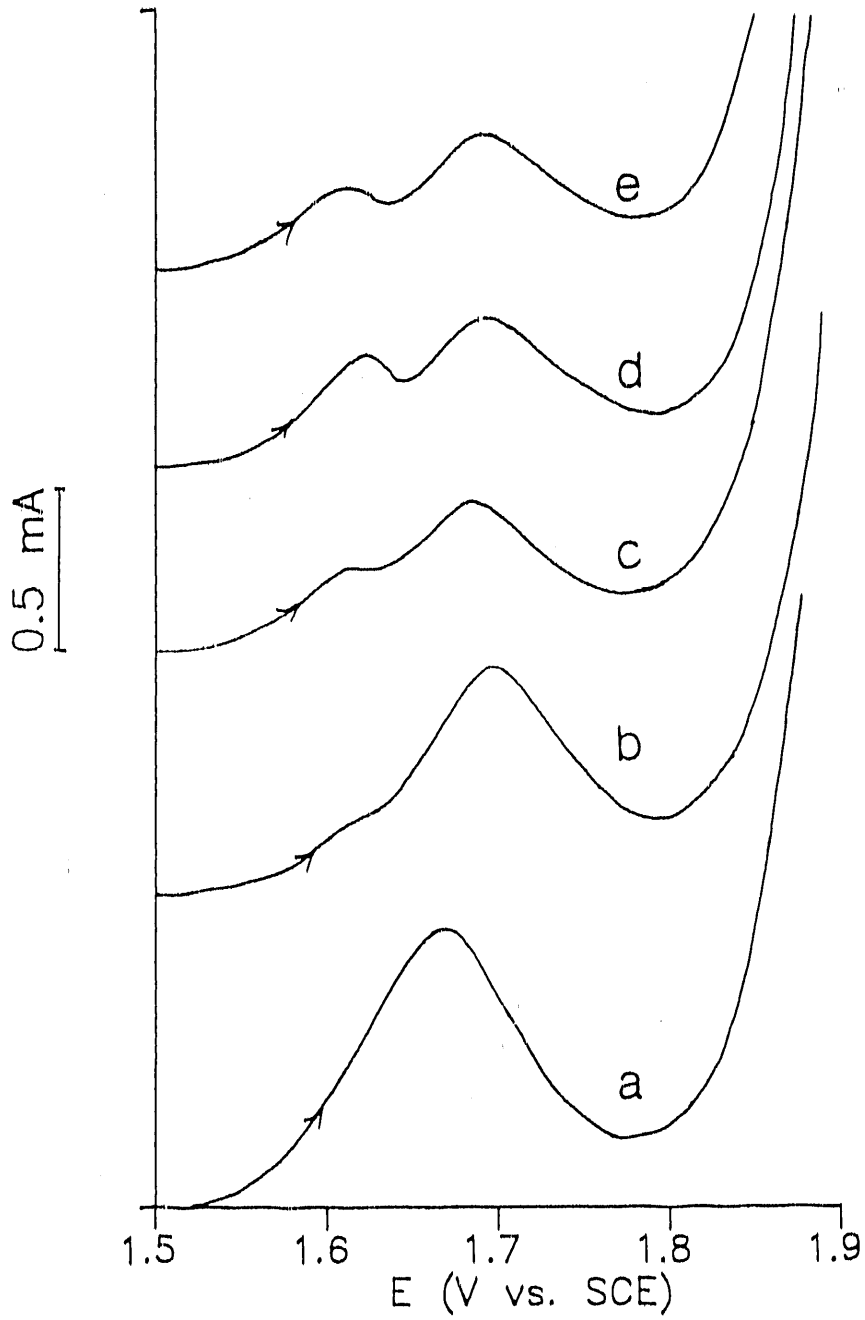

Figure 11C. Cyclic voltammograms of DMSO at Bi^{3+}-modified PbO_2 films

Conditions: 5 mM DMSO + 439 uM Bi^{3+}, 1 M $HClO_4$, 900 rev min^{-1}, 1 mV s^{-1}

Ratio of $[Bi^{3+}]/[Pb^{2+}]$ for the deposition of Bi-PbO_2 films: (a) 0, (b) 0.1, (c) 0.4, (d) 0.7, (e) 1.0

ACKNOWLEDGMENTS

I am very grateful to my advisor, Professor Dennis C. Johnson, for his guidance, encouragement, and patience during the past four years of my graduate studies. I have enjoyed every joke he has ever told, and will never forget that he gave me $10 as a reward for obtaining interesting results which showed break in the slopes of Koutecky-Levich plots. I believe that he still remembers the pizza I bought with that money.

I would like to thank the past and present group members I have worked with. Special thanks go to Brian Wels for setting up the data acquisition system for me and for making the lab so neat; Jianren Feng for giving me a typewriter and for his helpful discussions; Tiger Gordon for helping me with the EQCM measurements and for giving me a Chinese-version Bible; Doug Williams for letting me use his "Directory of Graduate Research" for so long, for kindly helping me with my English in many ways, and for letting me constantly bother him for no good reason; Hsiangpin Chang, Andy Tang, Larry Larew and Bill LaCourse for many things they have done for me; Warren Jackson, Rich Robert, Joe Vitt, and David Dobberpuhl. I thank them all for their friendships and for the pleasant environment they have created for the group.

There are so many people to thank and to remember. I am very lucky to have Professor Harvey Diehl, and Mr. Harvey Burkholder as my friends as I have learned so much from them; their enthusiasm will always inspire me. I thank Professor Marc D. Porter, and Professor R. Sam Houk

for their generosity for letting me use STM, and ICP mass spectrometry, respectively, in their research group. I appreciate my constant companion, Chien-Ching, for his support, helpful discussion, and his help with everything that has made my life in Ames meaningful.

Special thanks also go to the people of Machine Shop and Glass Shop in the Chemistry Department for their help.

This work was performed at Ames Laboratory under contract No. W-7405-eng-82 with the U. S. Department of Energy. The United States government has assigned the DOE Report number IS-T 1451 to this thesis.

END

DATE FILMED

11/15/90